Dynamic aeroelastic optimization of composite wings including fatigue considerations

Rajpal, D.

DOI
10.4233/uuid:fc33c568-b2f2-48c0-96cc-48221c69c2bb

Publication date
2021

Document Version
Final published version

Citation (APA)
Rajpal, D. (2021). *Dynamic aeroelastic optimization of composite wings including fatigue considerations*. [Dissertation (TU Delft), Delft University of Technology]. https://doi.org/10.4233/uuid:fc33c568-b2f2-48c0-96cc-48221c69c2bb

Dynamic Aeroelastic Optimization of Composite Wings including Fatigue Considerations

Dynamic Aeroelastic Optimization of Composite Wings including Fatigue Considerations

Proefschrift

ter verkrijging van de graad van doctor
aan de Technische Universiteit Delft,
op gezag van de Rector Magnificus Prof. dr. ir. T.H.J.J. van der Hagen,
voorzitter van het College voor Promoties, in het openbaar te verdedigen op vrijdag 26 maart 2021 om 10:00 uur

door

Darwin RAJPAL

Master of Science in Aerospace Engineering,
Delft University of Technology, the Netherlands
born in Ulhasnagar Thane, India.

This dissertation has been approved by the promotors

Composition of doctoral committee:

Rector Magnificus	chairperson
Prof. dr. C. Kassapoglou	Technische Universiteit Delft, promotor
Prof. dr. C. Bisagni	Technische Universiteit Delft, promotor
Dr. ir. R. De Breuker	Technische Universiteit Delft, promotor
Independent members:	
Prof. dr. J.E. Cooper	University of Bristol, UK
Prof. dr. W. Van Paepegem	Ghent University, Belgium
Prof. C.A. Dransfeld	Technische Universiteit Delft
Dr. M. Martinez	Clarkson University, USA
Reserve member	
Prof. dr. ir. R. Benedictus	Technische Universiteit Delft

This research was supported by Technische Universiteit Delft

Keyword: Composite Wing, Gust Loads, Fatigue, Structural Optimizations, Experimental Aeroelasticity

ISBN 978-94-6421-284-6

An electronic version of this dissertation is available at
http://repository.tudelft.nl/.

Dedicated to Mom, Dad,
Aakash and Bhawna

Summary

The COVID-19 pandemic had a significant impact on the aviation industry with more than 60% reduction in the passenger traffic in the year 2020 compared to year 2019. The passenger traffic which is now expected to reach the 2019 level only around the year 2024 will still continue to grow but at a lower pace compared to the pre pandemic levels. The environmental issues which were a major concern for the aviation industry before pandemic will still be relevant. The objective of achieving an environmentally friendly zero emission aircraft will not be met only with alternative fuels and propulsion concepts but also require advanced material technologies and novel designs.

A promising technology having the potential to improve the performance of an aircraft by improving the structural efficiency is the application of aeroelastic tailoring with the help of composite materials. However, incorporating aeroelastic tailoring with composite materials in the design process is not a trivial task. In the traditional design process, knowledge about the design increases, while the design freedom decreases as one goes from conceptual to preliminary and finally to the detailed design. For conventional designs, the lack of knowledge during the initial stages is compensated through empirical knowledge. However, the lack of such empirical knowledge for novel design and advanced technology, results in the need for increased physics-based knowledge during the initial design process.

In the research presented in this dissertation, the focus was on increasing knowledge in the early stages of the aeroelastic design process of a composite wing. As current state of art in aeroelastic tailoring does not include critical gust and fatigue loads, this thesis is focused on including critical gust loads and fatigue loading requirements in the preliminary aeroelastic optimization framework.

Taking into account gust loads during the initial phase of the design process is quite challenging as one has to scan approximately 10 million load cases to identify the worst-case gust load. Additionally, after every iteration, there is an update in the design which changes the aeroelastic properties of the wing leading to a change in critical gust load. As a result, a rescan of all the load cases is required at every new iteration in the design. To improve the efficiency of gust load analysis, a Model Order Reduction (MOR) methodology was implemented to predict the critical gust loads. The goal of the MOR techniques is to produce a system that shows equivalent response characteristics as the original, but consists

of significantly fewer state variables, leading to a reduction in computational cost.

A Reduced Order Aeroelastic Model (ROAM) was formulated by reducing the order of the unsteady vortex lattice model using the Balanced Proper Orthogonal Decomposition (BPOD) method and coupling it to the structural solver. The ROAM was based on the aeroelastic framework PROTEUS developed at Delft University of Technology (TU Delft). With the ROAM, it was demonstrated that the dominant modes of the aerodynamic model could be assumed to be constant for varying equivalent airspeed and Mach number, enabling the use of a single reduced model for the entire flight envelope. A comparison of the results from the full and reduced order aeroelastic model showed high accuracy of the latter and a large saving in computational cost.

Using the developed ROAM, a dynamic aeroelastic optimization of the Common Research Model (CRM) wing clamped at the root was carried out. The results showed that, in the case of a clamped composite wing, both static, as well as gust loads, are critical. Furthermore, the critical loads that sized the wing changed during the optimization process as the aeroelastic properties were changing due to the change in the design variables. This showed the importance of updating the critical loads during the dynamic aeroelastic optimization process.

Typically to account for fatigue in a composite structure, a knockdown factor is applied to the allowable stress levels of the laminate. These knockdown factors can become too conservative and result in a too high wing mass. Thus, an analytical model is formulated and integrated into the aeroelastic optimization process to account for fatigue instead of the knockdown factors. The analytical model to predict the fatigue life of a composite laminate is based on the residual strength degradation method developed by Kassapoglou to predict fatigue failure. Kassapoglou's method was extended by adding a Tsai Wu first ply failure theory to determine the failure of the laminate. Furthermore, it was assumed that the initial strength distribution would follow a Weibull distribution. The predictions of the fatigue model were compared to the test results of unidirectional (UD) and multidirectional (MD) glass/epoxy laminate for the Wisper and the New Wisper spectrum. Reasonable agreements were found between the predicted and the experimental results, with the analytical model being conservative by 1-2 orders of magnitude in fatigue life. Additionally, the analytical model was also extended to work with laminates described by lamination parameters instead of ply angles and stacking sequence. Since the failure criterion in the lamination parameter domain was conservative in nature, the life predictions were also conservative compared to the prediction for laminates defined by ply angles.

The developed analytical fatigue model was then integrated into the aeroelastic analysis and optimization tool PROTEUS. Two optimization studies of the CRM wing were carried out, one with fatigue as a constraint using the analytical fatigue model and another was the traditional one by using knockdown factors on material allowables to account for fatigue. To account for fatigue, the maximum design life of 40,000 flights based on Mini TWIST spectrum was assumed. Results show that a composite wing is not only critical in strength and buckling but also in fatigue when accounted for explicitly rather than using the conservative knockdown factors. When fatigue is accounted for by the analytical model, the middle part of the wing becomes critical in fatigue. As a result, optimum stiffness and thickness distributions lead to a higher washout and therefore reduced the load in the middle part. The critical gust and static loads for the optimum configurations are also different when fatigue is accounted for by the analytical model. The middle part of the wing, optimized with a fatigue constraint, is critical with respect to static loads, whereas the middle part of the wing, optimized with a conservative knockdown factor is critical with respect to gust loads. Furthermore, by including a mathematical fatigue model instead of a conservative knockdown factor, the weight of the wing is reduced by 22%.

To validate the developed preliminary aeroelastic design methodology taking into account fatigue and gust loads, an experimental campaign consisting of two wind tunnel tests and a fatigue test was conducted on a flexible composite wing with a span of 1.75 m and chord of 0.25 m designed to be critical in strength, buckling and fatigue. Additionally, since the design methodology did not take into account stiffness degradation during fatigue explicitly, the goal was also to understand the effect of fatigue on the stiffness of the wing and thus, on the aeroelastic response of the wing.

The aeroelastic part of the design methodology was validated with the wind tunnel tests as the experimental static and gust response of a composite wing matched the numerical predictions with reasonable accuracy with a maximum error of less than 8%. The fatigue tests led to degradation in the stiffness, resulting in an increase in tip deflection by 9%. The wing did not experience any failure at the end of the fatigue test and had sufficient residual strength to withstand the critical load. This validated the fatigue part of the design methodology. However, as the wing was not close to the failure, the analytical model could still be conservative in the fatigue prediction. The aeroelastic performance of the fatigued wing was compared with the pristine wing in the wind tunnel. There was a degradation in the lift curve slope of the fatigued wing when compared to the pristine wing which could be due to the degradation in stiffness due to fatigue. This degradation would result in a change in the cruise angle of attack, which then also needs to be taken into account during the optimization process to avoid degradation in aerodynamic performance because of fatigue over the design life.

In conclusion, with the use of MOR techniques and phenomenological methods, gust and fatigue loads can be accounted for in the preliminary aeroelastic design process respectively in an accurate and computationally inexpensive manner. By accounting for gust and fatigue loads, a lighter design with improved aeroelastic efficiency can be created at the preliminary stage of the design process, having the same reliability as the traditional methods.

Samenvatting

De COVID-19 pandemie heeft een aanzienlijke impact gehad op de luchtvaartsector met een daling van het passagiersverkeer met meer dan 60% in 2020 in vergelijking met 2019. Het passagiersverkeer, dat nu naar verwachting pas rond 2024 het niveau van 2019 zal bereiken, zal nog steeds blijven toenemen, maar in een lager tempo dan vóór de pandemie. De milieukwesties die vóór de pandemie een belangrijk punt van zorg waren voor de luchtvaartsector, zullen nog steeds relevant zijn. In de luchtvaart nemen het passagiers- en vrachtvervoer gestaag toe. De voorspelde verdubbeling van het luchtverkeer in de komende 20 jaar kan leiden tot een toename van de uitstoot van broeikasgassen en luchtverontreinigende stoffen. Om de klimaatverandering tegen te gaan is het dus nodig de efficiëntie van transportvliegtuigen te verbeteren. De doelstelling om te komen tot een milieuvriendelijk emissieloos vliegtuig zal niet alleen worden bereikt met alternatieve brandstoffen en aandrijvingsconcepten, maar vereist ook geavanceerde materiaaltechnologieën en nieuwe ontwerpen.

Een veelbelovende technologie die het potentieel heeft om de prestaties van een vliegtuig te verbeteren door de structurele efficiëntie te verbeteren, is de toepassing van aeroelastic tailoring met behulp van composietmaterialen. Het integreren van aeroelastic tailoring met composietmaterialen in het ontwerpproces is echter geen triviale taak. In het traditionele ontwerpproces neemt de kennis over het ontwerp toe, terwijl de ontwerpvrijheid afneemt naarmate men van conceptueel naar een voorlopig en tenslotte naar gedetailleerd ontwerp gaat. Bij conventionele ontwerpen wordt het gebrek aan kennis tijdens de initiële fase gecompenseerd door empirische kennis. Echter, het gebrek aan dergelijke empirische kennis voor nieuwe ontwerpen en geavanceerde technologie, resulteert in de behoefte aan meer op fysica gebaseerde kennis tijdens het initiële ontwerpproces.

In het onderzoek dat in deze dissertatie wordt gepresenteerd, lag de nadruk op het vergroten van kennis in de vroege stadia van het aeroelastische ontwerpproces van een composiet vleugel. Omdat de huidige stand van de techniek op het gebied van aeroelastische ontwerp geen rekening houdt met kritische windbelasting en vermoeiingsbelasting, richt dit proefschrift zich op het opnemen van kritische windbelasting en vermoeiingsbelastingseisen in de conceptuele aeroelastische optimalisatiemethode.

Rekening houden met windbelastingen in de beginfase van het ontwerpproces is

een lastige uitdaging, omdat men ongeveer 10 miljoen belastingsgevallen moet scannen om de ergste windbelasting te identificeren. Bovendien is er na elke iteratie een update in het ontwerp die de aeroelastische eigenschappen van de vleugel verandert, wat leidt tot een verandering in de kritische windbelasting. Als gevolg hiervan is bij elke nieuwe iteratie in het ontwerp een nieuwe scan van alle belastinggevallen nodig. Om de efficiëntie van de analyse van de windbelasting te verbeteren, werd een MOR-methodologie geïmplementeerd om de kritische windbelasting te voorspellen. Het doel van de MOR-technieken is een systeem te produceren dat gelijkwaardige responskenmerken vertoont als het origineel, maar uit aanzienlijk minder toestandsvariabelen bestaat, hetgeen leidt tot een vermindering van de rekentijd.

Een ROAM werd geformuleerd door de orde van het aerodynamische wervelmodel te reduceren met behulp van de BPOD methode en het te koppelen aan de structurele oplosser. De ROAM was gebaseerd op het aeroelastische computerprogramma PROTEUS, ontwikkeld aan de TU Delft. Met het ROAM werd aangetoond dat de dominante modi van het aërodynamische model constant konden worden verondersteld voor variërende equivalente luchtsnelheid en Machgetal, waardoor het gebruik van een enkel gereduceerd model voor alle mogelijke vliegcondities mogelijk werd. Een vergelijking van de resultaten van het aeroelastische model van de volledige en gereduceerde orde toonde een hoge nauwkeurigheid van het laatstgenoemde model en een grote besparing op de rekenkosten.

Met behulp van het ontwikkelde ROAM werd een dynamische aeroelastische optimalisatie uitgevoerd van de CRM vleugel die aan de wortel was vastgeklemd. De resultaten toonden aan dat, in het geval van een ingeklemde composiet vleugel, zowel statische als windbelastingen kritisch zijn. Bovendien veranderden de kritieke belastingen die het structurele vleugelontwerp bepalen tijdens het optimalisatieproces, omdat de aeroelastische eigenschappen veranderden als gevolg van de verandering in de ontwerpvariabelen. Dit toont het belang aan van het bijwerken van de kritische belastingen tijdens het dynamische aeroelastische optimalisatieproces.

Om rekening te houden met vermoeiing in een composietconstructie wordt een reductiefactor toegepast op de toelaatbare spanningsniveaus van de laminaten. Deze reductiefactoren kunnen te conservatief worden en resulteren in een te hoge vleugelmassa. Daarom wordt een analytisch model geformuleerd en geïntegreerd in het aeroelastische optimalisatieproces om rekening te houden met vermoeiing in plaats van met de reductiefactoren. Het analytische model om de vermoeiingslevensduur van een composiet laminaat te voorspellen is gebaseerd op de reststerkte degradatie methode ontwikkeld door Kassapoglou om vermoeiingsbreuk te voorspellen. Kassapoglou's methode werd uitgebreid met een Tsai Wu first ply failure theorie om het bezwijken van het laminaat te bepalen. Bovendien werd aangenomen dat de initiële sterkteverdeling een Weibullverdeling zou volgen. De voorspellingen van het vermoeiingsmodel werden vergeleken met de testresultaten van UD en MD glas/epoxy laminaat voor het Wisper en het New Wisper spectrum. Er werden redelijke overeenkomsten gevonden tussen de voorspelde en de experimentele resultaten, waarbij het analytische model conservatief was met 1-2 orden van grootte wat betreft vermoeiingslevensduur. Bovendien werd het analytische model uitgebreid om te kunnen werken met laminaten die worden beschreven door laminaatparameters in plaats van door de hoeken van de lagen en de stapelvolgorde. Aangezien het bezwijkcriterium in het domein van de lamineerparameters conservatief van aard was, waren de levensduurvoorspellingen ook conservatief in vergelijking met de voorspelling voor laminaten gedefinieerd door de hoeken van de lagen.

Het ontwikkelde analytische vermoeiingsmodel werd vervolgens geïntegreerd in het aeroelastische analyse- en optimalisatietool PROTEUS. Er werden twee optimalisatiestudies van de CRM-vleugel uitgevoerd, één met vermoeiing als beperking door gebruik te maken van het analytische vermoeiingsmodel en een andere was de traditionele studie, door gebruik te maken van de reductiefactoren op de toelaatbare materiaalmassa's om rekening te houden met vermoeiing. Om rekening te houden met vermoeiing werd uitgegaan van de maximale ontwerplevensduur van 40.000 vluchten op basis van het Mini TWIST spectrum. De resultaten tonen aan dat een composieten vleugel niet alleen kritisch is voor wat betreft sterkte en knik, maar ook voor wat betreft vermoeiing, wanneer er expliciet rekening mee wordt gehouden in plaats van gebruik te maken van de conservatieve reductiefactoren. Wanneer vermoeiing in rekening wordt gebracht door het analytische model, wordt het middelste deel van de vleugel kritisch in vermoeiing. Als gevolg hiervan leiden optimale stijfheids- en dikteverdelingen tot een hogere verdraaiing van de vleugeltip en daardoor een lagere belasting in het middendeel. De kritische windstoten en statische belastingen voor de optimale configuraties zijn ook verschillend wanneer vermoeiing in rekening wordt gebracht door het analytische model. Het middelste deel van de vleugel, geoptimaliseerd met een vermoeiingsbeperking, is kritisch met betrekking tot statische belastingen, terwijl het middelste deel van de vleugel, geoptimaliseerd met een conservatieve reductie factor, kritisch is met betrekking tot de windbelasting. Bovendien, door het opnemen van een mathematisch vermoeiingsmodel in plaats van een conservatieve knockdown factor, wordt het gewicht van de vleugel met 22

Om de ontwikkelde aeroelastische ontwerpmethodologie, die rekening houdt met vermoeiings- en windbelasting, te valideren, werd een experimentele campagne, bestaande uit twee windtunneltesten en een vermoeiingstest, uitgevoerd op een flexibele composietvleugel met een spanwijdte van 1,75 m en een koorde van 0,25 m die ontworpen was om kritisch te zijn op het gebied van sterkte, knik en vermoeiing. Aangezien de ontwerpmethodologie niet expliciet rekening hield met de degradatie van de stijfheid tijdens vermoeiing, was het doel ook om het effect van vermoeiing op de stijfheid van de vleugel en dus op de aeroelastische respons van de vleugel te begrijpen.

Het aeroelastische deel van de ontwerpmethodologie werd gevalideerd met windtunneltesten, aangezien de experimentele statische en windvlaagresponsie van een composietvleugel redelijk nauwkeurig overeenkwam met de numerieke voorspellingen, met een maximale fout van minder dan 8%. De vermoeiingstesten leidden tot degradatie van de stijfheid, resulterend in een toename van de tipdoorbuiging met 9%. De vleugel bezweek niet aan het einde van de vermoeiingstest en had voldoende reststerkte om de kritische belasting te weerstaan. Dit valideerde het vermoeiingsdeel van de ontwerpmethodologie. Echter, omdat de vleugel niet dicht bij bezwijken was, kon het analytische model nog steeds conservatief zijn in de vermoeiingsvoorspelling. De aeroelastische prestatie van de vermoeide vleugel werd vergeleken met de originele vleugel in de windtunnel. Er was een afname in de helling van de liftkromme van de vermoeide vleugel in vergelijking met de originele vleugel, wat te wijten zou kunnen zijn aan de afname van de stijfheid als gevolg van vermoeiing. Deze degradatie zou resulteren in een verandering van de invalshoek tijdens de kruisvlucht, waarmee dan ook rekening moet worden gehouden tijdens het optimalisatieproces om degradatie van de aërodynamische prestaties als gevolg van vermoeiing gedurende de ontwerplevensduur te voorkomen.

Concluderend kan worden gesteld dat met het gebruik van MOR-technieken en methoden, gebaseerd op fysica, op een nauwkeurige en rekenkundig goedkope manier rekening kan worden gehouden met windvlaag- en vermoeiingsbelastingen in het conceptuele aeroelastische ontwerpproces. Door rekening te houden met wind- en vermoeiingsbelastingen kan in het voorstadium van het ontwerpproces een lichter ontwerp met een verbeterde aeroelastische efficiëntie worden bereikt met dezelfde betrouwbaarheid als de traditionele methoden.

NOMENCLATURE

ROMAN SYMBOLS

$\mathbf{A}$	State matrix	–
$\mathbf{Ae}$	Aerodynamic influence coefficient	–
$\mathbf{As}$	Laminate in-plane stiffness matrix	N/m
$\mathbf{B}$	Input matrix	–
$\mathbf{C}$	Ouput matrix	–
$\mathbf{c}$	Vector with reduced states	–
C_l	Section lift coefficient	–
C_L	Wing lift coefficient	–
$\mathbf{D}$	Feedthrough matrix	–
$\mathbf{Df}$	Degradation factor	–
$\mathbf{d}$	Residual strength degradation ratio	–
E	Young's modulus	N/m^2
$\mathbf{e}_\gamma$	Vector along the vortex segment	–
$\mathbf{F}$	Force vector	N
$\mathbf{F}$	Force and moment vector	N,Nm
F	Fatigue factor	–
F_g	Flight profile alleviation factor	–
f	Modified Tsai Wu criterion	–
G	Shear modulus	N/m^2
$\mathbf{H}$	Transport of vorticity	–
H	Gust gradient	m
$\mathbf{K}$	Stiffness matrix	N/m^2
$\mathbf{M}$	Mass matrix	–
M	Mach number	–
N	Number of cycles to failure	–
N_t	Total cycles structure has to withstand	–
$\mathbf{n}$	Normal vector	–
$\mathbf{p}$	Structural degrees of freedom	m,rad

p	Probability of failure	–
R	Stress ratio	–
R_{tw}	Tsai Wu factor degradation ratio	–
S	Shear strength	N/m^2
s	Distance penetrated into the gust	m
t	Time	s
U	Gust velocity	m/s
$\mathbf{u}$	Input vector	–
$\mathbf{V}$	Velocity	m/s
$\mathbf{V_r}$	Reduced basis	–
V_{eq}	Equivalent airspeed	m/s
X_t	Longitudinal tensile strength	N/m^2
X_c	Longitudinal compressive strength	N/m^2
X	Mean of the distribution	–
$\mathbf{x}$	State vector	–
Y_t	Transverse tensile strength	N/m^2
Y_c	Transverse compressive strength	N/m^2
$\mathbf{y}$	Output vector	–

Greek Symbols

α	Angle of attack	rad
α	Weibull shape factor	–
β	Weibull scale factor	–
$\mathbf{\Gamma}$	Vortex strength vector	m^2/s
ϵ	Strain	-
λ	Eigenvalue	–
ν	Poisson's ratio	–
ρ	Density	kg/m^2
σ	Strength	N/m^2

Sub/Superscripts

1	Aligned with the fiber direction
2	Perpendicular to the fiber direction
∞	Freestream conditions
a	Aerodynamic
ae	Aeroelastic

b	Body surface
ds	Design gust velocity
eq	Equivalent speed
int	Initial
r	Residual strength
ref	reference velocity
s	Reduced states
s	Structural
sf	Static failure strength
st	Steady
TE	Trailing edge
$unst$	Unsteady
w	Wake surface
w_0	First row of wake elements
x	Along the x-direction
y	Along the y-direction
z	Along the z-direction

Abbreviations

CO_2	carbon dioxide
NOx	nitrogen oxide
V_{eq}	equivalent air speed
AFP	automatic fiber placement
AIC	aerodynamic influence coefficient
BEM	boundary element method
BMI	bismaleimide
BPOD	balanced proper orthogonal decomposition
BT	balanced truncation
CFD	computational fluid dynamics
CFRP	carbon fiber reinforced plastic
CoV	coefficient of variation
CRM	common research model
CS-25	certification specifications for large aeroplanes
DASML	Delft Aerospace Structures and Materials Laboratory
DLM	doublet lattice method
DLR	German Aerospace Center
EASA	European Aviation Safety Agency

FAA	Federal Aviation Administration
FOM	full order model
FPF	first ply failure
GCMMA	globally convergent method of moving asymptotes
GVT	ground vibration test
LE strip	leading edge strip
LTI	linear time-invariant
MD	multidirectional
MDO	multidisciplinary design optimization
Mini-TWIST	shortened version of the TWIST spectrum
MLE	maximum likelihood estimation
MOR	model order reduction
MT	model truncation
OFDR	optical frequency domain reflectometer
OJF	open jet facility
PDM	ply discount method
POD	proper orthogonal decomposition
RMSE	root-mean-square error
ROAM	reduced order aeroelastic model
ROM	reduced-order model
RTC	round the clock
SDM	stiffness degradation method
SVD	singular value decomposition
TU Delft	Delft University of Technology
UD	unidirectional
ULF	ultimate laminate failure
VLM	vortex lattice method

CONTENTS

1 Introduction

In the past two decades, aviation was experiencing a steady rise with both Boeing (2019) and Airbus (2017) predicting a projected growth by a factor of two within the next 20 years for the demand in air travel. However, the COVID-19 pandemic had a significant impact on the aviation industry as countries closed their borders and imposed travel restrictions in order to halt the spread of the virus. In comparison to 2019, there was a reduction of more than 60% in the passenger traffic in the year 2020 Bureau (2020). The passenger traffic is now expected to reach the 2019 level only around the year 2024 IATA (2020). The aviation will still continue to grow after 2024 but at a lower pace compared to the pre pandemic levels KPMG (2020). The environmental issues which were a major concern for the aviation industry before pandemic will still be relevant as the industry continues to grow. Thus climate change mitigation necessitates improvement in the efficiency of the transport aircraft.

To curb the global warming, the European Commission set out goals in the Flightpath 2050 report (Krein and Williams, 2012), which include, among others, a 75% reduction in Carbon Dioxide (CO_2) emissions per passenger kilometer, 90% reduction in Nitrogen Oxides (NOx) and 60% reduction in perceived noise by 2050 as compared to the aircraft in the year 2000. Even though these objectives were set before the pandemic, they are still relevant today and they do not seem to be realistic for conventional designs as it is becoming increasingly difficult to make the well-known wing and tube configuration more efficient. Advanced technologies and novel designs seem to have the potential to address the required leap in performance.

A promising technology having the potential to improve the performance of an aircraft by improving the structural efficiency is the application of aeroelastic tailoring with the help of composite materials. Aeroelastic tailoring is defined by SHIRK et al. (1986) as *the embodiment of directional stiffness into an aircraft structural design to control aeroelastic deformation, static or dynamic, in such a fashion as to affect the aerodynamic and structural performance of that aircraft in a beneficial way*. The aim of the aeroelastic tailoring is to optimize the bend-twist coupling of the wing in such a way that the resulting load distribution gives a lighter wing with improved aerodynamic performance.

With high specific strength, the use of composite materials is beneficial in terms of weight saving. A further advantage of the composite materials is their inherent anisotropic behavior, which can be tailored to achieve beneficial aeroelastic deformations. This improves the structural efficiency with a minimum weight penalty, resulting in higher performance during the flight. As a result, there is increased use of composites over the years in commercial aviation, as shown in Figure 1.1. With the advancement in manufacturing technologies and reduction in cost, commercial aircraft are increasingly using large proportions of composite materials.

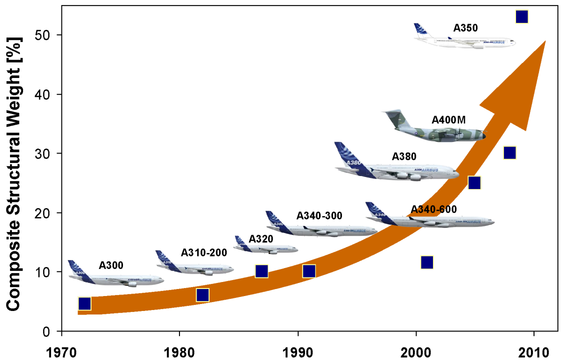

Figure 1.1: Usage of composite in Airbus aircraft (Fualdes, 2016).

Incorporating advanced technologies such as aeroelastic tailoring in the design process is not a trivial task. In the traditional design process, knowledge about the design increases, while the design freedom decreases as one goes from conceptual to preliminary and finally to the detailed design, as shown in Figure 1.2. For conventional designs, the lack of knowledge during the initial stages is compensated through empirical knowledge. However, the lack of such empirical knowledge for novel design results in the need for increased physics-based knowledge during the initial design process.

In the current thesis, the focus is on increasing knowledge in the early stages of

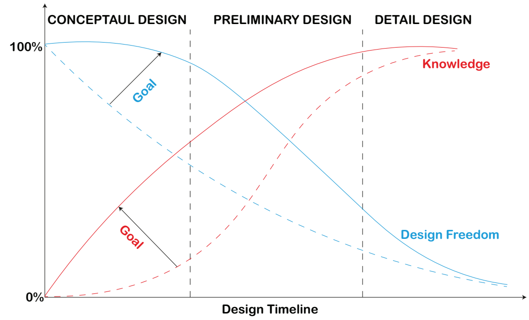

Figure 1.2: Trend of knowledge and freedom in aircraft design process (Mavris and DeLaurentis, 2000).

the aeroelastic design process of a composite wing. In the following sections, a survey of state of the art in the field of aeroelastic tailoring is described. Based on the shortcomings identified from the literature review, the research question that this thesis will be looking to answer will be derived. Finally, the outline of this dissertation is presented.

1.1 Aeroelastic Tailoring

In late 1960s/early 1970s, aeroelastic tailoring started gaining popularity with the introduction of fiber-reinforced materials (SHIRK et al., 1986; Weisshaar, 1981). However, the very first application of the concept of aeroelastic tailoring can be found way back in 1949 by Munk (1949), who oriented the grain of his wooden propeller blade to alter the directional stiffness properties of wood which would create desirable twist deformation when operated. The aeroelastic tailoring of forward-swept X-29 experimental aircraft using composite materials was one of the early success stories of the application of aeroelastic tailoring on the overall aircraft performance (Weisshaar, 1981).

Starnes Jr and Haftka (1979) explored the use of composite materials to minimize the weight of the wing with constraints on strength, buckling, displacement and twist. A balanced and symmetric laminate was used where the angles of the lamina was fixed but the thickness of the lamina served as a design variable. Green (1987) explored the possibilities for using general non-symmetric laminates in the aeroelastic tailoring studies to increase the flutter boundary. The results showed that non-symmetric laminates did not provide much improvement in the flutter boundary over the symmetric laminates. Taking into account the increased complexity in modelling and manufacturing for the non-symmetric laminates, there were no clear benefits of using non-symmetric laminates.

Combining static strength and aeroelastic stability, Isogai (1989) performed preliminary aeroelastic optimization with an objective of minimizing the weight of the wing box. The design variables used were the thickness distribution and the fiber orientation of the skin panels. Eastep et al. (1999) evaluated the effect of layup orientation on the optimized weight by using a fixed set of discrete ply angles $[0/45/-45/90]$. The design variables were the thickness of the layup and the orientation of the layup with respect to the wing axis. The constraints used in the optimization were static strength, flutter speed and aileron reversal. The study showed that the optimal designs of composite wings are relatively insensitive to the orientation of the laminate layup when the wing is subjected to multiple structural constraints (Eastep et al., 1999).

Guo and his co-workers (Guo, 2007; Guo et al., 2006, 2003) implemented a different strategy towards aeroelastic tailoring by fixing the number of plies in the laminate and hence the thickness of the laminate and varying the ply angles in the laminate to obtain the desired aeroelastic properties. The optimization was done for a minimum weight with aeroelastic and strength constraints. The results showed that compared to the metallic wing box, up to 30% increase of flutter speed for the composite wing box could be achieved by optimizing the fiber orientations of the wing skin and spar web laminates whereas compared with the quasi-isotropic layups, 18 percent increase in flutter speed was achieved.

A similar strategy to Guo was also adopted by Kim and Hwang (2005) to optimize the stacking sequence of the composite plate while keeping the thickness constant. Kim and Hwang focused on minimizing the strain energy by random gust loads. In this work, the concept of uncertainty and probabilistic methods were combined with aeroelastic tailoring approaches to obtain an optimized composite stacking sequence.

Arizono and Isogai (2005) optimized the laminate orientation along with the thicknesses of a cranked-arrow wing of a supersonic jet for minimum structural weight with constraints on strength, local buckling, and flutter. Strength and local buckling were evaluated for static load cases. Guo et al. (2012) presented an aeroelastic optimization of a large aircraft composite wing subject to multiple constraints, including strength, damage tolerance, and aeroelastic stability. Both skin thickness and the ply angles were used as the design variables. The damage tolerance was taken into account by the use of a knockdown factor on the stress allowables, which would limit the maximum strain experienced by the laminate. Additionally, both static loads and dynamic gusts were taken into account to size the structure. The results indicated that the final optimum design had around 30% weight saving compared to the initial design.

An alternative to the use of ply angles in composite optimization is the use of lamination parameters. The advantage of lamination parameters is that with a limited number of variables, a complete description of the laminate is obtained. Kameyama and Fukunaga (2007) used the lamination parameters to optimize a composite plate for a minimum weight with a constraint on aeroelastic divergence and flutter. The results showed the effectiveness of aeroelastic tailoring to optimize the aeroelastic stability boundary. Dillinger et al. (2013) used the concept of lamination parameters to optimize a composite wingbox structure with an objective of minimum weight or maximum aileron effectiveness with constraints on laminate failure and buckling. The static maneuver load cases were used to analyze the strength and buckling criteria. The results showed the superiority of the unbalanced laminates over balanced laminates for aeroelastic optimization problems. This work was extended by combining high fidelity Computational Fluid Dynamics (CFD) with low fidelity Doublet Lattice Method (DLM) aerodynamic solver to perform static aeroelastic stiffness optimization of a forward swept composite wing (Dillinger et al., 2019).

De Breuker and his co-workers have also focused on the use of lamination parameters in aeroelastic tailoring of composite wings (Jovanov, K. et al., 2019; Macquart et al., 2017; Natella and De Breuker, 2019; Silva et al., 2019; Werter and De Breuker, 2016). Werter and De Breuker (2016) developed a dynamic aeroelastic tailoring methodology using lamination parameters which could also take into account the effect of dynamic loads during optimization. Macquart et al. (2017) extended the framework of Werter and De Breuker by introducing blending constraints in the lamination parameter domain. The results show that by using blending constraints, the match between the optimized lamination parameters and the corresponding stacking sequences improves, leading to a better match in the aeroelastic response. Natella and De Breuker (2019) included the effect of the aerodynamics of the whole aircraft on the aeroelastic tailoring of the wing. The results show that including the aerodynamics of the full aircraft changes the lift distribution and the aerodynamic center, which leads to a change in the aeroelastic response resulting in changes up to 11% in the mass of the final design compared to design without the effect of the entire aircraft aerodynamics.

With the advancement of Automatic Fiber Placement (AFP) machines, there has been an interest in extending the composite design space for structures with the use of tow/fiber steering. AFP machines can manufacture tow steered composites by laying fibers along precise curvilinear paths to create variable-stiffness panels (Lukaszewicz et al., 2012). The effect of tow steering on the aeroelastic properties of composite plates has been investigated by several authors (Haddadpour and Zamani, 2012; Stanford et al., 2014; Stodieck et al., 2013). These studies showed considerable improvements in flutter and divergence speed of the variable-stiffness panels compared to constant-stiffness panels. Recently, the work on the plates has been extended by studying the advantage of fiber steering on the aeroelastic tailoring of the composite wingbox (Brooks et al., 2019; Stanford and Jutte, 2017; Stanford et al., 2016; Stodieck et al., 2015, 2017). The constraints considered in these studies are strength, buckling, aileron effectiveness, and flutter constraints. The results have shown a reduction in weight of approximately 10% compared to an aeroelastically tailored composite wing with unidirectional (UD) fibers, thus clearly establishing the benefits of variable-stiffness panels compared to constant-stiffness panels for aeroelastic tailoring.

Additionally Cooper and his co-workers (Georgiou et al., 2012; Manan and Cooper, 2009; Othman et al., 2019; Ouyang et al., 2013; Scarth et al., 2014) have focused on including the effect of uncertainties on the aeroelastic tailoring of the composite wings. The uncertainties in material properties, ply angles, ply thickness and Mach number were considered in the studies. There are two main conclusions from these studies. The first is that the Polynomial Chaos Expansion is more efficient than Monte Carlo Simulations in quantifying the effects of uncertainties however it can suffer from the curse of dimensionality as the number of estimated terms grows significantly with the number of random variables. The second is that the best compromise between weight, reliability and robustness is provided by simultaneous robust and reliability-based optimization as only reliability based design optimization leads to reduced robustness whereas optimizing for robustness can lead to sufficiently reliable design but with greater weight penalty.

1.2 Research Question

In a majority of the studies referenced above, static manoeuvre load cases are used to size the structure. With the increasing trend of wings becoming more flexible and lighter with the application of tailored composite materials, unsteady loads due to gusts can also become critical (Werter, 2017). In the studies which have included gust load cases (Guo et al., 2012; Stodieck et al., 2017; Werter, 2017), fixed gust lengths and flight points are used. However, in an optimization process, for every iteration, an update in the design of the wing would lead to a modification in the aeroelastic characteristics of the wing, which could result in a different critical gust load. As a result, at every iteration, a range of load cases across the entire flight envelope needs to be evaluated to determine the worst-case gust load.

The main design drivers in the aeroelastic optimization process based on state of the art, are stiffness, static strength, buckling and static and dynamic aeroelastic stability. In order to avoid fatigue problems, a conservative knockdown factor is applied to the allowable material strain levels (Guo et al., 2012). With this design philosophy, failure under repeated loading is avoided since the fatigue loads acting on the structure are too low to initiate or propagate any existing damage during anticipated life of the aircraft. As composite wing designs become more optimized for improved aeroelastic behavior and further weight savings, the difference between the magnitude of typical fatigue loads and the ultimate static strength of design becomes smaller. As a result, fatigue loading, which historically was not a design driver for the composite structure, now becomes more important and may impact the design. This means that using conservative knockdown factors would be too conservative and weight-inefficient.

In the current state of the art, the process of aeroelastic tailoring does not include critical gust and fatigue loads. With an aim to increase the knowledge in the current aeroelastic design framework, the main research question this thesis will be looking to answer is

> *Can critical gust and fatigue loads be integrated into a preliminary aeroelastic design process of a composite wing and what are there effects on the final design?*

In the quest to get the answer for the global research question mentioned above, the following sub questions will be answered

- How can critical gust loads be identified and included in every iteration in the aeroelastic optimization process of composite wings? What are the effects of including critical gust loads on the optimized design?
- How can the effect of fatigue be included in the aeroelastic tailoring process of the composite wings? How does the optimized design change due to inclusion of fatigue loads?
- To what extent does the formulated preliminary aeroelastic framework approximate the response of the wing when subjected to critical gust and fatigue loads? What is the effect of the fatigue on aeroelastic performance of the wing?

1.3 Dissertation outline

The thesis is organized into five chapters. In this chapter, a brief background on the topic was given. The state of art in the field of the aeroelastic tailoring was presented. The research questions that this thesis is going to answer was described.

The second chapter describes the use of Model Order Reduction (MOR) methodology to predict the critical gust loads. The Reduced Order Aeroelastic Model (ROAM) is formulated by reducing the aerodynamic system with a Balanced Proper Orthogonal Decomposition (BPOD) and coupling it to a structural solver. It is demonstrated that the dominant modes of the aerodynamic model can be assumed to be constant for varying equivalent airspeed and Mach number, enabling the use of a single reduced model for the entire flight envelope. A comparison of the results from the full and reduced order aeroelastic model shows high accuracy of the latter and a large saving in computational cost. A dynamic aeroelastic optimization framework is then formulated by coupling ROAM with the aeroelastic framework PROTEUS (Werter and De Breuker, 2016) developed at Delft University of Technology (TU Delft). The effects of including critical gust loads in the stiffness and thickness optimization of a composite wing are presented and discussed.

The third chapter sheds light on integrating a fatigue model in the aeroelastic design process. The analytical model to predict the fatigue life of a composite laminate formulated in this thesis is discussed. It is based on the method developed by Kassapoglou (Kassapoglou, 2007, 2010, 2011) to predict fatigue failure. The predictions of the model are validated for both constant amplitude and a variable amplitude loading on a Glass/Epoxy laminate. Furthermore, the analytical model is extended to work with laminates described using lamination parameters instead of ply angles and stacking sequence. Subsequently, the analytical fatigue model is then integrated into the PROTEUS and an aeroelastic optimization problem has been set up. The effect of including the analytical fatigue model instead of a conservative knockdown factor on the optimized design and the structural weight is then discussed.

In the fourth chapter, experiments are conducted to validate the numerical design methodology for optimizing composite wings subject to gust and fatigue loading requirements. A rectangular composite wing is designed to be critical in strength, buckling and fatigue. The optimized wing is manufactured with a hand layup technique using IM7/8552 prepreg. An experimental campaign comprising two wind tunnel tests and a fatigue test is performed. In the wind tunnel tests, both static and dynamic aeroelastic experiments are conducted to validate the numerical dynamic aeroelastic model. The fatigue test is used to validate the analytical fatigue model within the numerical design methodology and to understand the effect of fatigue on the structural and aeroelastic properties of the wings.

Finally, the fifth chapter presents the conclusion of the thesis. The research questions formulated at the start are revisited and reflected upon. The thesis ends with a list of recommendations for future research and further development of the preliminary aeroelastic design methodology.

2

Preliminary Aeroelastic Design of Composite Wings Subjected to Critical Gust Loads [1]

The journey of increasing the knowledge in the preliminary aeroelastic design methodology which this thesis is focused on starts with efforts on including critical gust loads in the aeroelastic design process.

Including the gust loads in an efficient and a reliable way during the initial phases of the design process is quite difficult. The first challenge is that there is no prior information on the flight points which will be critical with respect to gust loads. As per the requirements defined by the European Aviation Safety Agency (EASA) in the Certification Specifications for Large Aeroplanes (CS-25) (European Aviation Safety Agency, 2015), a range of load cases across the entire flight envelope has to be taken into consideration to determine the maximum loads the aircraft structure will experience. A ballpark approximation of the number of load cases to be taken into account can be in the order of 10 million (Khodaparast et al., 2012). This makes the process of finding the worst case gust loads computationally expensive. The second challenge is that as the design changes during optimization, the critical gusts might change as well and hence for every new iteration in the design process,

[1] This chapter is largely based on the journal paper Rajpal, D., Gillebaart, E. and De Breuker, R. (2019). *"Preliminary Aeroelastic Design of Composite Wings Subjected to Critical Gust Load"*, Aerospace Science and Technology, vol. 85, pp. 96-105.

the load cases have to be updated. This makes the inclusion of gust loads in the initial design process unfeasible.

The idea of improving the efficiency of the gust analysis has already received attention in recent years. Pototzky et al. (1991) used the concept of matched filter theory from signal processing to identify worst case stochastic gust loads. Fidkowski et al. (2008) also applied matched filter theory in combination with the Lyapunov equation to identify critical load for the stochastic gust in the conceptual aircraft design process. Knoblach (2013) used robust performance analysis from control theory to identify critical loads due to discrete 1-cosine gusts. In the work done under the European Seventh Framework Programme (FP7) project FFAST (Cavagna et al., 2013; Khodaparast and Cooper, 2013; Khodaparast et al., 2012), surrogate modelling, neural networks and optimization techniques were used for fast prediction of gust loads.

There has been a growing interest in using MOR techniques to predict gust loads in an efficient way. The goal of the MOR techniques is to produce a system that shows similar aeroelastic response characteristics as the original, but consists of significantly fewer state variables, leading to a reduction in computational cost. Majority of the work done (Bergmann et al., 2016; Thormann et al., 2016; Timme et al., 2017; Wales et al., 2016; Williams et al., 2017) was focused on using MOR techniques to reduce the CFD models to predict the gust response. In the early stages of the design process, there is a need to evaluate a multitude of designs. Hence, even with MOR techniques, CFD can still be computationally expensive. The industry standard (Reyes et al., 2017; Wilson et al., 2017), for gust loads, is the potential flow based aeroelastic solver such as MSC NASTRAN. There has not been sufficient focus in the literature on using the MOR methods for such solvers. Only recently Castellani et al. (2016) applied MOR technique to the potential flow based aeroelastic system for rapid prediction of dynamic gust loads. For the determination of critical loads, Castellani et al. created a reduced aeroelastic model at different flight points and used interpolation techniques to cover the entire flight envelope.

In the present chapter, aeroelastic system formulated using the MOR methodology will be used to predict the critical gust load. In the section 2.1, the ROAM is formulated by reducing the aerodynamic system with a BPOD and coupling it to a structural solver. In the current approach only the aerodynamic model is reduced because the dominant modes of the aerodynamic model can be assumed to be constant for varying equivalent airspeed and Mach number, enabling the use of a single reduced model for the entire flight envelope. In the next section, an optimization framework is formulated using the ROAM which accounts for worst case gust loads at every iteration. To demonstrate the efficacy of such a framework, aeroelastic tailoring of the NASA Common Research Model (CRM) wing (Vassberg et al., 2008) is carried out. Finally, a synopsis of the chapter is given.

2.1 Reduced Order Aeroelastic Model Formulation

The ROAM is based on the framework of PROTEUS, in-house aeroelastic tool, developed at TU Delft. Figure 2.1 depicts the schematic representation of the framework of the PROTEUS. The process starts with discretizing the wing into multiple spanwise sections, where each section is defined by one or more laminates in the chord wise direction. Based on the laminate properties, a cross sectional modeller especially developed to deal with anisotropic shell cross-sections, uses the cross-sectional geometry to generate the Timoshenko stiffness matrices. A geometrically non linear aeroelastic analysis is carried out for multiple load cases by coupling the geometrically nonlinear Timoshenko beam model to an unsteady vortex lattice aerodynamic model. A linear dynamic aeroelastic analysis is carried out around the nonlinear static equilibrium solution. In the post processing, with the help of the cross sectional modeller, the strains in the three-dimensional wing structure are retrieved. The obtained strains are used to calculate the strength and buckling properties of the wing which are then fed to the optimizer as constraints. A detailed description of the PROTEUS is given in work by Werter and De Breuker (2016). In the following subsections, the formulation of ROAM has been described.

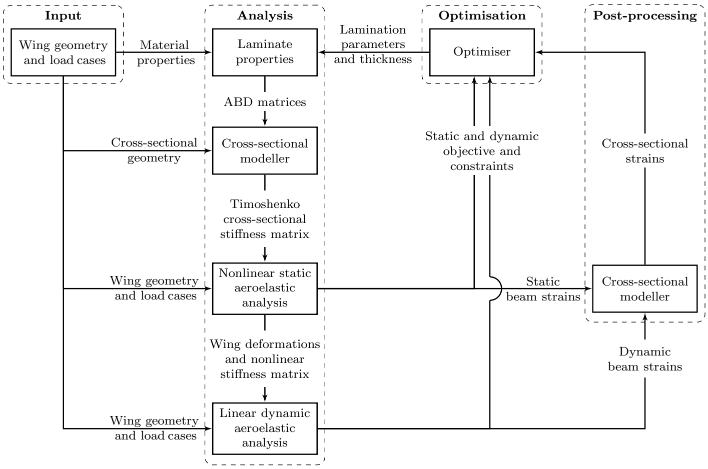

Figure 2.1: Framework of PROTEUS (Werter and De Breuker, 2016).

2.1.1 Full Order Aerodynamic model

In PROTEUS, the aerodynamic model is continuous-time state-space unsteady vortex lattice method based on the work of Werter et al. (2017). The unsteady vortex lattice is an efficient method, of comparable fidelity to the doublet lattice method at moderate Mach numbers, but without some of its restrictions: the wake and planform can be non planar, flow tangency is imposed on the statically deformed geometry, and in-plane deformations are captured (Murua et al., 2012). In the aerodynamic model, the wing is modelled as a thin wing with a prescribed wake using quadrilateral vortex rings with the collocation points in the center of the panels. Using the Kutta condition and Helmholtz theorem, a complete state-space system of equations for the potential flow is given by

$$\mathbf{Ae}\boldsymbol{\Gamma}^t = -\mathbf{V}_\infty \cdot \mathbf{n} \tag{2.1}$$

$$\boldsymbol{\Gamma}^t_{TE} = \boldsymbol{\Gamma}^t_{w_0} \tag{2.2}$$

$$\mathbf{H}_1\boldsymbol{\Gamma}^t = \mathbf{H}_2\boldsymbol{\Gamma}^{t-1} \tag{2.3}$$

where the matrix $\mathbf{Ae}$ contains the aerodynamic influence coefficients, $\mathbf{V}_\infty$ is the free stream velocity vector, $\mathbf{n}$ is the surface unit normal vector, $\boldsymbol{\Gamma}^t$ is the vector of unknown vortex ring strengths at time t, $\boldsymbol{\Gamma}^t_{TE}$ is the vector of unknown vortex ring strengths at the trailing edge of the wing at time t, $\boldsymbol{\Gamma}^t_{w_0}$ is the vector of unknown vortex ring strengths at the start of the wake at time t, and matrices $\mathbf{H}_1$ and $\mathbf{H}_2$ describe the transport of vorticity in the wake.

The vector with vortex ring strengths $\boldsymbol{\Gamma}$ can be split into three separate sets of unknowns: the body, Kutta, and wake unknowns. Using this separation of unknowns, the system of equations can be rewritten into the form of the standard state equation of a state-space system:

$$\dot{\mathbf{x}}_a = \mathbf{A}_a\mathbf{x}_a + \mathbf{B}_a\mathbf{u} \tag{2.4}$$

where $\mathbf{A}_a$ is the aerodynamic state matrix, $\mathbf{B}_a$ is the aerodynamic input matrix, $\mathbf{u}$ is the input vector containing the time derivative of the angle of attack per aerodynamic panel of the wing, and $\mathbf{x}_a$ is the aerodynamic state vector containing the vortex strengths in the wake and angles of attack. The dot over the $\mathbf{x}$ indicates the time derivative. Combining Equation (2.4) with expressions for the unsteady lift and moment acting on the wing, state-space system can be formulated as

$$\begin{aligned}\dot{\mathbf{x}}_a &= \mathbf{A}_a\mathbf{x}_a + \mathbf{B}_a\mathbf{u}\\ \mathbf{y}_a &= \mathbf{C}_a\mathbf{x}_a + \mathbf{D}_a\mathbf{u}\end{aligned} \tag{2.5}$$

where $\mathbf{y}_a$ is the output vector containing the aerodynamic forces and moments acting on the wing per spanwise section, $\mathbf{C}_a$ is aerodynamic output matrix and $\mathbf{D}_a$ is the aerodynamic feedthrough matrix. A more elaborate description of the aerodynamic modelling can be found in the work of Werter et al. (2017).

2.1.2 MODEL ORDER REDUCTION

The dimension or order n, of a state-space system is given by the number of states in the vector $\mathbf{x}_a$. A system with more states generally requires a higher computational cost. Besides system size, sparsity and system structure are also of importance for the computational cost. In this study, the dimension of the system is typically in the order of $10^3 \sim 10^4$ and the matrices are densely populated due to the use of a boundary element method. The dimension of the matrices can be significantly reduced and sparsity increased by applying the MOR method. The general approach for a MOR of Linear Time-Invariant (LTI) state-space systems is to project the original states onto a reduced basis:

$$\mathbf{x}_a = \mathbf{V}_r \mathbf{c} \tag{2.6}$$

where $\mathbf{c}$ is a vector with the r reduced states and $\mathbf{V}_r$ is the $n \times r$ reduced basis onto which the original states are projected. Inserting Equation (2.6) into Equation (2.5) results in a system with $r \ll n$ states:

$$\begin{aligned} \dot{\mathbf{c}} &= \mathbf{V}_r^{-1}\mathbf{A}_a\mathbf{V}_r\mathbf{c} + \mathbf{V}_r^{-1}\mathbf{B}_a\mathbf{u} = \mathbf{A}_r\mathbf{c} + \mathbf{B}_r\mathbf{u} \\ \mathbf{y}_a &= \mathbf{C}_a\mathbf{V}_r\mathbf{c} + \mathbf{D}_a\mathbf{u} = \mathbf{C}_r\mathbf{c} + \mathbf{D}_a\mathbf{u} \end{aligned} \tag{2.7}$$

Since $\mathbf{V}_r$ is rectangular matrix of rank r, $\mathbf{V}_r^{-1}$ represents the pseudo inverse of $\mathbf{V}_r$. The number of states r in the Reduced-order Model (ROM) depends on the required accuracy and the basis $\mathbf{V}_r$, but is typically in the order of $10 \sim 100$. There are four different MOR methods that are often used to provide the reduced basis. The methods are Model Truncation (MT), Balanced Truncation (BT), Proper Orthogonal Decomposition (POD) and BPOD. In a previous study performed by Gillebaart and De Breuker (2015) and Rajpal, Gillebaart and De Breuker (2019), four MOR methods were applied to a continuous-time state-space unsteady aerodynamic model and their specific properties, accuracy, robustness, and computational efficiency were investigated. The BPOD method provided the best combination of high accuracy with very few states, relatively low computational cost for a typical model size of interest, and sufficient robustness. Consequently in the current study BPOD method is chosen to compute the reduced basis for the aerodynamic system.

2.1.3 Reduced Order Aerodynamics

For the determination of critical loads, the aeroelastic system must be solved over a large number of flight points to calculate the various responses of the aircraft over the entire flight envelope. A significant saving in computational expense can be achieved if a reduced-order aeroelastic system can be used instead of a full order system. However, the full order aerodynamic system depends on parameters such as altitude, Mach number and velocity, hence every new flight point would necessitate a new ROAM. Thus an efficient way of applying the reduced-order aeroelastic system without the need of performing a new reduction at each flight point has been formulated.

Benner et al. (2015) have provided a comprehensive survey on MOR for a parametric state-space system. Generally, the approaches for the parametric model order reduction can be differentiated into local and global based methods. In the local based methods (Amsallem and Farhat, 2011; Lieu et al., 2006), the reduced basis required at a given point can be generated by interpolating local reduced bases generated at a fixed number of points in the parameter space. In the global based methods (Schmit and Glauser, 2003), a single reduced basis is generated by projecting the global matrix containing snapshots at various points in the parameter space. By projecting a global matrix, dominant modes across entire parameter space are selected, thus giving a good approximation. For the current aerodynamic system, a method similar to the global based methods is used. A reasonable assumption can be made that, for a given wing planform, the dominant aerodynamic modes will be the same for all the points inside the flight envelope. The basis for this assumption is explained below.

For every point inside the flight envelope, the aerodynamic state-space matrices depend upon the Equivalent Air Speed (V_{eq}), and the free stream Mach number, M. For the assumption to be valid, the dominant modes of the aerodynamic system should not change with a change in V_{eq} and M. With respect to V_{eq}, the aerodynamic system of equations described in Equations 2.1, 2.2 and 2.3 can be reformulated as

$$\mathbf{K}_1\mathbf{\Gamma}_b + \mathbf{K}_2\mathbf{\Gamma}_{w_0} + \mathbf{K}_3\mathbf{\Gamma}_w = -\mathbf{V}_\infty\mathbf{n}_x - \mathbf{V}_\infty\mathbf{n}_z\boldsymbol{\alpha} \tag{2.8}$$

$$\mathbf{K}_4\mathbf{\Gamma}_b + \mathbf{K}_5\mathbf{\Gamma}_{w_0} = 0 \tag{2.9}$$

$$\mathbf{K}_6(V_{eq})\mathbf{\Gamma}_w + \mathbf{K}_7(V_{eq})\mathbf{\Gamma}_{w_0} = \dot{\mathbf{\Gamma}}_w \tag{2.10}$$

where $\mathbf{K}_1$, $\mathbf{K}_2$ and $\mathbf{K}_3$ are a parts of the Aerodynamic Influence Coefficient (AIC) matrix, $\mathbf{K}_4$ and $\mathbf{K}_5$ connect the trailing edge panel to the first wake panel satisfying the Kutta condition, and $\mathbf{K}_6$ and $\mathbf{K}_7$ describe the transport of vorticity in the wake. The symbol $\boldsymbol{\alpha}$ represents the angle of attack. The subscripts b and w indicate the body and wake, respectively. Both $\mathbf{K}_6$ and $\mathbf{K}_7$ depend on V_{eq}. Note that V_{eq} needs to be consistent with $\mathbf{V}_\infty$. The AIC matrix also depends upon the velocity. A change in velocity necessitates a change in the trim angle, which leads to a change in angle between the body and the wake and thus a change of the AIC matrix. However, in a linear analysis, for small deviations in the trim angle, the AIC matrix can be assumed to be constant. Expressing $\mathbf{\Gamma}_b$ and $\mathbf{\Gamma}_{w_0}$ as function of $\mathbf{\Gamma}_w$, the state equation of state-space system can be derived as

$$\dot{\mathbf{\Gamma}}_w = \mathbf{K}_8(V_{eq})\mathbf{\Gamma}_w + \mathbf{K}_9(V_{eq})\boldsymbol{\alpha} + \mathbf{K}_{10}(V_{eq}) \tag{2.11}$$

where $\mathbf{K}_8$, $\mathbf{K}_9$ and $\mathbf{K}_{10}$ have linear dependencies on equivalent airspeed.

To compute the aerodynamic output, forces and moments are split into steady component and an unsteady component. The steady component of the aerodynamic forces is given by

$$\mathbf{F}_{st} = \rho\mathbf{V}_\infty \times \mathbf{\Gamma} = \rho\mathbf{V}_\infty \times \mathbf{e}_\Gamma\Gamma \tag{2.12}$$

where $\mathbf{e}_\Gamma$ is the vector along the vortex segment, Γ is the vortex strength of the vortex segment and ρ represents the density. The unsteady component of the aerodynamic forces is given by

$$\mathbf{F}_{unst} = \rho\widehat{\mathbf{V}}_\infty \times \widehat{\mathbf{e}}_\Gamma \frac{\partial \Gamma_{i,j}}{\partial t}\mathbf{H}_{i,j} \tag{2.13}$$

where $\widehat{\mathbf{V}}_\infty$ is the unit vector in the direction of the free stream velocity, $\widehat{\mathbf{e}}_\Gamma$ is the unit vector in the direction of the leading vortex segment and $\mathbf{H}$ is the AIC matrix. By defining a reference axis with respect to which the aerodynamic moments are computed, the total aerodynamic forces and moments are expressed as

$$\begin{bmatrix}\mathbf{F}_a\\ \mathbf{M}_a\end{bmatrix} = \begin{bmatrix}\mathbf{F}_{st}\\ \mathbf{M}_{st}\end{bmatrix} + \begin{bmatrix}\mathbf{F}_{unst}\\ \mathbf{M}_{unst}\end{bmatrix} = \mathbf{L}_1(V_{eq})\mathbf{\Gamma}_b + \mathbf{L}_2(V_{eq})\dot{\mathbf{\Gamma}}_b \tag{2.14}$$

where $\mathbf{L}_1$ and $\mathbf{L}_2$ have linear dependencies on equivalent airspeed. Relating $\mathbf{\Gamma}_b$ to $\mathbf{\Gamma}_w$ leads to

$$\begin{bmatrix}\mathbf{F}_a\\ \mathbf{M}_a\end{bmatrix} = \mathbf{L}_9(V_{eq})\mathbf{\Gamma}_w + \mathbf{L}_{10}(V_{eq})\alpha + \mathbf{L}_8(V_{eq})\dot{\alpha} + \mathbf{L}_{11}(V_{eq}) \tag{2.15}$$

Using Equations 2.11 and 2.15, the aerodynamic state-space equation is given as

$$\begin{aligned}\dot{\mathbf{x}}_a &= \begin{bmatrix}\mathbf{K}_8(V_{eq}) & \mathbf{K}_9(V_{eq})\\ 0 & 0\end{bmatrix}\mathbf{x}_a + \begin{bmatrix}0 & \mathbf{K}_{10}(V_{eq})\\ \mathbf{I} & 0\end{bmatrix}\mathbf{u},\\ \mathbf{y}_a &= \begin{bmatrix}\mathbf{L}_9(V_{eq}) & \mathbf{L}_{10}(V_{eq})\end{bmatrix}\mathbf{x}_a + \begin{bmatrix}\mathbf{L}_8(V_{eq}) & \mathbf{L}_{11}(V_{eq})\end{bmatrix}\mathbf{u},\end{aligned} \tag{2.16}$$

Thus the aerodynamic system can be assumed to have an affine dependency on the velocity. The aerodynamic state-space system can then be formulated as

$$\begin{aligned}\dot{\mathbf{x}}_a &= \mathbf{F}_1(V_{eq})\hat{\mathbf{A}}_\mathbf{a}\mathbf{x}_a + \mathbf{F}_2(V_{eq})\hat{\mathbf{B}}_a\mathbf{u},\\ \mathbf{y}_a &= \mathbf{F}_3(V_{eq})\hat{\mathbf{C}}_a\mathbf{x}_a + \mathbf{F}_4(V_{eq})\hat{\mathbf{D}}_a\mathbf{u},\end{aligned} \tag{2.17}$$

where the modified state-space matrices are now independent of the equivalent airspeed, and the influence of the airspeed is collected in the matrices $\mathbf{F}_1$ to $\mathbf{F}_4$. These matrices are found by taking out the dependencies of the equivalent airspeed during the formulation of the state-space system. As a result, the characteristics of the state matrix will remain the same for different velocities, validating the assumption that dominant aerodynamic modes for different velocities can be assumed to be the same.

Before describing the effect of Mach number on the mode shapes, the effect of the change in aspect ratio on the aerodynamic mode shapes is investigated. In Figure 2.2 the aerodynamic mode shapes for a backward swept wing are shown for four different aspect ratios of the wing. The aspect ratios are 9.5, 8, 6.5 and 5. Please note that only the shapes along the chordwise and spanwise directions with the origin at the root trailing edge point are displayed to enable a good comparison between the mode shapes for different aspect ratios.

The mode shapes for the first three, most dominant modes, are practically constant with changing the aspect ratio of the wing. Up to mode 7 the shapes remain

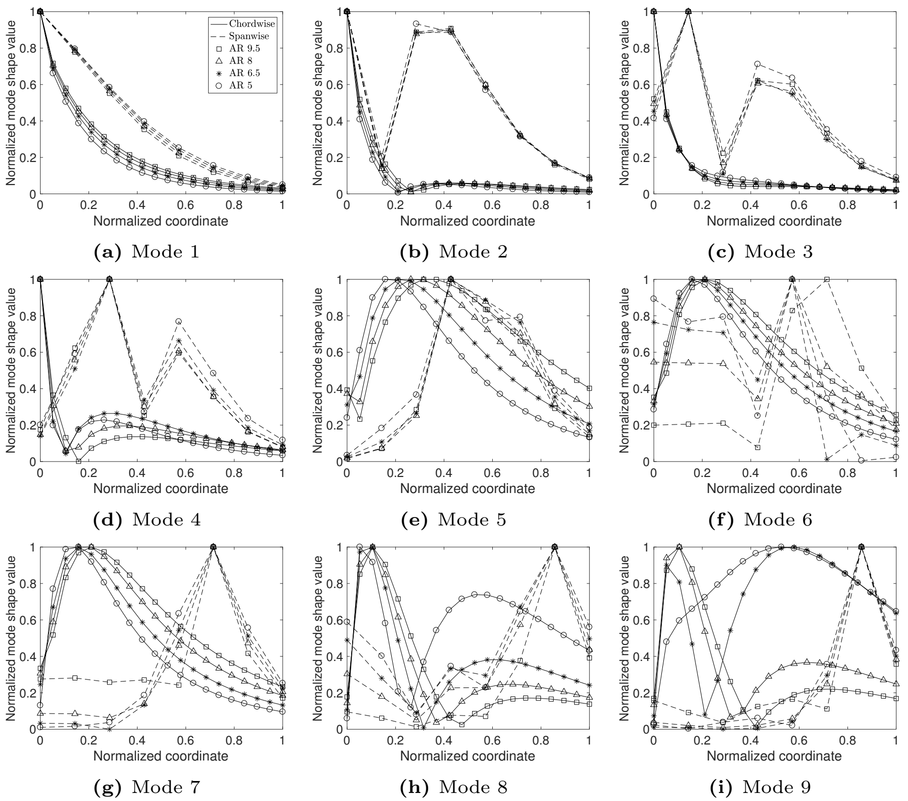

Figure 2.2: First 9 BPOD aerodynamic mode shapes for a untapered, swept backward wing for different aspect ratios.

very similar. As the mode number increases further, a larger difference is seen with increasing aspect ratio, although the trend is still similar. A similar trend is also observed for a forward swept wing. A conclusion can then be made that the shapes for the first 7 dominant aerodynamic modes remain almost similar for different aspect ratio.

With respect to the Mach number effects, the application of Prandtl-Glauert transformation brings the parametric dependency of the aerodynamic system on the Mach number. The Prandtl-Glauert transformation scales the geometry in the x-direction by a factor $\sqrt{1-M^2}$, effectively changing the aspect ratio of the wing. The first seven dominant modes of the aerodynamic system stay nearly constant with the change in the aspect ratio. Hence, a change in Mach number results in a nearly no change in the dominant modes. Thus, with the assumptions mentioned before, a reduced basis constructed at one flight point can reasonably span the entire flight envelope.

2.1.4 Reduced Order Aeroelastic Framework

In the present work, the reduced-order aerodynamic system, as described in the previous section, generated using BPOD, replaces the full order unsteady aerodynamic model in the PROTEUS framework. For the purpose of completeness, the state-space equation for the coupled dynamic system is derived. The governing equation of a linear dynamic structural model is given by:

$$\mathbf{M}\ddot{\mathbf{p}} + \mathbf{K}\mathbf{p} = \mathbf{F}_s \tag{2.18}$$

where $\mathbf{M}$ is the global mass matrix, $\mathbf{K}$ is the global stiffness matrix, $\mathbf{p}$ contains the structural degrees of freedom and $\mathbf{F}_s$ is the structural force vector. This system of equations can be converted to a first order state-space system by including both $\dot{\mathbf{p}}$ and $\mathbf{p}$ in the vector of state variables, resulting in:

$$\begin{pmatrix} \ddot{\mathbf{p}} \\ \dot{\mathbf{p}} \end{pmatrix} = \begin{bmatrix} \mathbf{0} & -\mathbf{M}^{-1}\mathbf{K} \\ \mathbf{I} & \mathbf{0} \end{bmatrix} \begin{pmatrix} \dot{\mathbf{p}} \\ \mathbf{p} \end{pmatrix} + \begin{bmatrix} \mathbf{M}^{-1} \\ \mathbf{0} \end{bmatrix} \begin{pmatrix} \mathbf{F}_s \\ \mathbf{0} \end{pmatrix} \tag{2.19}$$

$$\begin{pmatrix} \ddot{\mathbf{p}} \\ \dot{\mathbf{p}} \end{pmatrix} = \mathbf{A}_s \begin{pmatrix} \dot{\mathbf{p}} \\ \mathbf{p} \end{pmatrix} + \mathbf{B}_s \begin{pmatrix} \mathbf{F}_s \\ \mathbf{0} \end{pmatrix} \tag{2.20}$$

where $\mathbf{I}$ is the identity matrix, $\mathbf{0}$ the zero matrix, and $\mathbf{A}_s$ and $\mathbf{B}_s$ the structural state and input matrices, respectively. Coupling Equations 2.7 and 2.20 and performing some algebraic manipulation, results in the reduced-order dynamic aeroelastic state-space system:

$$\begin{aligned} \dot{\mathbf{x}} &= \mathbf{A}_{ae}\mathbf{x} + \mathbf{B}_{ae}\mathbf{u} \\ \begin{pmatrix} \mathbf{F} \\ \mathbf{p} \end{pmatrix} &= \mathbf{C}_{ae}\mathbf{x} + \mathbf{D}_{ae}\mathbf{u} \end{aligned} \tag{2.21}$$

where the state vector $\mathbf{x}$ is given by $\begin{bmatrix} \mathbf{c} & \dot{\mathbf{p}} & \mathbf{p} \end{bmatrix}^T$, $\mathbf{F}$ contains aerodynamic lift and moment forces rotated in structural coordinate system and $\mathbf{A}_{ae}$, $\mathbf{B}_{ae}$, $\mathbf{C}_{ae}$ and $\mathbf{D}_{ae}$ are the aeroelastic state, input, output and feedthrough matrices.

2.1.5 Common Research Model

The NASA CRM (Vassberg et al., 2008), originally developed for the 4th AIAA drag prediction workshop, is used as a case study for the current analysis. The main characteristics of the aircraft are summarized in Table 2.1. Figure 2.3 depicts the wing planform. The wing consist of 54 ribs with a rib spacing of 0.55 m that are taken into account as concentrated masses. Additionally, fuel, engine, leading edge devices and trailing edge devices are also accounted for as concentrated masses. The top and bottom skin of the wing are strengthened with the help of stringers that run along the span of the wing.

Table 2.1: Characteristics of the CRM wing.

Parameter	Value
Span	58.8 m
Leading edge sweep angle	35 degrees
Wing aspect ratio	8.4
Taper ratio	0.275
Planform wing area	412 m^2
Cruise Mach	0.85
Design Range	14,300 km
Design Payload	45,000 kg
Maximum takeoff weight	296,000 kg

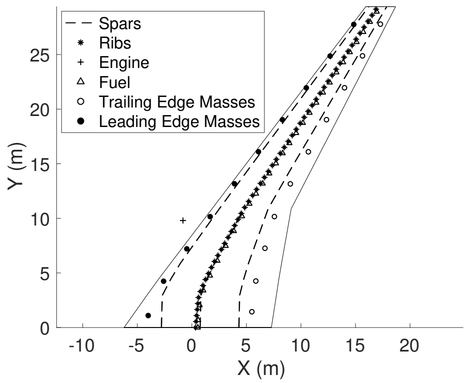

Figure 2.3: CRM wing planform.

2.1.6 Response to Varying Gust Length

To demonstrate the application of the reduced-order aeroelastic framework in determining the gust response of aircraft, the CRM wing model is subjected to a discrete 1-cosine gust of varying gust lengths. The 1-cosine profile for the discrete gust is given by European Aviation Safety Agency (2015)

$$U = \frac{U_{ds}}{2}\left(1 - \cos\left(\frac{\pi s}{H}\right)\right) \tag{2.22}$$

where U is the gust velocity, s the distance penetrated into the gust, H the gust gradient, and U_{ds} the design gust velocity defined as

$$U_{ds} = U_{ref} F_g \left(\frac{H}{350}\right)^{1/6} \tag{2.23}$$

where U_{ref} is the reference velocity that reduces bi-linearly from 17.07 m/s at sea level to 13.41 m/s at 4,572 m and then to 6.36 m/s at 18,288 m, and F_g is the flight profile alleviation factor related to the aircraft maximum take-off weight and maximum landing weight.

Figure 2.4 depicts the four different gust velocity profiles having gust gradients of 9 m, 30 m, 80 m and 110 m. Figures 2.5 and 2.6 depict the root bending moment and root torsional moment responses of the CRM wing to the four different gust gradients as obtained by the Full-order Model (FOM) and the ROAM, using 20 out of 1,188 modes, for a flight point of $M = 0.73$ at an altitude of 11,000 m. As can be seen, the error in the responses from the ROAM as compared to the responses from the FOM is less than 0.5% across the entire time history. With respect to computational efficiency, the ROAM took 160 s to build and 1.2 s to simulate whereas the FOM took 29.3 s to simulate. The time required for building the ROAM outweighs the benefit in this case, because only a small number of flight points are included. The simulation time, however, is decreased by 96%, so if more flight points will be included, the reduction in simulation time will at some point outweigh the time spend on building the ROAM, as is demonstrated in the next subsection.

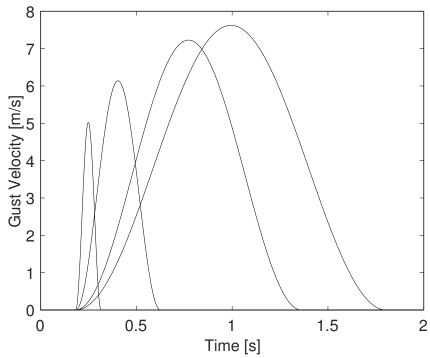

Figure 2.4: Gust Profile for gust gradients of 9 m, 30 m, 80 m and 110 m.

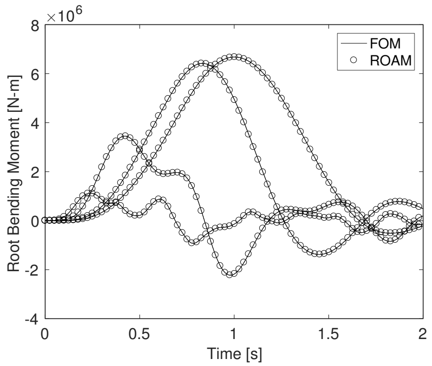

Figure 2.5: Root bending moment response for the FOM and ROAM of the CRM wing.

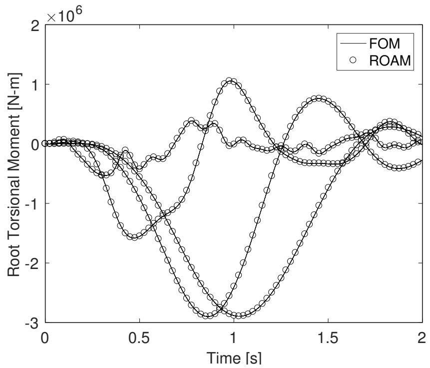

Figure 2.6: Root torsional moment response for the FOM and ROAM of the CRM wing.

2.1.7 RESPONSE ACROSS THE FLIGHT ENVELOPE

To demonstrate the applicability of the reduction method, the response of the standard backward swept CRM wing and a forward swept version of the CRM wing using both the ROAM and the FOM is evaluated at 36 different flight points across the flight envelope. For each flight point, 68 different gust gradients, ranging from 9 m to 107 m, are considered, bringing the total number of evaluated flight points to 2,448. For the froward swept version, a forward sweep of 36 degrees is applied on the leading edge. Figure 2.7 depicts the different flight points considered in this study. A reduced basis is calculated at the cruise condition with a cruise speed of 220 m/s at 10 km altitude and a Mach number of 0.73. The altitude has been reduced from the standard 11 km to 10 km in order to bring down the Mach number and remain within the validity of the high subsonic potential flow theory. The first 20 out of a total of 1,188 aerodynamic modes of this basis are used as the global reduced basis for the ROAM.

The load plots over the complete flight envelope, also called potato plots, for combination of root bending moment, root shear force and root torsional moment for both backward swept wing and forward swept wing are shown in Figures 2.8, 2.9, 2.10 and 2.11. Note that the convex hull functionality is used to extract the points on the edge of the loads envelope and the solid line is used to connect the discrete FOM points in the figures. A good agreement of the ROAM with the FOM across the entire flight envelope is obtained with the maximum error being less than 0.5%.

Table 2.2 compares the computational effort required by the FOM and the ROAM for sweeping the flight envelope. The time related to the model setup for the ROAM is kept low by using the single reduced basis as the global basis, as was explained before. The achieved reduction in simulation time is an order of magnitude larger than the extra time required for creating the ROAM, resulting in an 85.5% saving in the computational effort in identifying the critical loads.

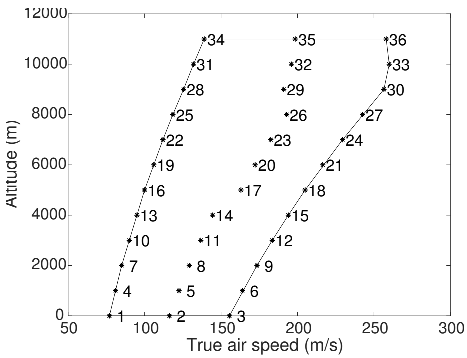

Figure 2.7: Flight envelope.

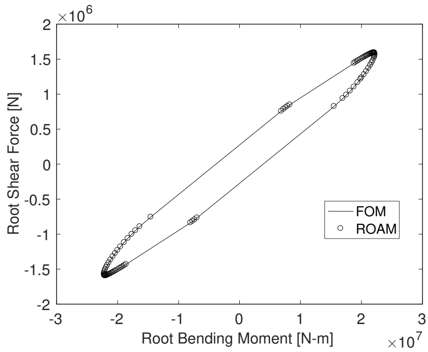

Figure 2.8: Root bending moment versus shear force for the backward swept CRM.

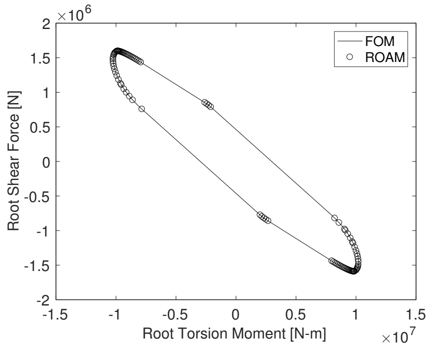

Figure 2.9: Root torsion moment versus shear force for the backward swept CRM.

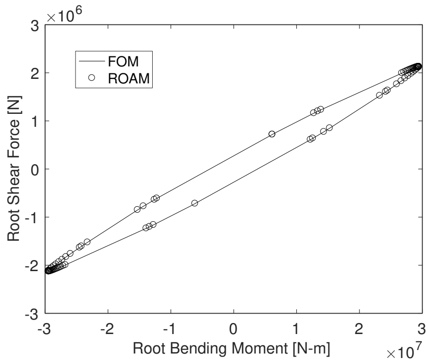

Figure 2.10: Root bending moment versus shear force for the forward swept CRM.

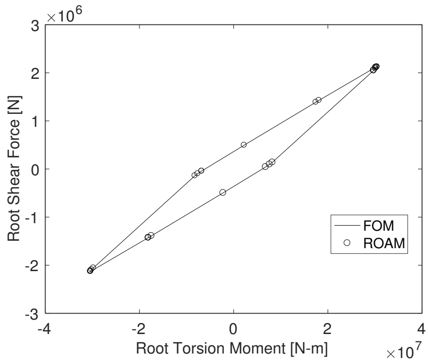

Figure 2.11: Root torsion moment versus shear force for the forward swept CRM.

Table 2.2: Breakdown of computational time required for the critical load identification (Values in the bracket indicate savings in computational time of ROAM simulations with respect to FOM simulations in terms of percentage).

	Model setup (min)	**Simulation time** (min)	**Total time** (min)
FOM	0	171	171
ROAM	2.7	22.1	24.8
Difference	2.7 (-)	148.9 (87.1%)	146.2 (85.5%)

2.2 Dynamic Aeroelastic Optimization Framework

As has been mentioned before, in the case of gust loads, there is no prior information on the flight point which leads to the critical load. During the optimization process, for every iteration, an update in the design of the wing would lead to a modification in the aeroelastic characteristics of the wing, which could result in a different critical gust load. As a result, at every iteration, a range of load cases across the entire flight envelope needs to be evaluated to determine the worst case gust load. Hence an optimization framework, depicted in Figure 2.12, is formulated which has the capability to determine the critical gust load at every iteration in a computationally efficient manner. It starts with the identification of the worst gust load for the initial design using the ROAM. Next, for the given critical static and gust load conditions, PROTEUS analyses the initial design and calculates the analytical sensitivities which are then fed to the optimizer. The optimizer calculates the new design variables which are fed to ROAM as well as PROTEUS. ROAM analyzes the entire flight envelope with respect to the new design variables, identifies the critical loads and feeds it back to PROTEUS. The process continues until an optimum has been reached. Since the analytical sensitivities of the objective function and constraints, including the sensitivities of the critical gust loads, are available, the gradient based optimizer Globally Convergent Method of Moving Asymptotes (GCMMA) developed by Svanberg (2002) is used.

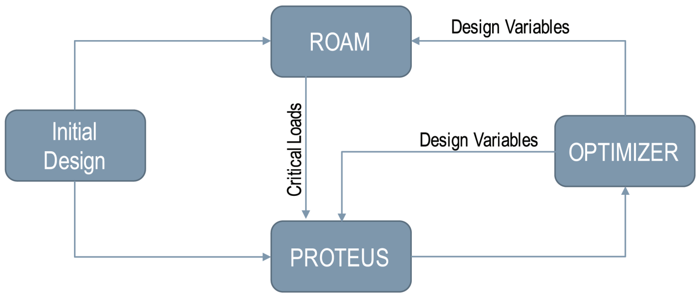

Figure 2.12: Schematic representation of the optimization framework.

2.2.1 Setup of Dynamic Aeroelastic Optimization Problem

In the current study, for the aeroelastic tailoring of the CRM wing, clamped at root, gust load analysis is carried out on 64 flight points and at every iteration, to identify the critical gust loads, all the 64 points are evaluated. Table 2.3 shows the material properties used for the CRM wing. To account for the effect of material scatter, barely visible impact damage and environmental effects, the strength allowables are knocked down by 58.4% (Kassapoglou, 2013). Table 2.4 gives the information regarding the optimization setup considered in the current study. The objective is to minimize the structural weight of the wing. The wing is divided into 10 spanwise sections. Each section of the top skin and the bottom skin consists of two laminates in the chordwise direction and each section of each spar has one laminate. This distribution results in 64 unique laminates. The laminates are represented by lamination parameters which describe the in-plane and out-of-plane behaviour of the composite laminates which are symmetric and unbalanced. For every laminate, there are eight lamination parameters and one thickness variable resulting in a total number of 576 design variables. Figure 2.13 depicts the laminate distribution along the top skin of the wing. It also shows the stiffness for each laminate, where the wing stiffness distribution is represented by the polar plot of thickness normalized modulus of elasticity $\hat{\mathbf{E}}_{11}(\theta)$ which is given by

$$\hat{\mathbf{E}}_{11}(\theta) = \frac{1}{\hat{\mathbf{As}}_{11}^{-1}(\theta)} \tag{2.24}$$

where $\hat{\mathbf{As}}$ is the thickness normalized membrane stiffness matrix and θ ranges from 0 to 360 degrees.

Table 2.3: Material properties.

Property	Value
E_{11} (GPa)	147
E_{22} (GPa)	10.3
G_{12} (GPa)	7
ν_{12} (−)	0.27
ρ (kg/m^3)	1600
X_t (MPa)	2280
X_c (MPa)	1725
Y_t (MPa)	57
Y_c (MPa)	228
S (MPa)	76

Table 2.4: Optimization setup.

Type	Parameter	# responses
Objective	Minimize Wing Mass	1
Design Variables	Lamination Parameter Laminate Thickness	576
Constraints	Laminate Feasibility	384
	Static Strength	1024/load case
	Buckling	4096/load case
	Aeroelastic Stability	10/load case
	Aileron Effectiveness	1/load case
	Local Angle of Attack	22/load case

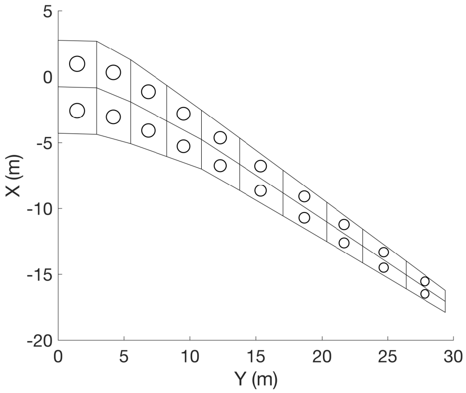

Figure 2.13: Laminate Distribution of the top skin of CRM.

Lamination feasibility equations formulated by Hammer et al. (1997), Raju et al. (2014) and Wu et al. (2015) are applied to make sure that the lamination parameters represent actual ply distributions. The static strength of the laminate is assessed by the failure envelope calculated using Tsai-Wu criterion formulated for lamination parameter domain by Khani et al. (2011). The stability of the panel in buckling is based on an idealized buckling model formulated by Dillinger et al. (2013). To ensure that the wing is aeroelastically stable, the real part of the eigenvalues of the state matrix should be less than zero within the flutter flight envelope. The local angle of attack is constrained to a maximum of 12 degrees and a minimum of -12 degrees. The aileron effectiveness computed as the negative ratio of the roll coefficient induced by the aileron deflection and the roll coefficient due to the roll manoeuvre, is set to a minimum of 0.1 to ensure reasonable handling quality (Dillinger et al., 2013).

Table 2.5 gives the information on the static load cases which are used for the current study. These load cases provided by NASA, represent the cruise condition, 2.5g symmetric pull up manoeuvre and -1g symmetric push down manoeuvre. With respect to gust load cases, 84 flight points covering the entire flight envelope are investigated. Figure 2.14 displays the flight envelope with their respective flight point ID. For each flight point, 40 gust gradients both positive as well as negative, ranging from 9 m to 107 m are considered. To simulate the effect of different mass configurations on the gust loads, 40 different fuel configurations were selected for initial evaluation. These configurations were selected based on requirements given by EASA CS-25 (European Aviation Safety Agency, 2015) which states that:

1. “Load combinations must include each fuel load in the range from zero fuel to the selected maximum fuel.”

2. “Any critical fuel loading conditions, not shown to be extremely improbable, which may result from mismanagement of fuel.”

Out of these 40 configurations, 6 critical combinations, depicted in Table 2.6, are included in the gust loads analysis. Thus, in total, 20,160 load cases will be scanned to determine the critical loads. For each gust load case, the wing response is analyzed at six time instances namely maximum and minimum root bending moment, maximum and minimum tip displacement and maximum and minimum tip twist. It will be shown later in the results part of the chapter that with these six instances, the most critical load on the wing across the entire time history of the gust can be approximated.

Table 2.5: List of static load cases.

Load case ID	$\mathbf{V_{eq}}$ (m/s)	**Altitude** (m)	**Load Factor**	**Fuel level/Max fuel** (%)
1	136	11000	1	70
2	240	3000	2.5	80
3	198	0	-1	80

Table 2.6: Details of fuel configurations considered in gust load cases.

Fuel Mass Case ID	**Fuel Tank 1** (%)	**Fuel Tank 2** (%)	**Fuel Tank 3** (%)	**Fuel Tank 4** (%)
1	0	0	0	0
2	80	0	0	0
3	0	0	0	80
4	0	0	80	80
5	80	0	0	80
6	80	80	80	80

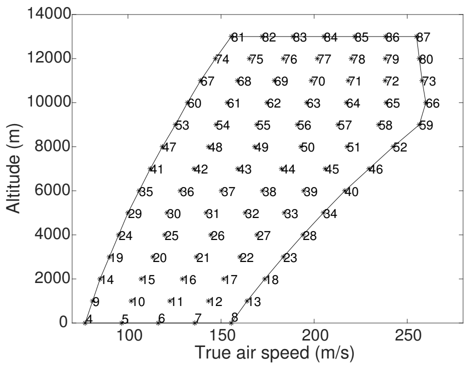

Figure 2.14: Flight envelope depicting the 84 flight points that were investigated. Each flight point represented by an Astrix is a combination of true air speed and altitude.

2.2.2 Optimization Results

It took 42 iterations to obtain an optimized configuration resulting in a structural weight of 8,684 kg which is 86.5% of the initial weight. Figure 2.15 shows the stiffness and the thickness distribution of the optimized CRM wing. The strain, and buckling constraints can be seen in Figure 2.16. The inner half of the wing is mainly dominated by strength and buckling constraints, whereas the outer half is dominated by aileron efficiency and strength constraints. In the inner half, the region near the wing root is dominated by buckling and as a result, the out of plane stiffness properties are more pronounced as compared to the rest of the wing. The middle part of the wing is sized by the strength and hence the in-plane stiffness distributions are oriented along the wing axis to maximize the load carrying capabilities of the wing. The thickness in the inner half of the wing increases from the root till the region around the engine. Additionally, the front part has a higher thickness as compared to the aft, thus shifting the elastic axis forward and introducing wash-out twist upon wing bending which alleviates the load. In the outer half of the wing, the in-plane stiffness distributions are oriented aft to increase the aileron effectiveness. Furthermore, the aft part is thicker than the front part, shifting the elastic axis aft thus making it beneficial in terms of aileron effectiveness.

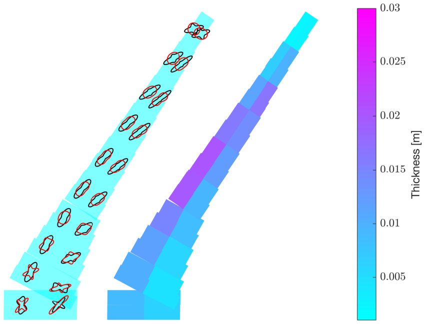

(a) Top Skin

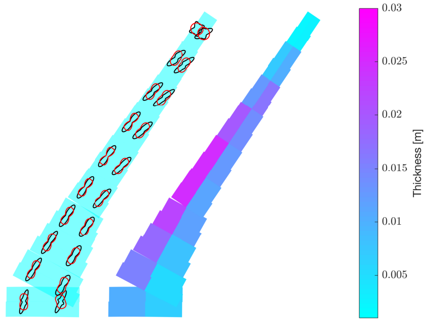

(b) Bottom Skin

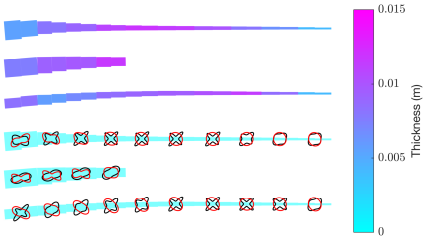

(c) Spars

Figure 2.15: Stiffness and thickness distribution for the optimized CRM wing (In-plane stiffness: black, out-of-plane stiffness: red).

Figures 2.17 and 2.18 depict the critical loads at various iterations in the optimization process on the top and bottom skin of the CRM wing respectively. For each laminate, the number outside the bracket indicates the critical flight point, the number inside the bracket indicates the fuel mass case ID and the colour indicates the critical gust gradient. The laminates with grey colour are critical with respect to the static load cases. Flight points 1, 2 and 3 are static load cases described in Table 2.5 and the rest are the gust flight points as shown in Figure 2.14.

Looking at the critical loads, the change in the design variables leads to modification in the aeroelastic properties of the wing, which results in the variation of critical loads. Figure 2.19 shows the mean change in the design variables along the optimization process and Figure 2.20 shows the corresponding change in the

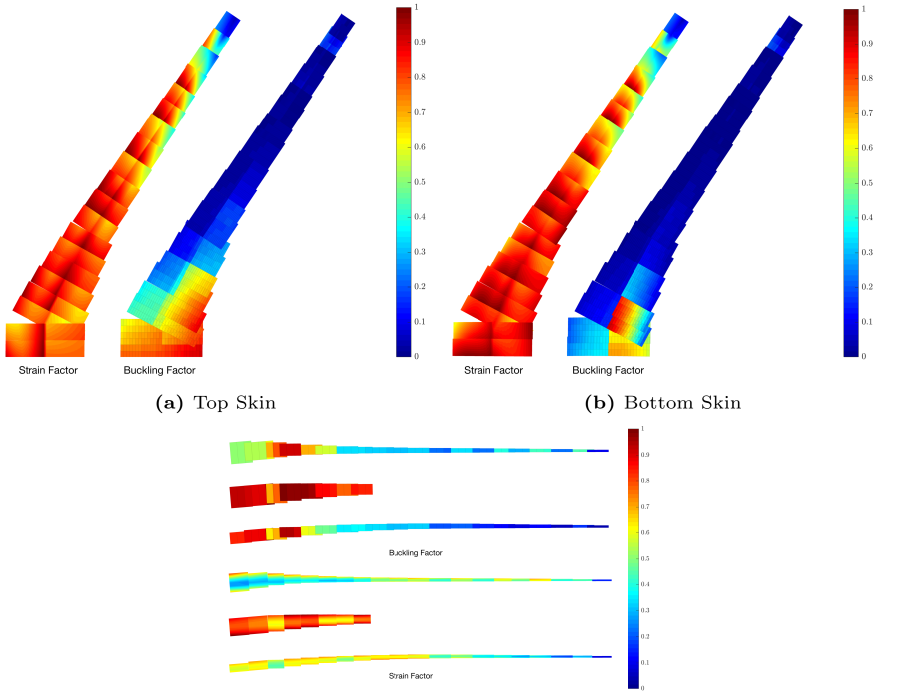

(a) Top Skin **(b)** Bottom Skin

(c) Spars

Figure 2.16: Strain and buckling factor distribution on the optimized CRM wing.

frequency of the first bending mode. Additionally, Figure 2.21 shows for every iteration, the number of critical load cases that have been added or removed with respect to the previous iteration. As can be seen, the biggest change in the design variable as well as the first bending mode frequency happens in the first few iterations. As a result, the change in the critical loads is also significant in the first few iterations. Thus, in the case of the dynamic aeroelastic optimization process, the worst case gust loads need to be determined at every new iteration during the first few steps as the change in the later steps is minimal.

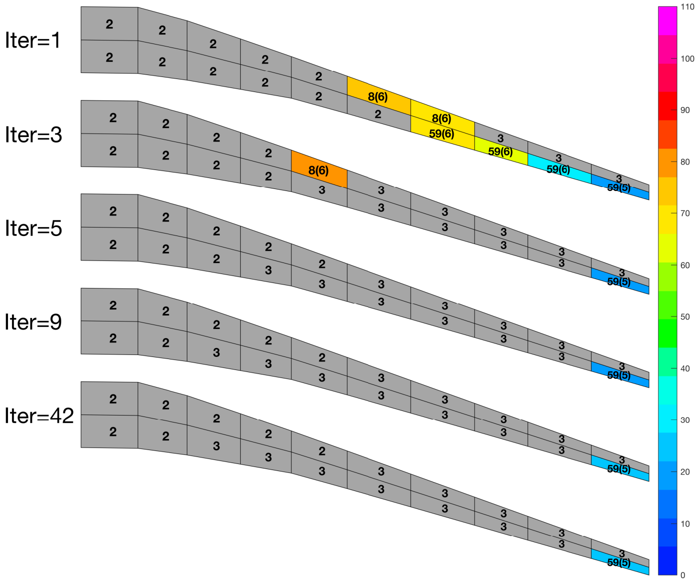

Figure 2.17: Critical flight points and gust gradients on the top skin during the optimization process.

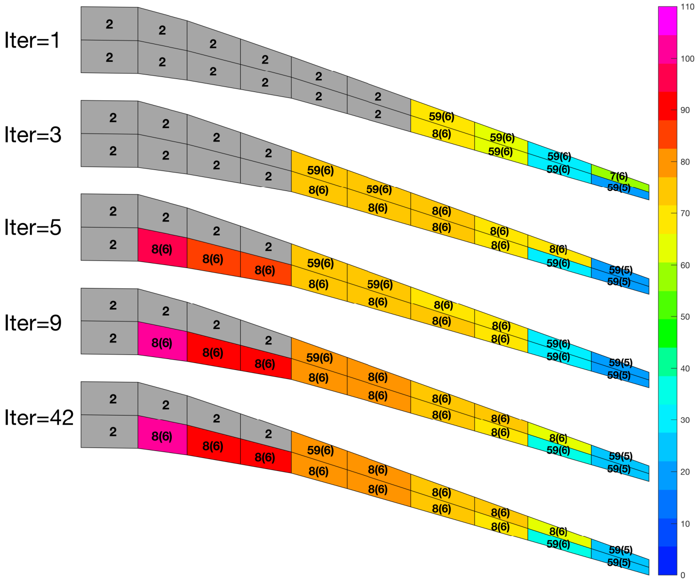

Figure 2.18: Critical flight points and gust gradients on the bottom skin during the optimization process.

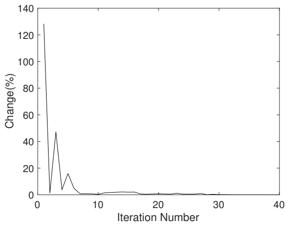

Figure 2.19: Mean change in the design variables.

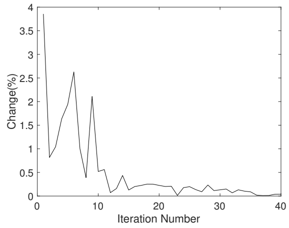

Figure 2.20: Change in the first bending frequency.

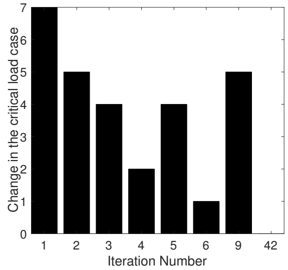

Figure 2.21: Total number of the change in the critical load cases.

To understand the importance of updating critical loads during the optimization process, the CRM wing is optimized with respect to the critical loads determined only for the initial design. Figure 2.22 shows the maximum strain factor for each laminate of the optimized wing obtained by analyzing the entire flight envelope. As can be seen, the optimized wing violates the strength constraints by a maximum of 5%. This is due to the fact that the critical loads are different than the loads that the wing is optimized for. Although for the current design, the maximum violation is of only 5%, in the area of loads, such a small violation can cause a huge penalty in terms of weight of the wing. Additionally, the magnitude of the violation depends on how close the initial design is with respect to the optimum configuration. If there is a big difference, then the violation could be bigger as well. The failure of the optimized wing under gust loads illustrates the importance of identifying gust loads at various iteration in the design process.

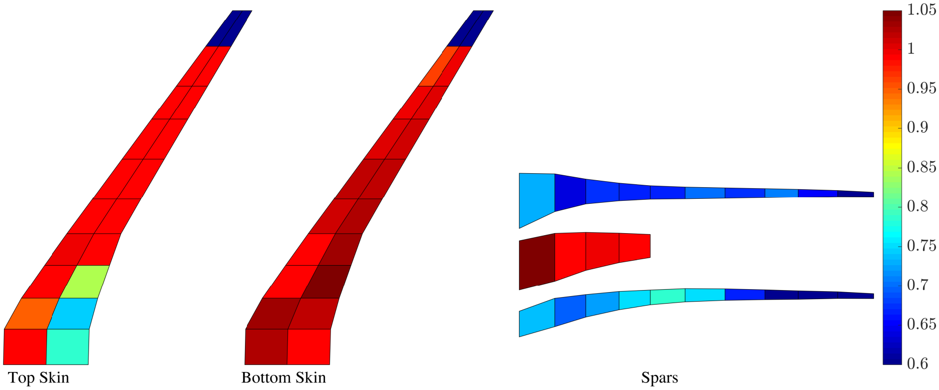

Figure 2.22: Strain factor distribution of the CRM wing optimized with a fixed set of critical loads.

Gust response is dominated by the dynamic pressure and the reference gust velocity. As per the certification requirements, the reference gust velocity decreases as the altitude increases. Hence, along with cruise load case, the points at sea level also are responsible for the critical gust loads. With respect to gust gradient, critical length increases as we move from the outer part towards the inner part of the wing. And with respect to fuel mass configurations, fuel mass case 6 is the critical fuel mass case for the entire wing except for the outer laminates in which fuel mass case 5 becomes critical.

It should be noted that the present study is performed on a clamped wing only. Due to the flight dynamics, the gust loads on a free flying aircraft are usually lower than on a clamped wing as the rigid body motion of the aircraft reduces the load experienced by the wing. However, the critical gust load cases are still expected to change during the optimization process. The methodology, proposed to identify critical gust loads at every iteration and include it in the optimization for the clamped wings, can be adapted to a free flying aircraft as well.

As was mentioned before, the wing response is evaluated at six instances per gust load. To prove the validity of this approach, the highest strain factor for the optimized wing is calculated by analyzing wing response at every instance of the time history and compared with the highest strain factors analyzed by taking into account only 6 aforementioned instances in the response. Figure 2.23 shows the increase in strain factor by taking the entire time history into account. The highest difference is about 0.5%, thus validating the approach taken.

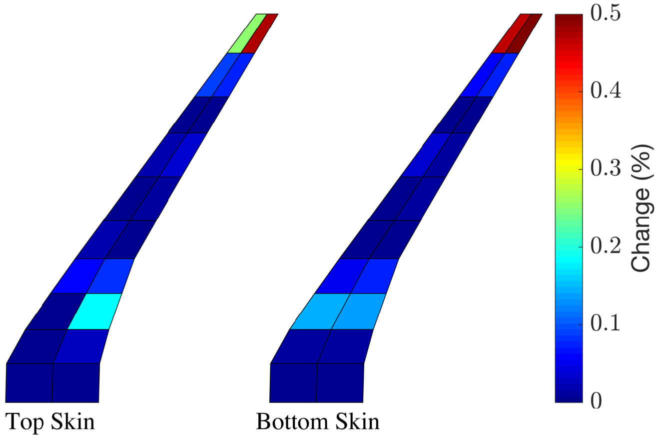

Figure 2.23: Comparison of the strain factor determined for the entire time history with strain factor determined only at 6 aforementioned instances.

2.3 SYNOPSIS

In this chapter, a dynamic aeroelastic optimization method was formulated using the ROAM. The ROAM which is based on PROTEUS was created by reducing the order of the unsteady vortex lattice model and coupling it to the structural solver. The combination of high accuracy with very few states, relatively low computational cost for a typical model size of interest, and sufficient robustness, made the BPOD the most suitable MOR method for the aeroelastic framework.

The ROAM formulated using the BPOD method predicts the wing responses caused by different gust gradients very accurately. To be able to efficiently cover the complete flight envelope of an aircraft for a given wing planform, a new formulation for the state-space system was derived where the influence of the equivalent airspeed was isolated from the state-space matrices. Furthermore, it was demonstrated that the Mach number, which in this vortex lattice model is implemented using the Prandtl-Glauert correction, has a negligible effect on the reduced basis. A single ROM could thus be used to analyze the aeroelastic loads throughout the flight envelope, reducing the computational cost significantly. The comparison of the loads acting on a backward and forward swept version of the NASA CRM obtained with the ROAM and FOM proved the validity of the assumption. A considerable saving in computational cost of about 89% for the analysis of 2,448 flight points, was obtained using this method.

Using the developed ROAM, a dynamic aeroelastic optimization framework was formulated and thickness and stiffness optimization of the CRM wing clamped at the root was carried out. The results showed that both static as well as gust loads are critical for a composite clamped wing. Furthermore, the change in the design variables was highest during the first few iterations which lead to a considerable change in the critical loads in the first few iterations. This showed the importance of updating the critical loads along the dynamic aeroelastic optimization process.

3

AEROELASTIC OPTIMIZATION OF COMPOSITE WINGS SUBJECTED TO FATIGUE LOADS [1]

The previous chapter dealt with including the critical gust loads in the aeroelastic design process. In this chapter, the journey towards increasing the knowledge in the preliminary aeroelastic design continues by focusing on integrating fatigue loading requirements in the aeroelastic design methodology of composite wings.

Fatigue damage in composites is a complex process involving different mechanisms, such as matrix cracking, fiber breakage, delamination and fiber/matrix debonding. As a result, fatigue life prediction becomes much more complicated as compared to metals. A nice overview of the different fatigue prediction algorithms exists in the literature (Degrieck and Van Paepegem, 2001; Passipoularidis and Brøndsted, 2010; Post et al., 2008). Fatigue models can be divided mostly into three categories, empirical, phenomenological and progressive damage models. Empirical models such as Miner's rule (Miner et al., 1945) use the information from S-N curve or Goodman diagrams to define a damage parameter which keeps track of the fatigue life. The parameter starts with 0 and increases until the value equals 1 which indicates the final failure. The S-N curves and Goodman dia-

[1] This chapter is largely based on the journal paper Rajpal, D., Kassapoglou, C. and De Breuker, R. (2019). *"Aeroelastic optimization of composite wings including fatigue loading requirements"*, Composite Structures, vol. 227.

grams are obtained by carrying out an experimental campaign calculating fatigue life of multiple test coupons under various levels of constant amplitude loading. Phenomenological models (Paepegem et al., 2001; Whitworth, 1997) calculate the fatigue life by measuring the degradation in a macroscopic material property. This property can be the stiffness (Brunbauer and Pinter, 2015) or the strength (Philippidis and Passipoularidis, 2007) of the material. In the progressive damage models (Bergmann and Prinz, 1989; Dahlen and Springer, 1994), composite properties are predicted and deteriorated by modelling microscopic failures that occur on fibres, matrix and fibre/matrix interface. These models are quite complex and time consuming to run, due to the various damage mechanisms occurring in composites and the extensive simulations needed to track damage evolution.

In the current thesis, the focus is on using residual strength phenomenological models for predicting the fatigue life of a composite. The residual strength wear out model has an inherent failure criterion: failure occurs when residual strength degrades to the maximum applied stress. There has been significant research on applying different residual strength degradation theories under a variety of loading conditions. Philippidis and Passipoularidis (2007) give a detailed overview of the different theories available in the literature and their validity with respect to experiments. One of the first degradation models for the residual strength which was the linear residual strength degradation approach was presented by Broutman and Sahu (1972). The approach was based on differential rate type equation which was also used in models by Schaff and Davidson (1997*a*,*b*), Hahn and Kim (1975) and Hashin (1985). Chou and Croman (1978) and Yang along with his colleagues (Yang and Du, 1983; Yang, 1978*a*; Yang and Jones, 1978; Yang and Sun, 1980) used a similar type of rate equation along with probability distribution of static strength, fatigue life and residual strength. Several other authors also worked on residual strength degradation model such as Adam et al. (1986), Epaarachchi and Clausen (2003) and Reifsnider and Stinchcomb (1986). The majority of the models requires empirical parameters that are determined by using experiments and curve-fitting. This makes the universal application of fatigue models quite difficult. Based on the models developed by Broutman and Sahu (1972), Kassapoglou (Kassapoglou, 2007, 2010, 2011) formulated a residual strength wear out model without the need of parameters obtained from fatigue tests.

In the present chapter, an analytical model based on the Kassapoglou method has been formulated to determine the fatigue life of a composite laminate. In the section 3.1, a brief overview of the Kassapoglou method is described. The analytical model is then formulated and validated for a constant amplitude as well as a variable amplitude fatigue test by comparing the prediction on a Glass/Epoxy laminate subjected to Wisper spectrum (Tenhave, 1992) and New Wisper spectrum (Bulder et al., 2002). To integrate into an aeroelastic optimization framework, the analytical fatigue model is modified to work with the composite laminates described by lamination parameters instead of stacking sequence and ply angles.

In the next section, the analytical fatigue model is integrated into the aeroelastic optimization framework. The aeroelastic tailoring of the NASA CRM (Vassberg et al., 2008) wing is carried out to investigate the effect of including fatigue as one of the design constraints along with strength, buckling and aeroelastic stability. Finally, a synopsis of the chapter is given.

3.1 Fatigue Model Formulation

The analytical fatigue model combines the Kassapoglou method (Kassapoglou, 2007, 2010, 2011, 2015) with the first ply failure theory to determine the fatigue life under a constant amplitude as well as a spectrum loading.

3.1.1 Kassapoglou Residual Strength Degradation Method

For the sake of completeness, the relevant steps involved in assessing the fatigue life using the Kassapoglou method (Kassapoglou, 2007, 2010, 2011, 2015) are summarized below.

1. For the given loads, stresses in each ply of the laminate can be determined using the classical laminate theory.

2. Based on the applied stress σ, the probability p that the residual strength of the ply is not higher than the applied stress in the ply is calculated. For the first cycle, the residual strength σ_r is equal to the static failure strength σ_{sf}. The value of p will depend on the type of statistical distribution and stress ratio R. Generally, the static strength allowables for a composite material follow a normal distribution, two parameter Weibull or lognormal distribution (Kassapoglou, 2015).

3. Once the probability of failure is determined, the number of cycles to failure (Kassapoglou, 2007), N, if the failure mode does not change and p is constant, is determined by

$$N = -\frac{1}{\ln(1-p)} \tag{3.1}$$

4. Residual strength of the ply after n cycles of the applied stress is determined through a degradation model (Kassapoglou, 2015) given by

$$\sigma_r = \sigma_{sf}(1 - (1 - \frac{\sigma}{\sigma_{sf}})\frac{n}{N-1}) \tag{3.2}$$

5. If the applied stress in any ply is higher than the residual strength of the ply, the laminate fails. Otherwise, the statistical parameters of the static

strength, such as mean and standard deviation in case of a normal distribution are degraded and the process continues until the maximum number of cycles has been reached or the laminate has failed.

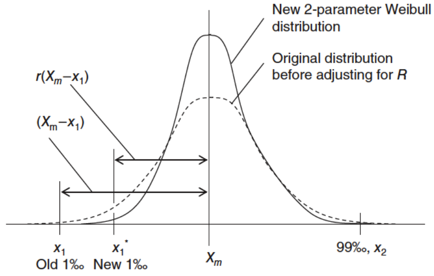

Figure 3.1: Modification of the probability distribution for stress ratio other than 0 (Kassapoglou, 2015).

For the values of stress ratio R other than 0, the value of p, needs to be modified to account for the fact that cyclic stress does not start from 0 but some finite value. This is taken into account by modifying the statistical distribution of the residual strength. Figure 3.1 depicts the assumed change in the distribution for the stress ratio other than 0. The 1% value of the distribution is shifted towards the mean of the distribution by a factor r which is given by

$$\begin{aligned} r &= 1 - R, 0 < R < 1 \\ r &= 1 - \frac{1}{R}, R > 1 \end{aligned} \tag{3.3}$$

The mean and the 99% values are kept constant. The resulting distribution is assumed to be two parameter Weibull distribution. The shape and the scale parameter can be obtained by solving iteratively Equation (3.4) which is expressed as

$$\begin{aligned} \beta(1 - \frac{1}{\alpha}) &= X \\ e^{-\frac{x_1^\alpha}{\beta}} - e^{-\frac{x_2^\alpha}{\beta}} &= 0.98 \end{aligned} \tag{3.4}$$

where x_1 is the 1% value of the new distribution, x_2 is the 99% value of the original distribution, α is the shape parameter of the Weibull distribution, β is the scale parameter of the Weibull distribution and X is the mean of the original distribution.

3.1.2 FORMULATION OF ANALYTICAL FATIGUE MODEL

In the current analytical model, instead of comparing the applied stress to the residual strength of the ply, the first ply failure theory is used to determine if there is a failure in the structure due to the degradation of the residual strength. Four first ply failure theories, namely Tsai-Hill, Tsai-Wu, Hashin and Puck were individually combined with the Kassapoglou method and their accuracy is compared to the results from experiments and the original Kassapoglou method (Kassapoglou, 2007) for different stress ratios in Figure 3.2. A $[[\pm 45/0_2]_2]_s$ T800/5245 bismaleimide (BMI) laminate is used for the comparison. Table 3.1 shows the strength allowables as well as the mean and the standard deviation of the material used. Results show that the Kassapoglou residual strength degradation model combined with all the failure theories is conservative with respect to the experimental results. Keeping in mind the accuracy along with the ease of implementation, Tsai-Wu is chosen as the most suitable failure theory to predict the fatigue life. However, it is understood that the Tsai-Wu failure criterion does not always match test results, especially under biaxial compression, but it gives a good indication of first ply failure for other loading situations. Furthermore, the approach presented here can easily be modified to include a different failure criterion if necessary.

Table 3.1: Material properties of T800/5245 ply (Gathercole et al., 1994).

Property	Mean Value	Standard Deviation
E_{11} (GPa)	147	
E_{22} (GPa)	10.3	
G_{12} (GPa)	7	
ν_{12} (-)	0.27	
X_t (MPa)	3460	318.32
X_c (MPa)	1730	171.27
Y_t (MPa)	50	4.60
Y_c (MPa)	165	16.34
S (MPa)	75	7.43

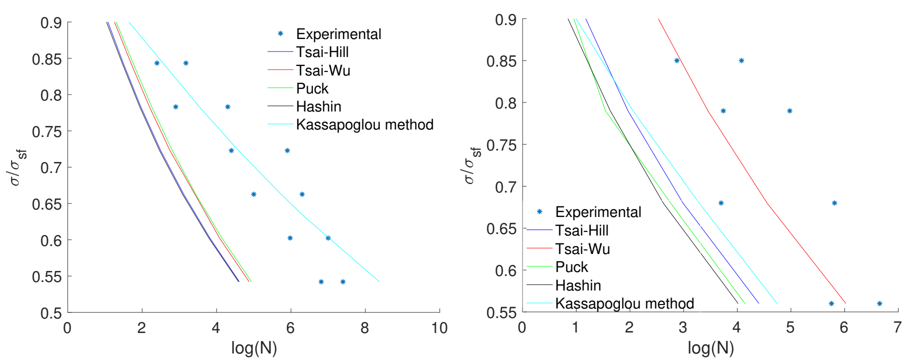

(a) R=0.1 **(b)** R=10

Figure 3.2: Comparison of 4 failure theories with results from the experimental and the original Kassapoglou model (Kassapoglou, 2007).

For the current analytical model, an assumption is made that the initial static strength follows a two parameter Weibull distribution. This assumption can be justified by the fact that the fatigue life of a composite material generally follows a two parameter Weibull distribution (Hwang and Han, 1987; Yang, 1978*b*; Yao and Himmel, 1999). Since Equation (3.2) describing the degradation of the residual strength is linear, both the residual strength and the initial static strength will also follow a two parameter Weibull distribution.

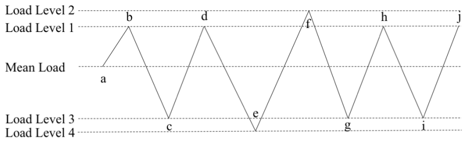

Figure 3.3: Simple spectrum with 4 load levels.

To predict failure under the spectrum loading, let us assume that the residual strength has a two parameter Weibull distribution with scale parameter α_{int} and a shape parameter β_{int} obtained by fitting a Weibull distribution to the stochastic static strength data. A simple spectrum loading comprising of peaks and valleys at different load levels is shown in Figure 3.3. At peak points in the spectrum, the stress ratio is obtained by taking into account the stress applied at the valley before the peak with stress applied at the peak. During the first cycle, the load increases to point a in the spectrum. As this is assumed to have stress ratio $R = 0$, no modification of R is necessary according to Equations (3.3) and (3.4). When the load reaches point a, residual strength and the Weibull parameters are degraded following steps 1-4 and the Tsai-Wu failure criterion is evaluated. If there is no failure, then, the load excursion from point a to point b is applied. At point b, the R value is calculated by using the stress values at a and b. If $R \neq 0$, the current Weibull parameters are modified using Equations (3.3) and (3.4). Then, the process of updating the residual strength and Weibull parameters is repeated and the Tsai-Wu failure criterion is evaluated again. For the load excursion from b to c, it is assumed again that c corresponds to $R = 0$. From this point on, and as long as the Tsai-Wu criterion does not indicate failure, the process is repeated following the steps described above.

With composite materials, there is a high scatter in fatigue life due to anisotropic heterogeneous characteristics, such as lay-up, manufacturing defects and imperfections, test complications, and environment (Tomblin and Seneviratne, 2011). To account for scatter in the calculation of the fatigue life, the B-basis reliability is used. The definition of a B value is that at least 90% of the population of values is expected to be equal to or exceed a particular property with confidence of 95%. Over a wide variety of tests on different carbon/epoxy materials, it has been found that on an S-N diagram, the stress reduction corresponding to the difference between B-Basis and mean life is approximately 20% (Tomblin and Seneviratne, 2011; Whitehead et al., 1986). Thus, in the analytical model, the calculated fatigue life is knocked down by 20%, to incorporate the effects of scatter. It should be noted that this 20% knockdown is an approximation and, given enough data, more accurate estimates of the B-Basis life can be obtained.

The analytical fatigue model is validated for spectrum loading by comparing it to the test results from the Glass/Epoxy laminate for the Wisper Spectrum (Tenhave, 1992) and the New Wisper Spectrum (Bulder et al., 2002). The experimental data was obtained from the OPTIMAT BLADES project (OPTIMAT, 2002) in which an extensive experimental campaign on a Glass/Epoxy material used in the Wind Turbine Rotor Blades industry was performed. Two types of lay up were considered in the tests; a UD layup $[0_4]$ and a multidirectional (MD) $[[\pm 45/0]_4/\pm 45]$ lay-up. To calculate the Weibull distribution parameters for the initial static strength of the ply, data corresponding to R03 coupon from the OPTIMAT database (OPTIMAT, 2002) is used. Outliers from this dataset are removed and the Maximum Likelihood Estimation (MLE) method is used to estimate the shape and the scale parameters. Table 3.2 shows the static strength allowables of the ply along with their shape and scale parameters.

Table 3.2: Properties of Glass/Epoxy laminate used in OPTIMAT project (OPTIMAT, 2002).

Property	Mean Value	Scale	Shape
E_{11} (GPa)	41.5		
E_{22} (GPa)	15		
G_{12} (GPa)	8.6		
ν_{12} (-)	0.36		
X_t (MPa)	802	854	10.12
X_c (MPa)	509	532.81	11.02
Y_t (MPa)	55	56.34	21.75
Y_c (MPa)	161	165.62	22.56
S (MPa)	53	80.61	23.56

Figure 3.4 compares the fatigue life of the UD ply predicted by the analytical model to the experimental results for the single stress ratio as well as the spectrum load. There is a reasonable agreement observed between the analytical model and the experimental results for all the cases except for the stress ratio of 10. As there is high scatter in fatigue life and material properties are not accurately known, theoretical prediction of fatigue life which is conservative and within 1-2 orders of magnitude from the experimental data can be considered as reasonable agreement. For stress ratio of 10, the prediction of the analytical model is a bit on the conservative side. The number of cycles predicted by the analytical model is 2-3 orders of magnitude lower than the experimental results. This discrepancy is expected given the fact that under compression, several failure modes such as micro-buckling, matrix local yielding and shear failure may compete and interact. This interaction of failure modes is not accounted for in the model as formulated.

The MD laminate consists of ± 45 non-woven glass roving lamina and 0 degree UD

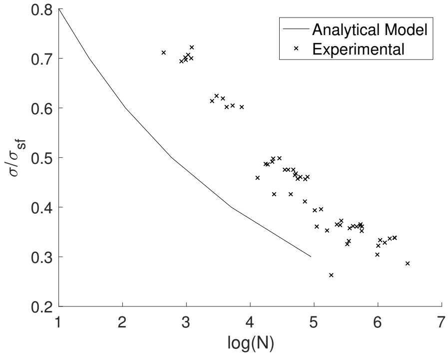

(a) R=0.1

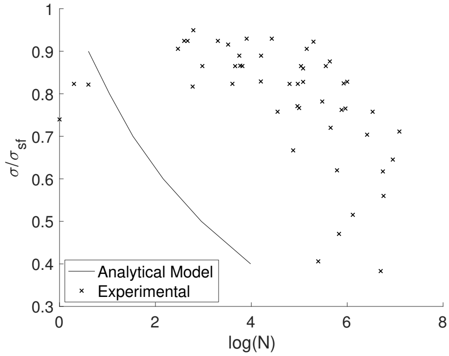

(b) R=10

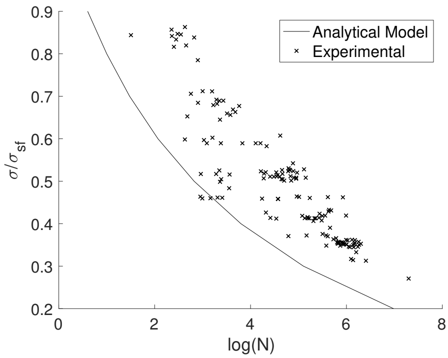

(c) R=-1

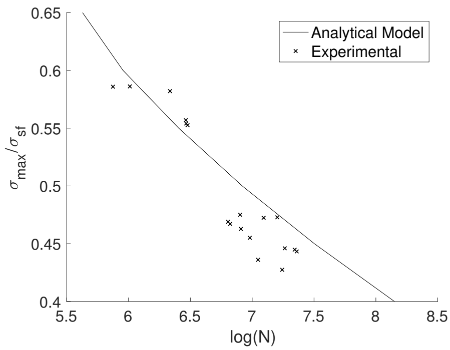

(d) Wisper Spectrum

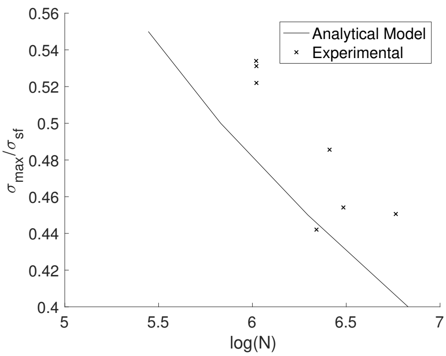

(e) New Wisper Spectrum

Figure 3.4: Comparison of fatigue life predicted by analytical model and experimental results for the UD laminate.

ply. As there is no static strength information available for the ±45 non-woven glass roving, the ±45 lamina is represented by two UD plies; one oriented at 45 degrees and the other at -45 degrees, each having half the thickness of the ±45 lamina. In Table 3.3, the static strength of the MD laminate, modelled with only UD plies and calculated using the Tsai-Wu failure criterion, is compared to the actual strength values obtained from the OPTIMAT database. As can be seen, the Tsai-Wu values are on average 55% lower than the experimental values. The conservativeness of Tsai-Wu is because the analysis is done using First Ply Failure (FPF) methodology.

The ±45 plies fail at a lower stress level compared to the 0 plies and, as a result, the static strength values are conservative. In reality, the MD laminate will carry considerable load after the failure of ±45 plies. The static strength of the laminate then has to be predicted using progressive failure models with Ultimate Laminate Failure (ULF) failure criteria. To model the progressive failure of a laminate, a Stiffness Degradation Method (SDM) is formulated. In SDM, the damaged plies after the initial failure are modeled by reduced stiffnesses. Since Tsai-Wu is an interactive theory, there is no information on the mode of failure. Thus to use Tsai-Wu in SDM methodology, an assumption is made that if the stresses in the longitudinal direction are the main contributor to the failure index, then fiber has failed otherwise the matrix has failed (Liu and Tsai, 1998).

For the current MD laminate, failure in the ±45 plies is matrix dominated and hence the transverse and the shear stiffness moduli are degraded as follows

$$E_{22_{new}} = Df_1 E_{22} \tag{3.5}$$

$$G_{12_{new}} = Df_2 G_{12} \tag{3.6}$$

The values of the degradation factors Df_1 and Df_2 are obtained by performing an optimization with an objective function of reducing the sum of two errors: the first error is between the stress-strain curve predicted using the SDM model and the experimental stress-strain data available in the OPTIMAT database, and the second error is between the ultimate tensile strength predicted by the SDM model and the experiments. This multi-objective optimization results in 0.88 and 0.97 as the values for Df_1 and Df_2, respectively. As can be seen in Table 3.3, the SDM model gives a better estimate of the static strength in tension for the MD laminate. The static strength for compression still shows a significant difference and the main reason for that is the modelling of the ±45 plies in the laminate. The non-woven glass roving has a higher compressive strength compared to the combination of UD plies, hence the difference in the static strength values.

Figure 3.5 compares the fatigue life predictions by the analytical model using the SDM methodology to the experimental results for the MD laminate. For stress ratio of 0.1 and 10, there is a good agreement on the fatigue life as the life predictions from analytical model are 1-2 order of magnitude lower compared to the experimental results. For the stress ratio of -1 and the spectrum loading,

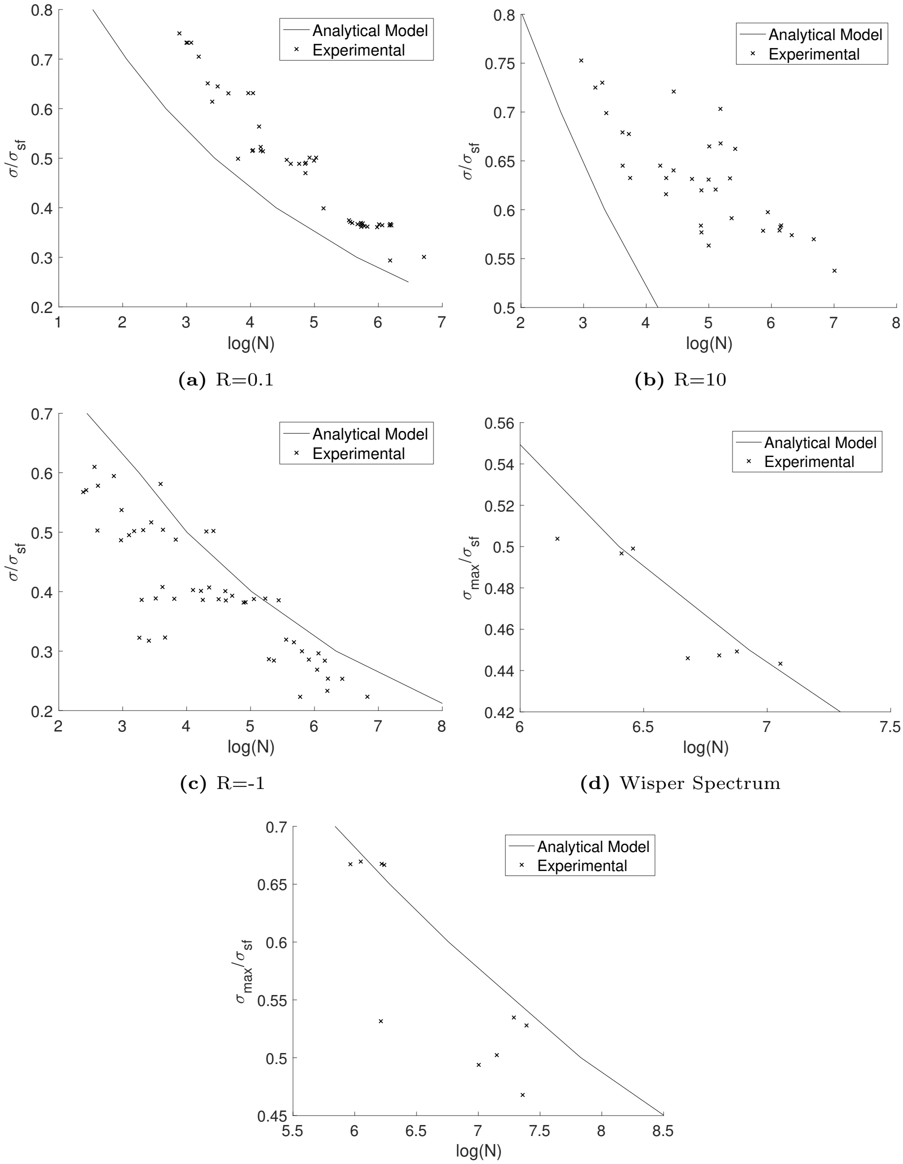

(a) R=0.1

(b) R=10

(c) R=-1

(d) Wisper Spectrum

(e) New Wisper Spectrum

Figure 3.5: Comparison of fatigue life predicted by analytical model and experimental results for the MD laminate.

even though the predictions are slightly nonconservative as the majority of experimental results are 1 order of magnitude lower than the predictions, it is a good

Table 3.3: Static strength allowables of the MD laminate.

Parameter	**Experimental Data**	**Tsai-Wu** FPF	**Tsai-Wu** SDM
σ_t^{ult} **[MPa]**	532	184	473
σ_c^{ult} **[MPa]**	458	262	262

match as the analytical prediction can be considered to be within the scatter of the fatigue data.

Even though the comparisons to test results shown here are for glass/epoxy laminates having standard ply angles, the analytical fatigue model is still valid for carbon/epoxy specimens as well as non standard fiber orientations. Comparisons with carbon/epoxy laminates, showing good to excellent agreement with predictions, can be found in Kassapoglou (2007). In addition, it should be emphasized that the analytical model is based on two quantities: (i) the probability p that the strength of a given specimen is less than the applied cyclic stress at a given number of cycles, and (ii) the residual strength which evolves with cycles. Of the two, the probability p is defined by the creation and evolution of damage during cycling. Therefore, any differences in the type of damage and its progress, arising due to the difference in the material or the orientation of the fiber, are accounted for by the calculation of p as a function of cycles.

3.1.3 Assumptions in Analytical Fatigue Model

The process to predict failure by analyzing each step of a spectrum load until the laminate fails can become computationally expensive. For example, on an Intel i5 2.7 GHz single core processor, it took 3 hours to analyze the UD ply for the New Wisper spectrum with the maximum applied stress of 0.5 times the static failure stress. If an entire wing needs to be analyzed, the computational time would be in the range of 100 hours, which becomes quite expensive for a preliminary optimization process. Hence, three assumptions have been made which can decrease the computational time quite significantly. In this section, the first two assumptions are discussed and the third assumption will be explained later in the chapter. To understand the basis of the first two assumptions, consider a simple spectrum shown in Figure 3.3.

The first assumption is that the ratio of degradation remains constant for a given load cycle. Looking at Figure 3.3, the second load cycle consisting of points c and d, is similar to the fourth and the fifth load cycle consisting of points g, h, i and j respectively. Instead of repeating the analysis at the individual points, the model parameters can directly be degraded using the ratio calculated at the first instance. For example, the residual strength, if the combination of c and d repeats, n times is given by

$$\sigma_{r_2} = \sigma_{r_1} d_1^n \tag{3.7}$$

where σ_{r_1} is the residual strength before the first point of the load cycle, σ_{r_2} is the residual strength after the n similar load cycles and d_1 is the residual strength degradation ratio calculated during the first instance of the particular load cycle. Thus, for the fourth and the fifth load cycle, the degradation ratio can be applied directly to the residual strength and the Weibull distribution parameters.

A spectrum loading generally consists of a block of cycles which are repeated multiple times. The second assumption is then the extension of the first assumption over the entire block of the cycles. The ratio of degradation remains constant over the entire block. To explain the second assumption, consider a spectrum load made up by repeating the block of cycles described in Figure 3.3 seven times. To calculate the fatigue life over the entire spectrum, the degradation in different parameters is calculated by

$$x_2 = x_1 d_2^n \tag{3.8}$$

where x_1 is the value of the parameter at the start of the block, x_2 is the value of the parameter after the block is repeated n times (end of the spectrum) and d_2 is the degradation ratio of the parameter calculated during the first sequence of the block.

The second assumption can become nonconservative as the ratio of the degradation increases with the decrease in the residual strength. Thus, to be on the conservative side, the entire block of the cycles needs to be analyzed and the ratio of the degradation needs to be updated again after every third sequence. With this approach, the fatigue life for the spectrum load made up by repeating the block of cycles described in Figure 3.3 seven times is determined first by analyzing the first sequence of the block and calculating the degradation ratio for different parameters. Then the effect of the second and third sequence is directly calculated by degrading the model parameters by their respective ratios calculated for the first sequence. The degradation ratio is updated by analyzing the fourth sequence of the block and is then used to degrade the properties for the fifth and sixth sequence and finally the seventh sequence is analyzed. Thus, the entire block of cycles is analyzed only three times instead of seven times resulting in a reduced computational effort.

Table 3.4 compares the residual strength after the application of the New Wisper spectrum on the UD laminate obtained from the full analysis and the analysis with the assumptions included. The maximum applied stress is 0.5 times the static failure stress. The second column lists the maximum change in the residual strength, and the third column shows the difference in the computational time required to perform the analysis. As can be seen, by implementing both the first and the second assumption, there is a good agreement with the original model with the error being less than 1%. With the use of these assumptions, the analytical model becomes faster by almost 93%.

Table 3.4: Validity of the assumptions made to predict the fatigue life.

Assumption Type	ΔX (%)	Δt (%)
1	0.0013	85.2
2	0.92	56.4
Both 1 and 2	0.97	92.8

3.1.4 Modification for Lamination Parameter Space

For the aeroelastic optimization process described in Chapter 2, lamination parameters are used to represent the composite laminate. With the current fatigue model, only the laminates described by ply angles and stacking sequences can be analyzed. With the lamination parameters, there is no information on the number of the plies or the angle of the plies. As a result, the fatigue model is modified such that it can be applied to the lamination parameter domain.

From hereon, the analytical model to predict failure in the laminate described by ply angle and stacking sequence will be called the original model. To determine if the laminate has failed, the Tsai-Wu failure criterion has been implemented in the original model. The failure criterion in its original form explicitly depends on the ply angles and the stacking sequence. To adapt it for the lamination parameters, Khani et al. (2011) formulated a failure envelope based on the conservative approximation of the Tsai-Wu failure criterion that does not explicitly depend on the ply angle. The approach assumes that all ply angles could be present at any location through the thickness of the laminate and thus is safe regardless of the ply angle. In the current fatigue model, for the failure criterion, this modified Tsai-Wu failure envelope is implemented.

As the failure envelope works with the principal strains, the fatigue model is modified to work on principal strains rather than lamina stresses. Figure 3.6 depicts the flowchart of the fatigue model to determine failure for a composite defined by the lamination parameters. To determine the probability of failure, which is needed for calculating cycles to failure N, instead of comparing the lamina stresses in each ply to their residual strength, the value of the modified Tsai-Wu criterion of the entire laminate is compared to the failure index, which at the start is equal to 1. For this purpose, the Weibull distribution parameters of the Tsai-Wu criterion need to be calculated. Based on the statistical distribution of the static strength allowables, 100,000 set of inputs to the Tsai-Wu failure criterion are randomly generated. A deterministic computation of the failure criterion on the randomly generated input is performed and the Weibull distribution of the modified Tsai-Wu is estimated. Figure 3.7 shows an example of the histogram generated by calculating the modified Tsai-Wu failure index for a set of 100,000 random input variables.

In the original model, the degradation in the residual strength of the ply is calcu-

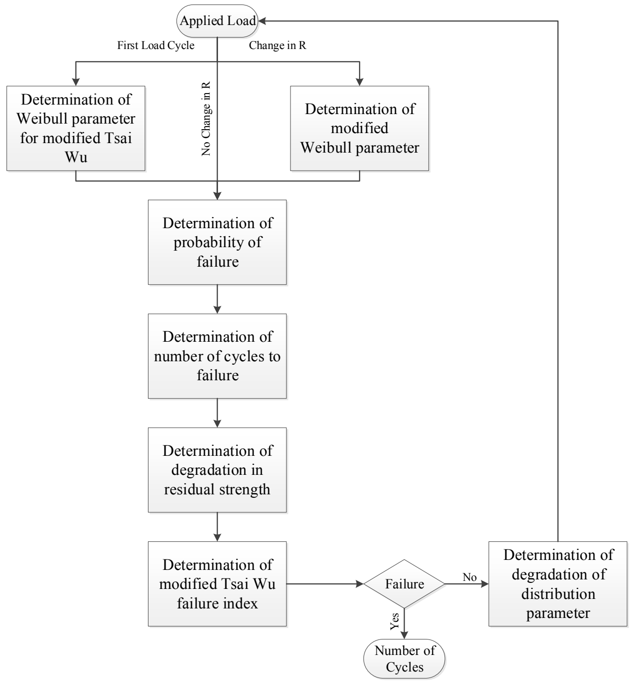

Figure 3.6: Algorithm for the modified fatigue model.

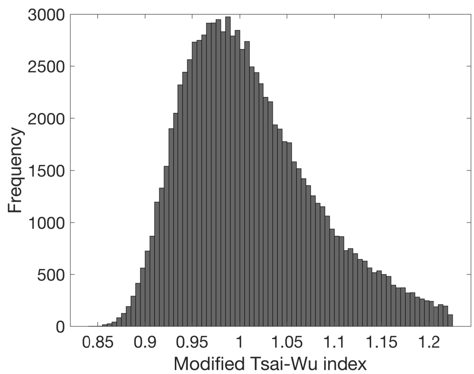

Figure 3.7: Histogram of the modified Tsai-Wu failure index generated using 100,000 sets of random input.

lated with Equation (3.2). In the case of the modified model, the stress terms in the equation are replaced by principal strains. The equation for the degradation in residual strength can then be expressed as

$$\begin{aligned}\sigma_r &= \sigma_{sf}(1-(1-\frac{\epsilon_i}{\epsilon_{sf}})\frac{n}{N-1}\\ \epsilon_r &= \epsilon_{sf}(1-(1-\frac{\epsilon_i}{\epsilon_{sf}})\frac{n}{N-1}\end{aligned} \tag{3.9}$$

where ϵ_i represents the principal strain of the laminate based on the applied stress and ϵ_{sf} represents the principal strain at which the laminate will fail.

The distribution parameters of the modified Tsai-Wu criterion are degraded by R_{tw}, which is expressed as

$$R_{tw} = \frac{f}{f_r} \tag{3.10}$$

where f is the value of the modified Tsai-Wu criterion before the residual strength degradation and f_r is the value of the modified Tsai-Wu criterion after the residual strength degradation.

Figure 3.8 compares the result by the original model and the modified model for the OPTIMAT MD ply subjected to New Wisper spectrum. As expected, because of the conservative nature of the modified Tsai-Wu criterion (Khani et al., 2011), the fatigue predictions of the modified fatigue model are conservative compared to the original model.

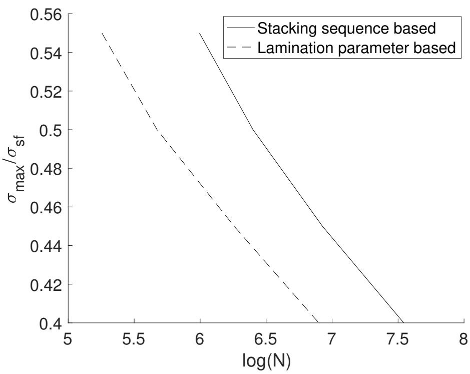

Figure 3.8: Comparing life prediction of model with lamination parameter and model with stacking sequence.

3.2 DYNAMIC AEROELASTIC OPTIMIZATION WITH FATIGUE LOADING

To understand the effect of including the proposed fatigue analysis over using the traditional knockdown factor in the design of the composite wing, the analytical fatigue model is integrated into the aeroelastic framework, PROTEUS. The framework of PROTEUS is described in Chapter 2 and Werter and De Breuker (2016). In the current study, along with strength and buckling, fatigue properties of the wing will also be calculated using the analytical fatigue model and fed as a constraint to the optimizer.

3.2.1 FATIGUE CONSTRAINT SETUP

To analyze the wing for fatigue, a shortened version of the TWIST spectrum (Mini-TWIST) (Lowak et al., 1979) is used as the load spectrum. The Mini-TWIST spectrum consists of ten flight levels where each flight level has ten different levels of stress ratio. The stress ratio has been normalized to the stress level at cruise condition. At each stress ratio, the number of cycles is different. The ten flight levels are repeated in a random manner to make a block of 4,000 flights which is equal to 58,442 cycles. In reality, cycles with highest load levels occur randomly during the fatigue life and hence out of the ten flight levels in the spectrum, care needs to be taken that the first four flight levels having the highest stress ratio are not clustered together as they might have the highest effect on fatigue. The block of 4,000 flights is repeated 10 times, equivalent to 40,000 flights which is considered as the maximum life of the aircraft. A fatigue factor F is calculated for every laminate by subjecting it to Mini-TWIST spectrum for 10 times. F is defined as

$$F = f\frac{N_t}{N} \tag{3.11}$$

where f is the modified Tsai-Wu failure criterion at the time of failure, N_t represents the total cycles the structure has to withstand and N represents the total cycles to failure. If the laminate does not fail after the 40,000 flights, f is then the maximum modified Tsai-Wu failure criterion calculated in the spectrum.

For each laminate, running the fatigue model for 40,000 flights can become time consuming. Looking at the process to calculate the fatigue life in the lamination parameter domain, calculation of the Weibull parameters for different stress ratios is computationally the most expensive. In an effort to speed up the process, in addition to the two aforementioned assumptions discussed in section 3.1.3, a third assumption is made. The ratio of change in the Weibull parameters for all the patches remains constant. The patch could be a design region or a laminate. Consider a wing consisting of ten patches. The statistical distribution of the static strength of the material is described by Weibull parameters α_{int} and β_{int}.

The wing is subjected to the Mini-TWIST spectrum. At the second load step, the R ratio changes and hence Weibull distribution is modified as well. The new Weibull parameters $\alpha_{1_{new}}$ and $\beta_{1_{new}}$ for the first patch are calculated using Equations (3.3) and (3.4) (it is recommended to use the most critical patch as determined by the highest value of the Tsai-Wu criterion). The modified Weibull parameters for rest of the patches are then calculated by

$$\begin{aligned}\alpha_{i_{new}} &= \alpha_{i_{int}} \frac{\alpha_{1_{new}}}{\alpha_{1_{int}}} \\ \beta_{i_{new}} &= \beta_{i_{int}} \frac{\beta_{1_{new}}}{\beta_{1_{int}}}\end{aligned} \tag{3.12}$$

where i is the patch number ranging from two to ten.

Thus, Weibull parameters at a new stress ratio are determined only for the single laminate. The Weibull parameters for all the other laminates are based on the ratio of change in the Weibull parameters of that single laminate. Figure 3.9 depicts the delta plot of the percentage change in the residual strength value of the laminates with and without the third assumption. The overall difference is less than 0.5%. The wing used is a CRM wing which is described in the next section. In terms of computational efficiency, without the third assumption it takes 104 minutes to run a block of 4,000 flights and with the third assumption, it takes two minutes. Thus, only with the third assumption, 98% saving in the computational effort is achieved without sacrificing much in terms of accuracy.

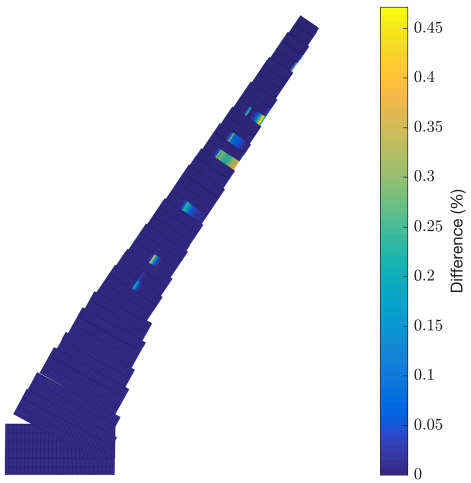

Figure 3.9: Delta plot of residual strength with and without third assumption.

3.2.2 OPTIMIZATION APPROACH

The NASA CRM, defined in Section 2.1.5, is used as a case study for the current analysis. Two optimization studies are performed: (i) an aeroelastic optimization without fatigue as a constraint, and (ii) an aeroelastic optimization with fatigue as a constraint. In the first one, a traditional knockdown factor of 0.39 is applied to account for fatigue, damage and material scatter and a knockdown factor of 0.8 is applied to account for environment. Thus a net knockdown factor of 0.312 is applied to the stress allowables. In the second case, knockdown factors of 0.65 and 0.8 are applied to account for damage and environment respectively. Thus a net knockdown factor of 0.52 is applied to the stress allowables. Additionally, as was mentioned before, in the analytical model, the fatigue life is also reduced by 20% to account for fatigue scatter. The UD AS4/8552 carbon/epoxy composite prepreg is used as the reference material. Table 3.5 shows the material properties along with the Weibull distribution parameters (Clarkson, 2011). The optimization problem is shown in Table 3.6. The objective of the study is to minimize the structural weight of the wing. The wing is divided into 10 sections along the spanwise direction. For the top skin and the bottom skin, each spanwise section consists of two laminates in the chord-wise direction and for the spars, each spanwise section has only one laminate in the chord-wise direction. This results in 64 unique laminates. Laminates are symmetric and unbalanced. Every laminate is described by eight lamination parameters and one thickness variable, resulting in a total of 576 design variables.

Table 3.5: Material properties of AS4/8552.

Property	**Mean Value** (GPa)	**Scale** (GPa)	**Shape** (-)
E_{11}	128		
E_{22}	19.3		
G_{12}	4.8		
ν_{12}	0.3		
X_t	1.99	2.06	12.05
X_c	1.39	1.43	16.59
Y_t	0.064	0.067	11.12
Y_c	0.27	0.28	17.32
S	0.092	0.094	17.32

With respect to constraints, a similar strategy as explained in Section 2.2.1 is implemented. Additionally, a constraint on fatigue is also implemented where the analytical fatigue model is used to calculate the fatigue life of the laminate. The laminate should not fatigue during the design life of the aircraft which in the current case is assumed to be 40,000 flights with the aforementioned Mini-TWIST spectrum.

Table 3.7 gives the information on the static load cases which are used for the current study. These load cases which were provided by NASA, represent the

Table 3.6: Optimization setup.

Type	Parameter	# parameters
Objective	Minimize Wing Mass	1
Design Variables	Lamination Parameter Laminate Thickness	576
Constraints	Laminate Feasibility	384
	Static Strength	1,024/load case
	Buckling	4,096/load case
	Fatigue	3,875
	Aeroelastic Stability	10/load case
	Local Angle of Attack	22/load case
	Total Constraints	4,259+5,152/load case

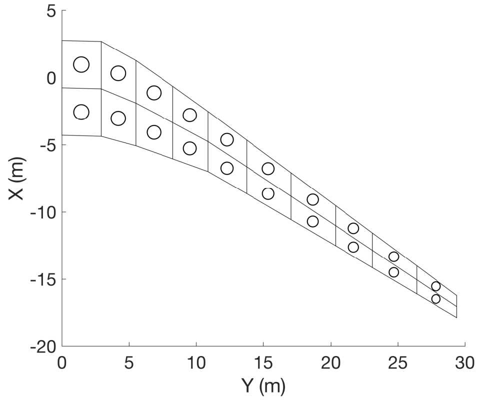

Figure 3.10: Laminate Distribution of the top skin of CRM.

cruise condition, 2.5g symmetric pull up manoeuvre and -1g symmetric push down manoeuvre. With respect to gust load cases, 84 flight points covering the entire flight envelope are investigated. For each flight point, 40 gust gradients both positive as well as negative, ranging from 9 m to 107 m are considered. Figure 3.11 displays the flight envelope with their respective flight point ID. These load cases represent the limit load which is defined as the maximum load the wing expects in service. To satisfy the requirements for the ultimate load, an additional safety factor of 1.5 is applied to the strength and buckling values calculated for the limit loads.

Table 3.7: List of load cases.

Load case ID	V_{eq} (m/s)	Altitude (m)	Load Factor (-)	Fuel level/Max fuel (%)
1	136	11,000	1	70
2	240	3,000	2.5	80
3	198	0	-1	80

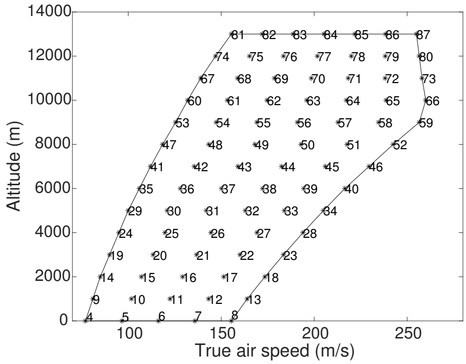

Figure 3.11: Flight Envelope.

3.2.3 Optimization Results

Figure 3.12 plots the critical constraints for both the optimization studies, one with and one without the analytical fatigue model. For the sake of simplicity, from hereon, the case without the fatigue model will be referred to as Study with Knockdown Factors (SKF) and the case with the fatigue model will be referred to as Study with Analytical Fatigue Model (SAFM). For SKF, the wing is critical in both strength and buckling. The inboard part of the top skin and spar is buckling critical whereas the outer part is critical in strength. The bottom skin is mainly driven by strength. In the case of SAFM, similar trends can be observed. However, the wing is also critical in fatigue. The middle/outboard part of both top and bottom skins and the inboard part of the front spar are sized by fatigue.

Figure 3.13 shows the stiffness and the thickness distribution of the optimization studies. With respect to Figure 3.13, the region near the wing root is dominated by buckling and as a result, the out of plane stiffness properties are more pronounced as compared to the rest of the wing in both the studies. With respect to middle and outboard parts of the wing, for both the studies, the in plane stiffnesses in the top skin are oriented forward to increase the nose down twist and shift the load inboard. Figure 3.14 compares the twist distribution at 1g and 2.5g condition for wing optimized in SKF and SAFM. The middle part of the wing is critical in fatigue in SAFM, resulting in a stiffness tailoring and thickness distribution which leads to a higher washout and hence reduced load compared to the wing in SKF. Looking at the in plane stiffness in the inboard part of the bottom skin, in SKF, the in plane stiffness shape is narrower than SAFM, indicating more concentration of plies in 0 direction to increase the load carrying capacity as it has lower strength allowables because of the conservative knockdown factor.

Figure 3.15 compares the critical static and gust loads acting on the bottom skin of the optimized wing for both the studies. For each laminate, the number indicates the critical flight point and the colour indicates the critical gust gradient. The laminates with grey colour are critical with respect to the static load cases. Flight points 1, 2 and 3 are static load cases described in Table 3.7 and the rest are the gust flight points as shown in Figure 3.11. As can be seen, the middle part of the wing, where fatigue is critical in SAFM, has different critical loads as compared to the wing in SKF. The wing optimized with fatigue model is more critical to static loads in the middle part whereas the wing optimized with conservative knockdown factor is more critical to gust loads in the middle part.

Looking at the thickness distribution, as expected, the optimized wings in SKF where a knockdown of 68% is applied to the material allowables, are thicker compared to the wings in SAFM. The weight of the wing in SKF is 12,129 kg, whereas, in SAFM, the wing weighs 9,416 kg. Thus, by including analytical fatigue model, the weight of the wing can be reduced by approximately 22%. Additionally, the maximum fatigue factor for the wing in SKF is 0.75, which reconfirms the point that the knockdown factor applied to account for fatigue is conservative in nature.

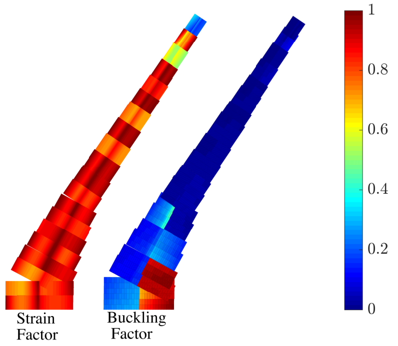

(a) Top Skin without fatigue model

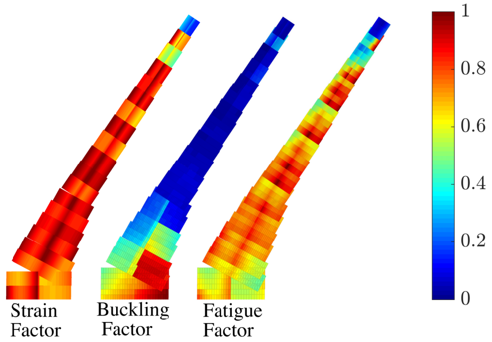

(b) Top Skin with fatigue model

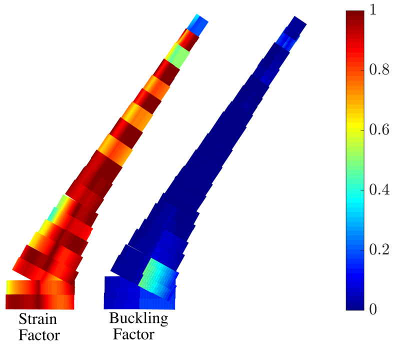

(c) Bottom Skin without fatigue model

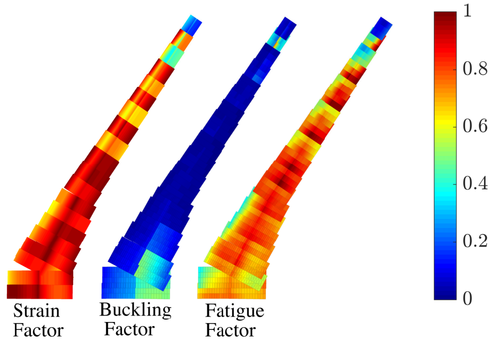

(d) Bottom Skin with fatigue model

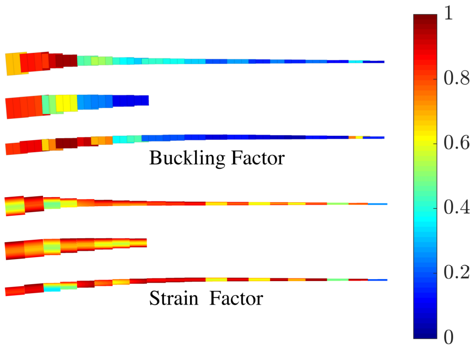

(e) Spars without fatigue model

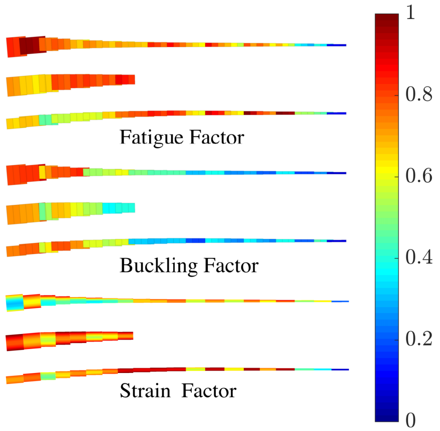

(f) Spars with fatigue model

Figure 3.12: Value of the critical constraints for the optimized CRM wing.

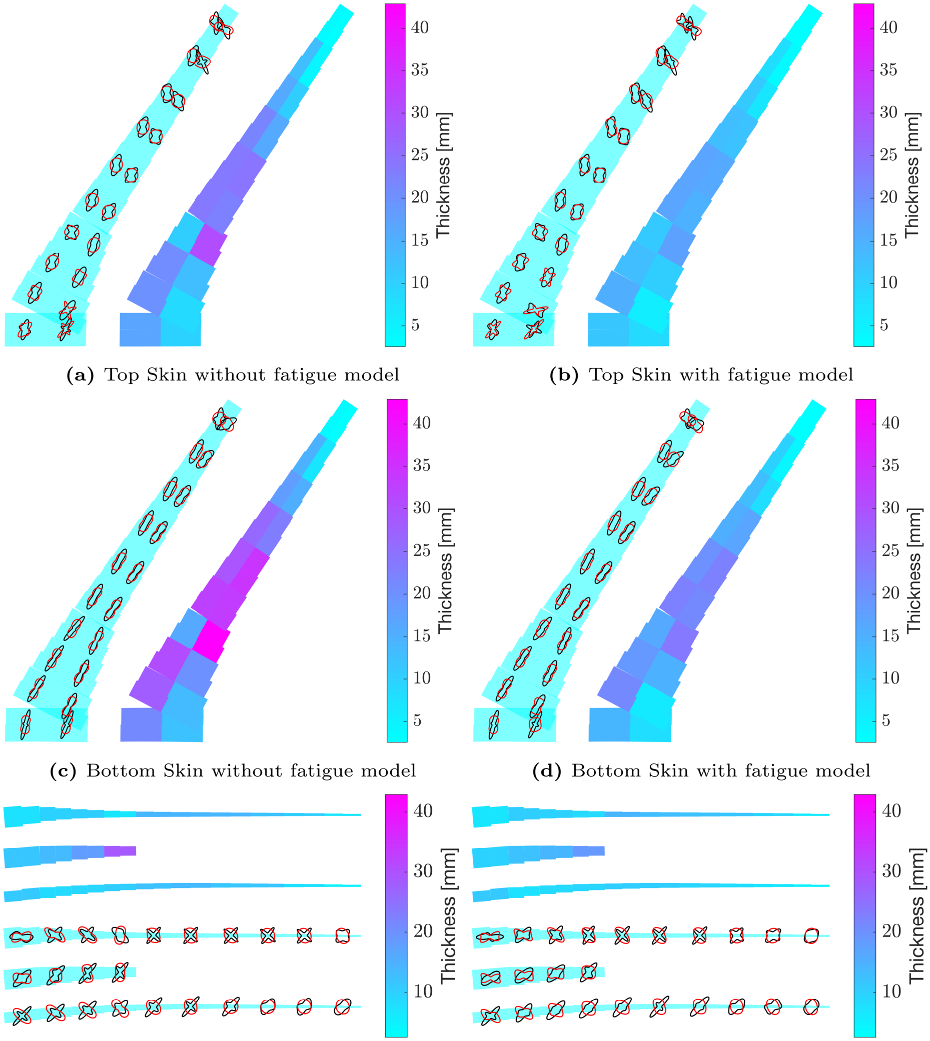

(a) Top Skin without fatigue model (b) Top Skin with fatigue model

(c) Bottom Skin without fatigue model (d) Bottom Skin with fatigue model

(e) Spars without fatigue model (f) Spars with fatigue model

Figure 3.13: Stiffness and thickness distribution for the optimized CRM wing (In-plane stiffness: black, out-of-plane stiffness: red).

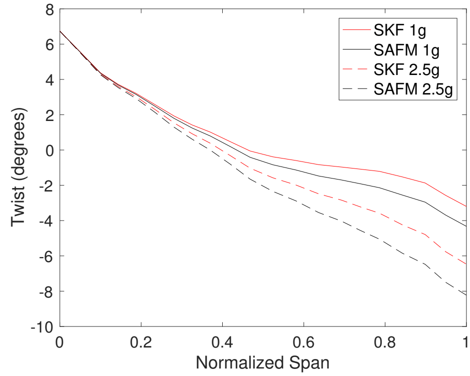

Figure 3.14: Total twist distribution for the CRM wing optimized in SKF and SAFM.

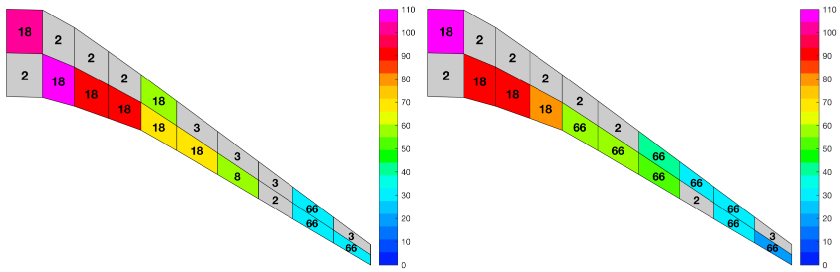

(a) Bottom Skin with fatigue model **(b)** Bottom Skin without fatigue model

Figure 3.15: Critical static and gust loads on the bottom skin of the optimized CRM wing.

3.3 SYNOPSIS

An aeroelastic optimization method including fatigue as a constraint for composite wings was formulated in this chapter. Fatigue was accounted in the optimization using the analytical fatigue model. The analytical fatigue model is a residual strength degradation model based on the method developed by Kassapoglou.

Kassapoglou's method was extended by adding a first ply failure theory to determine the failure of the laminate. Different first ply failure theories were compared to the experimental data and Tsai Wu was found to have the best mix of accuracy and ease of implementation. Furthermore, it was assumed that the initial strength distribution would follow a Weibull distribution. The predictions of the fatigue model were compared to the test results of UD and MD glass/epoxy laminate for the Wisper and the New Wisper spectrum. Reasonable agreements were found between the predicted and the experimental results, with the analytical model being conservative. Additionally, the analytical model was also extended to work with laminates described by lamination parameters instead of ply angles and stacking sequence. Since the failure criterion in the lamination parameter domain was conservative in nature, the life predictions were also conservative compared to the prediction for laminates defined by ply angles.

The developed analytical fatigue model was integrated into the aeroelastic optimization tool PROTEUS. Two optimization studies of the CRM wing were carried out, one with traditional knockdown factors applied on material allowables to account for fatigue and another one with fatigue as a constraint using the analytical fatigue model. To account for fatigue, the maximum design life of 40,000 flights based on Mini TWIST spectrum was assumed.

Results show that a composite wing is not only critical in strength and buckling but also in fatigue when accounted for explicitly rather than using the conservative knockdown factors which limit the fatigue loads to a small fraction of the limit load. The middle part of the wing is critical in fatigue and as a result, optimum stiffness and thickness distributions designed lead to a higher tip washout and thus reduced the load in the middle part. The critical gust and static loads for the optimum configurations are also different when fatigue is accounted for by the analytical model. The middle part of the wing optimized with fatigue constraint is critical with respect to static loads whereas the middle part of the wing optimized with conservative knockdown factor is critical with respect to gust loads. Furthermore, by including a mathematical fatigue model instead of a conservative knockdown factor, the weight of the wing is reduced by 22%.

4

FATIGUE AND DYNAMIC AEROELASTIC EXPERIMENTS INCLUDING THE EFFECT OF FATIGUE ON THE AEROELASTIC PERFORMANCE OF THE WING [1]

The previous two chapters have described the formulation of the aeroelastic optimization methodology with integrated gust and fatigue loading requirements. To validate the developed methodology, this chapter presents the design, manufacturing, and testing of an aeroelastically tailored composite wings. Additionally, in this chapter the effect of fatigue on the aeroelastic response of the wing is also discussed.

There is limited literature available on the aeroelastic experimental data sets of tailored composite wings. Early research has been focused on testing of wings modeled as plates (Chen and Dugundji, 1987; Landsberger and Dugundji, 1985; Sherrer et al., 1981) which are tailored to improve aeroelastic behavior using the bend-twist coupling of the composite laminate. However, for the representative

[1] This chapter is largely based on the journal paper Rajpal, D. et al. (2021) *"Design and testing of a aeroelastically tailored composite wing under fatigue and gust loading including the effect of fatigue on the aeroelastic performance*, Composite Structures, under review.

wing structure, a closed-cell cross-sectional configuration is used where the improved aeroelastic behavior originates from the extension-shear coupling of the individual laminates of the cross-section. At the German Aerospace Center (DLR), there has been a concentrated effort on optimization, manufacturing and testing of an aeroelastically tailored wing with representative cross section using composite materials (Meddaikar et al., 2017, 2016; Ritter et al., 2017). In these studies, the wing is manufactured using load-carrying skins filled with foam. The foam is used to provide resistance against buckling. Ribs and spars are not included in the wing, in order to simplify the manufacturing.

More recently at TU Delft, Werter et al. (2016) have manufactured and tested aeroelastically tailored wings having load-carrying skins filled with foam in the wind tunnel under static maneuver loadings. The designed wing employed constant thickness and stiffness along the span, such that a manufacturable stacking sequence could be obtained by a sweep over ply angles. Although the wings tested at DLR and TU Delft have tailored composite skins, they all feature foam as internal structure in place of spars and ribs. Thus, they are not entirely representative of a realistic wing as they miss the typical wingbox structure.

The current chapter extends the work done by Werter et al. (2016) by first designing and manufacturing a composite wing with an actual wing box, which includes ribs and spars such that there are clear load carrying paths; second, by testing under gust loading conditions, and third by performing fatigue tests on it. For this purpose, a carbon fiber rectangular wing is optimized subjected to static and gust loads, including the analytical fatigue model introduced in Chapter 3. The optimized wing is manufactured using UD prepreg and undergoes an experimental test campaign. The test campaign has the following steps:

1. The pristine wing is tested in the low subsonic Open Jet Facility (OJF) wind tunnel (Open Jet Facility) at the TU Delft under static and dynamic (gust) conditions. The data from this wind tunnel test is used to validate the numerical methodology of evaluating gust loads. The data will also be used to benchmark the performance of the pristine wing.

2. In the second step, using a MTS 100KN fatigue machine, the wing is fatigued to a predefined number of cycles that it is designed for. The data from the fatigue tests are used to validate the analytical model formulated for fatigue.

3. The fatigued wing is finally tested again in the wind tunnel under static and gust conditions. With this test, the effect of fatigue on the aeroelastic response of the wing is analyzed by comparing it to the response of the pristine wing measured in step 1.

The chapter starts with giving an overview of the design methodology in Section 4.1, which is formulated to optimize a manufacturable and tailored composite wing. In Section 4.2, the optimization problem is introduced and the optimized design is explained. This is followed by Section 4.3, which explains the manufacturing process of the composite wing. The experimental setup is described in Section 4.4. Finally, the experimental results are analyzed in Section 4.5, followed by the synopsis in Section 4.6.

4.1 Setup of Design Framework

To design and manufacture a composite wing optimized for gust loads and fatigue loads, a design framework is formulated, which includes, along with PROTEUS, OptiBLESS (Macquart, 2016), an open-source stacking-sequence-retrieval algorithm, and a commercial software MSCNastran.

OptiBLESS is an open-source toolbox used to retrieve blended and manufacturable stacking sequences from the lamination parameters optimized by PROTEUS. This toolbox employs a patch-based optimization strategy including blending to obtain a blendable stacking sequence from several sets of lamination parameters representing different neighboring laminates. In OptiBLESS, the stacking sequence is considered blended when the plies of the thinnest laminate patch span the entire structural component. A detailed explanation of the capabilities and the methodologies employed in OptiBLESS is given in Macquart (2016).

MSC Nastran is a standard tool for aeroelastic computation within the aerospace industry. The reason for coupling the approach with a finite element software such as MSC Nastran is threefold.

- The first reason is to have a numerical model which includes the spar flanges, since these are not modeled in PROTEUS. This is necessary in order to verify that the flange is sufficiently strong to resist crippling.
- The second reason is the correction of conservative buckling calculations in PROTEUS, which is based on idealized buckling model derived by Dillinger (2015). Besides this, the presence of spar flanges results in a stiffening effect on the wing structure, which reduces the strains in the laminates and thus needs to be accounted for in PROTEUS. By means of the higher fidelity model in Nastran, it is possible to assess the level of the conservativeness of PROTEUS analysis and apply a correction.
- Finally, using a finer mesh in MSC Nastran, a better approximation of the local stresses in the bonded spar flange and skin is obtained. The local stresses are needed to make sure the shear stress experienced by the spars, which will be transferred through the bond line, is lower than the shear strength of the adhesive bond itself.

A MATLAB routine is developed to translate the beam model from PROTEUS into a 2D shell model in MSC Nastran, making use of the wing geometry and of the laminates' properties. By combining MSC Nastran with PROTEUS, a multi fidelity design framework is formulated which optimizes the wing in a computationally efficient manner as compared to optimizing the wing only with MSC Nastran.

Figure 4.1 shows the flow diagram of the design framework used to optimize the composite wing. The first step consists of defining the wing geometry, the load cases, the initial laminate distribution and pertinent material properties. Furthermore, an initial width is chosen for the flange, which is later used for the generation of the Nastran model of the wing. The flange width is constant along the span. Based on the input variables, objective functions, design variables and constraints, stiffness and thickness optimization of the composite wing is performed within PROTEUS. This optimized design is fed to OptiBLESS, which transforms the results from the lamination parameter domain to the stacking sequence domain. After this operation, a manufacturable design in terms of feasible laminates is obtained. The new lamination parameters, associated with the stacking sequence found by OptiBLESS, are calculated and fed to PROTEUS, which analyzes the design to evaluate the incurred changes in the aeroelastic behavior. Following this step, the PROTEUS design is converted into a MSC Nastran aeroelastic model. For the first loop of the process, the model is evaluated with an initial flange width and the level of the conservativeness of PROTEUS is assessed so that the strain and buckling constraints can be corrected. From the second loop onward, a check is performed on the crippling load of the flange as defined in Kassapoglou (2013) and the maximum shear stress in the bond line. If the crippling load and maximum shear stress requirements are satisfied, the process is stopped; otherwise, a new flange size is selected and the optimization constraints are updated according to the new conservativeness assessment.

A more detailed analysis of the design framework is given in Mitrotta et al. (2020).

4.2 OPTIMIZATION STUDY

4.2.1 OPTIMIZATION APPROACH

Using the aforementioned framework, an aeroelastically tailored rectangular wing having a span of 1.75 m and a chord of 0.25 m is designed by taking into account gust and fatigue loading requirements. The wing geometrical parameters are summarized in Table 4.1. The wing has two spars located at 25% and 65% of the chord. The location of the rear spar is defined such as to guarantee a minimum web height of at least 15 mm. A total of 13 ribs is used, with spacing increasing from wing root to tip. The ribs at the root are clustered together as the skin panels are more prone to buckle. For the present case, the wing is divided into three design regions. An overview of the design regions, together with the layout

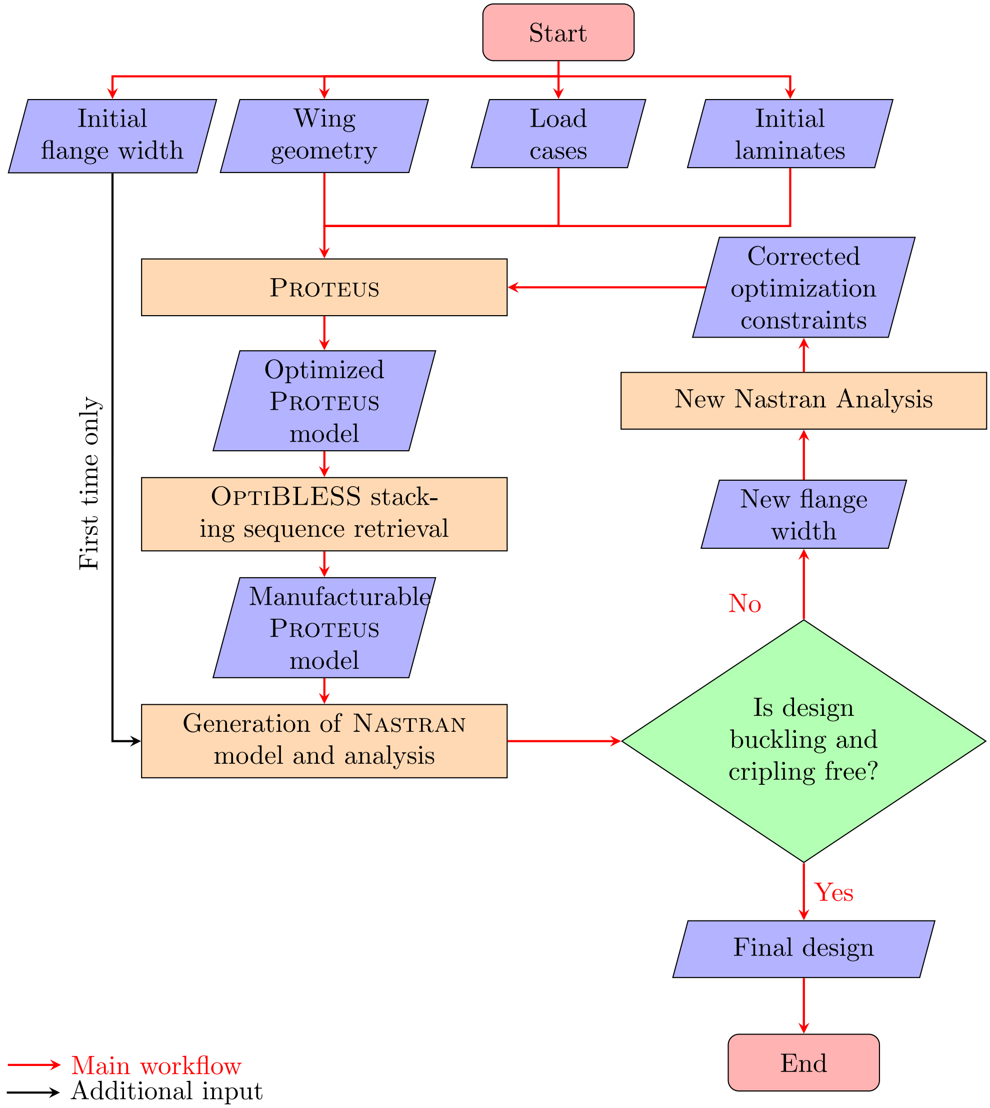

Figure 4.1: Flow diagram of the design framework.

of spars and ribs, is given in Figure 4.2.

Table 4.2 shows the material properties used for the experimental wing. Knockdown factors of 0.65 and 0.80 are used to account for damage and environment, respectively, resulting in a net knockdown factor of 0.52 which is applied to the stress allowables. Table 4.3 gives the information regarding the optimization setup

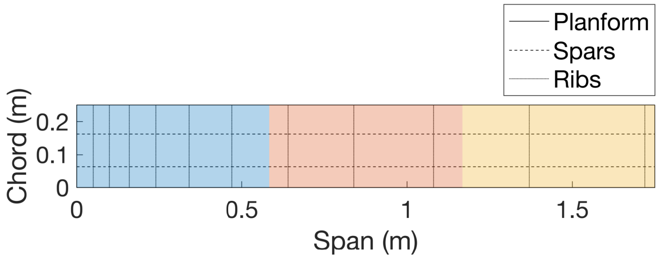

Figure 4.2: Wing planform with layout of spars and ribs. The different colors indicate the design regions.

Table 4.1: Characteristics of the experimental composite wing.

Parameter	Value
Half Span	1.75 m
Leading edge sweep angle	0 degrees
Front spar location, % chord	25
Rear spar location, % chord	65
Number of Ribs, % chord	13
Wing aspect ratio	14
Taper ratio	1
Wing chord	0.25 m
Airfoil	NACA 0010

considered in the current study.

With a goal of obtaining a light and flexible wing, the objective of the optimization is set to maximize the wing tip deflection and minimize the wing weight. The laminates in the upper and lower skins and the front and the rear spars are optimized while the laminates in the ribs are pre-defined. The top and bottom skins of the wing are divided into three spanwise laminates, whereas the front and rear spars are represented by a single laminate each. This distribution results in eight unique laminates. Laminates are symmetric and allowed to be unbalanced. For every laminate, there are eight lamination parameters and one thickness variable resulting in a total number of 72 design variables. However, the thickness of the spars is set to be 0.524 mm, corresponding to four plies, which is not further optimized. This choice is made for ease of manufacturing and to reduce the complexity of the crippling assessment. Consequently, the number of active design variables is reduced to 70. The distribution of the laminates along the top skin is shown in Figure 4.3. In the initial design, all the laminates are balanced and quasi-isotropic. In each of the laminates shown in Figure 4.3, the stiffness distribution is depicted.

With respect to constraints, a similar strategy as explained in Section 2.2.1 is implemented. Additionally, the fatigue life of the laminate is calculated for the load spectrum, which is based on Mini-TWIST (Lowak et al., 1979). Table 4.4

Table 4.2: Material properties.

Property	**Value**
E_{11} (GPa)	148.3
E_{22} (GPa)	9.3
G_{12} (GPa)	4.7
ν_{12} (−)	0.32
ρ (kg/m^3)	1,570
X_t (MPa)	2,500
X_c (MPa)	1,716
Y_t (MPa)	64
Y_c (MPa)	285.7
S (MPa)	91.2

Table 4.3: Optimization setup.

Type	**Parameter**	**# responses**
Objective	Maximize wing tip deflection + Minimize wing weight	2
Design Variables	Lamination Parameter Laminate Thickness	70
Constraints	Laminate Feasibility	72
	Static Strength	416/load case
	Buckling	768/load case
	Fatigue	184
	Aeroelastic Stability	10/load case

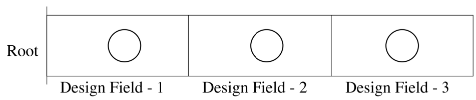

Figure 4.3: Initial guess for laminate distribution of the top skin of experimental wing.

depicts the load spectrum used to evaluate the fatigue of the designed composite wing. The spectrum consists of eight load levels where each level has thirteen different levels of stress ratio. The stress ratio has been normalized to the stress level at cruise condition. At each stress ratio, the number of cycles is different for different load levels. The eight levels are repeated based on the frequency, in a random manner to make a one block which is equal to 10,000 cycles. In reality, cycles with highest load levels occur randomly during the fatigue life and hence out of the eight levels in the spectrum, care needs to be taken that the first three levels having the highest stress ratio are not clustered together as they might have the highest effect on fatigue. The block of 10,000 cycles is repeated 10 times, to accumulate 100,000 cycles which is considered as the maximum life of the wing. For evaluating the fatigue life of the laminate, the loads obtained from the cruise load case are used as a mean load on top of which the fatigue spectrum is applied.

Table 4.4: Load spectrum used to evaluate fatigue.

		Number and magnitude of amplitude level												
Load level	Frequency per block	1 3.08	2 2.97	3 2.82	4 2.69	5 2.56	6 2.3	7 1.78	8 0.97	9 0.69	10 0.56	11 0.29	12 0.22	13 0.17
		Number of Cycles per load type												
A	1	1	4	4	4	16	18	15	2	1	8	18	15	24
B	1		4	4	4	10	11	16	1	4	5	11	16	19
C	3			4	4	18	7	16	2	5	9	7	16	12
D	19				1	31	1	1	1	1	15	1	1	4
E	120					26	1	1			13	1	1	6
F	260						1	1					1	1
G	382							1					1	1
H	220							1					1	
Total Number of Cycles per block		1	8	20	39	3,789	449	1,080	28	39	1,885	449	1,080	1,517

Table 4.5 gives the information on the load cases which are used for the current study. The first three load cases represent the static manoeuver load cases. The fourth load case is a gust load case where, for the given combination of velocity and angle of attack, ten gust gradients ranging from 2 m to 6 m were applied. These load cases represent the limit load, which is defined as the maximum load the wing is expected to experience in service. To satisfy the requirements for the ultimate load, an additional safety factor of 1.5 is applied to the strength and buckling values calculated for the limit loads.

Table 4.5: List of static and gust load cases.

Load case ID	$\mathbf{V_{eq}}$ (m/s)	**Altitude** (m)	**Load Factor** (-)	**Angle of Attack** (degrees)
1	28	0	1	3
2	28	0	2.5	7.5
3	28	0	-1	-3
4	28	0	1	3

4.2.2 OPTIMIZATION RESULTS

The optimization with PROTEUS results in stiffness and thickness distribution shown in Figure 4.4. The strain, buckling and fatigue factors of the optimized design are shown in Figure 4.5 (where more than 1 denotes failure). The inner part of the top skin and the first rib bay of the second laminate for both top and bottom skin are dominated by buckling and fatigue. With respect to strains, only the middle part of the bottom skin of the wing adjacent to the ply drop between first and the second laminate is critical. Since the thickness at the transition point between the first and the second laminate of the bottom skin drops by 40%, this region is sensitive to buckling, fatigue and strain. Looking at the stiffness distribution in Figure 4.4, the optimizer achieves the objective of maximizing the tip deflection by orienting the in-plane stiffness in all the laminates forward relative to the wing axis, resulting in reduced stiffness in the wing axis direction and thus maximizing the flexibility. For the laminates, which are critical in buckling, the out of plane stiffness is tailored as well.

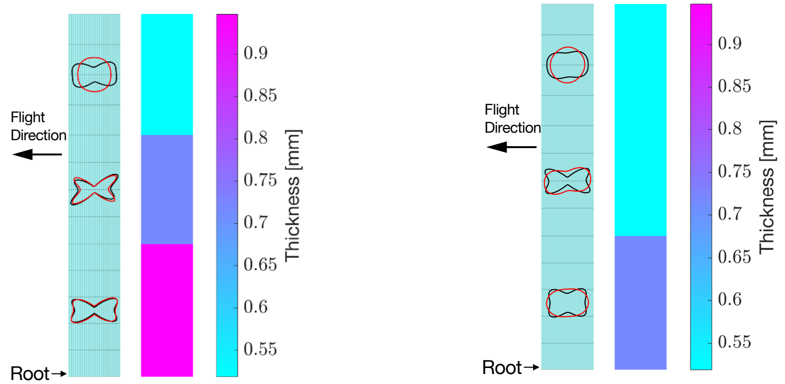

(a) Top Skin. **(b)** Bottom Skin.

Figure 4.4: Stiffness and thickness distribution for the optimized wing (Black: In-plane stiffness, Red: Out-of-plane stiffness.).

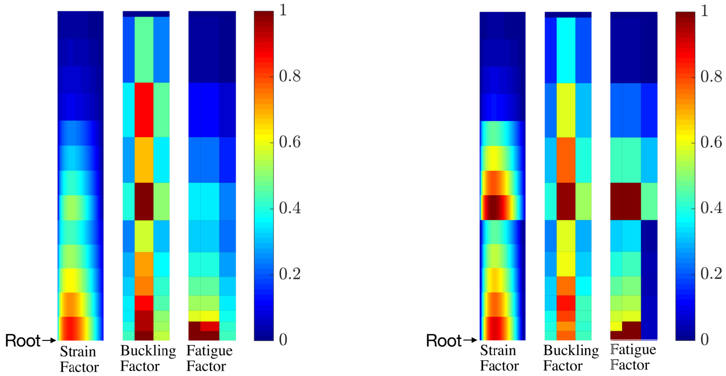

(a) Top Skin. **(b)** Bottom Skin.

Figure 4.5: Strain and buckling factor distribution on the optimized wing.

OptiBLESS is then used to retrieve the blended stacking sequences from the lamination parameters optimized by PROTEUS. The resulting stacking sequences of top and bottom skins and the spars are given in Table 4.6. The front and rear spars have the same stacking sequence and since they are not critical for any constraints, they are not mentioned further in the current discussion. The use of OptiBLESS to retrieve blended stacking sequences inevitably affects the thickness and stiffness of the laminates. The effect can be observed in Figure 4.6. The only laminate undergoing a change in laminate thickness smaller than 5% is the one corresponding to the first design region of the top skin. All the other laminates experience a 10 to 30 percent change in thickness, caused by the fact that the blended laminate thickness must be a multiple of the ply thickness. Moreover, it can be observed that, in most cases, the blended laminates are thinner than the optimal laminates. The reason for this is twofold. First, the result of the optimization performed in OptiBLESS is influenced by the bounds set in terms of number of plies. In the present case, the bounds are set such that manufacturable design is not conservative with respect to the PROTEUS result. Furthermore, the simultaneous symmetry and blending constraints on the laminates forces the OptiBLESS to remove an even number of plies at the ply drops. This leads to thinner laminates in the outboard region compared to PROTEUS result.

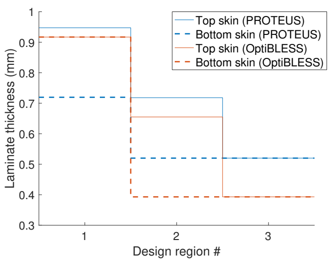

(a) Laminate thickness.

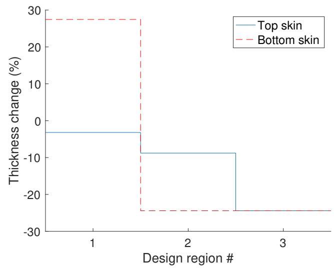

(b) Change in laminate thickness.

Figure 4.6: Comparison between the thickness of non blended and blended laminates obtained from PROTEUS and OptiBLESS, respectively.

As far as the change in stiffness is concerned, Figure 4.7 shows a comparison between the stiffness polars of the optimum and of the blended laminates. As already noticed with the stacking sequence table, the stiffness is mainly directed away from the span axis, both for the optimum and the blended laminates and especially considering the in-plane stiffness. However, substantial differences can be observed between the stiffness of the optimum and the blended laminates. Only the in-plane stiffnesses of the first design region of both skins are well matched and the quality of the match deteriorates progressively in the following design regions. This is the consequence of blending requirements combined with the relatively small number of available plies. In fact, the laminate of the first design region of each skin is the thickest and this gives to the optimizer used in OptiBLESS a design space large enough to match the optimum stiffness. However, when switching to the laminate of the adjacent patch, the design space is reduced both by the need to continue some plies from the previous patch and by the reduced number of plies. This makes the matching of both in-plane and out-of-plane stiffnesses over the entire skin very challenging.

Table 4.6: Stacking sequence table of top and bottom skins and spars, ply angles in degrees.

Top skin			Bottom skin			Spar		
Design region #			Design region #			Design region #		
1	2	3	1	2	3	1	2	3
55	55	55	−75	−75	−75	70	70	70
−65	−65		50			−60	−60	−60
75			−30			−60	−60	−60
−70	−70	−70	55	55	55	70	70	70
75			−30					
−65	−65		50					
55	55	55	−75	−75	−75			

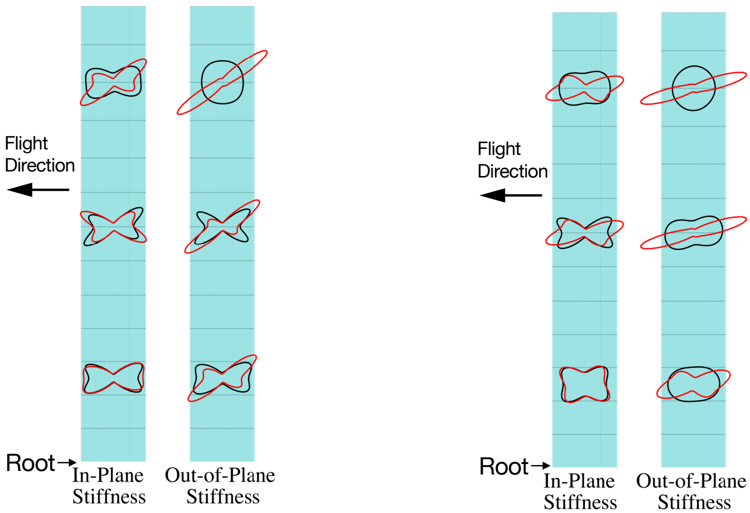

(a) Top Skin.

(b) Bottom Skin.

Figure 4.7: Comparison between the stiffness polars of non blended and blended laminates obtained from PROTEUS and OptiBLESS respectively (Black: PROTEUS design, Red: OptiBLESS design.).

4.3 Manufacturing of the Wing

The optimized wing with a span of 1.8 m and a chord of 0.25 m is manufactured using a hand layup technique using IM7/8552 UD prepreg. The experimental wing is extended by 50 mm at the root with respect to the nominal span of 1.75 m. An aluminum block is inserted inside the first 50 mm of the wing-box section to facilitate the clamping mechanism of the wing. A female half mold is used to manufacture the skins and male mold is used to manufacture the spars. Both molds are milled out of aluminum. To connect the top and the bottom skins, a bridging strip called as Leading Edge Strip (LE strip) is also manufactured using a separate aluminum male mold. All the molds are designed with a tolerance of 0.5 mm. The ribs are cut from prefabricated 3 mm thick quasi-isotropic carbon fiber plates. All the components, namely: top skin, bottom skin, front spar, rear spar and the LE strip are cured individually and then bonded together using Araldite AW 4858. To monitor strains experienced by the wing, an optical strain fiber sensor is attached in a criss-cross pattern to the bottom skin of the wing using a super-glue. The advantage of such a strain fiber is the high resolution of the strains obtained along the length of the fiber. The optical fiber used for strain sensing in the current experiment is a 5 m long LUNA HD-FOS strain sensor. The sensor is based on Rayleigh backscattering.

The manufacturing procedure of building the composite wing is segmented into six main parts, starting with cutting of the necessary patches, laying-up of the patches in the mold followed by curing, trimming, surface preparation and finally bonding. The following steps give more insight into the steps involved in manufacturing of the composite wing.

- In the first step, the UD prepreg roll is cut into the individual patches having required dimensions and ply orientation using the GERBER laminate cutting machine at the Delft Aerospace Structures and Materials Laboratory (DASML). The cutting bench, along with the prepreg roll, can be seen in Figure 4.8a. Since the width of the roll, used to cut the patches, is 1200 mm, it is not possible to have single patches having a length of 1.75 m with fiber orientations larger than 40 degrees. Therefore, for patches having fiber orientations larger than 40 degrees, smaller sub-patches are joined by aligning them side by side along the fiber orientation to get a longer patch. Care is taken to make sure that no two such joints in adjacent plies lined up with each other in order to facilitate load transfer and minimize stress concentration effects. Figure 4.8b shows the side view of the layup of the top skin where the dashed line indicates the region of the joined sub-patches.

- The trimmed patches are moved to the laminating clean-room facility at the DASML where the process of laying-up is performed. The patches are placed on the mold based on the stacking sequence of each part as detailed in Table 4.6. After every three layers, debulking of the stacked plies for around 5 minutes is done to consolidate the plies to the tooling and force out any trapped air caught between the individual layers. Once all the plies are layed up, the mold is covered with perforated foil to allow the excess resin to flow out. A breather material is put on top of the perforated foil and finally, a vacuum bag covers the entire part. Figure 4.8c depicts the top skin being debulked after laying up the first three layers and Figure 4.8d shows the top skin vacuum bagged just before putting it in the autoclave for curing.

- The vacuum bagged part is then cured in the autoclave. The cure process followed the cycle recommended by the material supplier which lasts approximately 6 hours.

- The cured skins, spars and the LE strip are trimmed into the right dimensions and the ribs are cut from the quasi-isotropic carbon fiber plates to the required dimensions using a CNC water-jet cutting machine.

- To achieve good adhesion and improve the durability of the bonded structures, the surface to be bonded is mechanically abraded using sandpaper and cleaned using acetone to remove any contaminations. A limited number of contact angle measurement tests (water break) is done to make sure the quality of the surface preparation is optimal for bonding.

- Once all the parts are trimmed and the surfaces are prepared for bonding, the bonding of the entire wing starts. Since there is a tolerance of 0.5 mm in the mold designs, a constant bond line thickness of 0.5 mm is targeted. Care is taken to avoid creation of bond-lines with varying thickness by uniformly spreading the adhesive paste along the bonded surface. In the bonding process, first, the front and the rear spars and the ribs are bonded using the aforementioned adhesive paste. Figure 4.8e depicts the bonded skeleton of ribs and spars.

- Next, the top skin is placed in the mold and the skeleton is bonded to the top skin. The LE strip is also bonded to the top skin of the wing. Weights are placed on the skeleton to get a good bond between the spars, ribs and the skin. Figure 4.8f shows the skeleton placed on the top skin. Additionally, a chemically etched aluminum block is also bonded to the root of the top skin. This block is later used to clamp the wing to the test setup.

- The optical strain fiber is then attached to the bottom skin of the wing using a super-glue. In the first half of the bottom skin, the fiber is layed out in a criss-cross pattern to get strains in 3 directions, which can then be later post-processed to get normal strains and shear strain. In the criss-cross pattern, the angle between the each segment is 90 degrees and the length of each segment is 25 mm. The segments are oriented at 45 degrees and -45 degrees alternatively with respect to the span of the wing. The radius of the corner is 5 mm. Due to the constraint on the length of the fiber, in the second half of the wing, the fiber is layed out in a straight line along the span of the wing. The drawing of the fiber pattern is shown in Figure 4.8g.

- Finally, the wing is closed by placing, the bottom skin with the fiber attached, on the top skin with the skeleton, and glued together with the adhesive paste. Care is taken to match a number of locations around the perimeter of upper and lower skin and that the upper skin is lowered uniformly to the lower one to avoid the creation of bond-lines with varying thickness. Figure 4.8h shows the bottom skin with the attached fiber and the top skin with skeleton glued just before closing the wing.

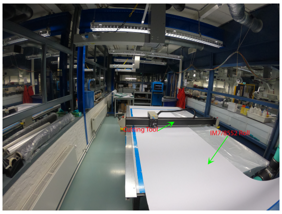

(a) The GERBER laminate cutting bench.

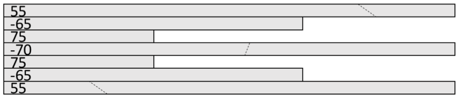

(b) Side view of the layup of the top skin (Text indicates the ply angle and the dashed line indicates the region of the joined sub-patches).

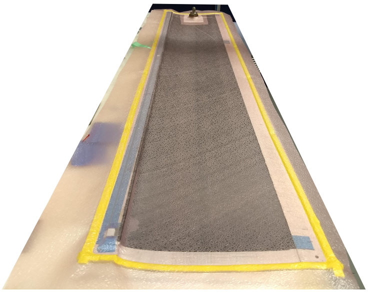

(c) Debulking of the top skin of the wing.

(d) Vacuum bagging of the top skin of the wing.

(e) Bonded skeleton consisting of spars and ribs.

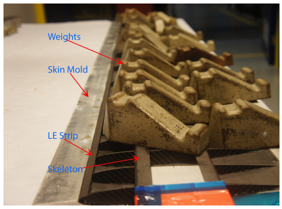

(f) Skeleton being bonded to the top skin of the wing.

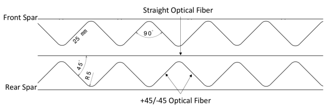

(g) Drawing of the fiber-pattern.

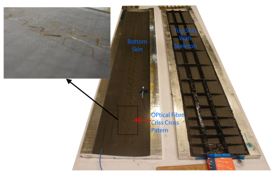

(h) Two halves of the wing before being closed.

Figure 4.8: Manufacturing process.

4.4 Experimental Setup

The aim of the experimental campaign is twofold.

1. The first one is to validate the numerical methodology of designing a composite wing with fatigue as an active constraint.

2. The second is to assess the effect of fatigue on the aeroelastic response of the wing.

For this purpose, a five month experimental campaign is conducted which involves two wind tunnel tests and one fatigue test. The Ground Vibration Test (GVT) of the wing is performed using the fatigue test assembly.

4.4.1 Wind Tunnel

The static and dynamic aeroelastic experiments are performed in the wind tunnel at the TU Delft. The wind tunnel is an OJF with an octagonal test section of 2.85 m $\times$ 2.85 m and has a maximum velocity of up to 35 m/s. The test setup consists of the gust generator, the manufactured composite wing and the measurement systems. Figure 4.9 depicts the experimental setup along with the major components.

The gust generator is a device that produces unsteady flows in the form of sine and cosine gusts. The gusts are produced by two rectangular gust vanes with a symmetric NACA 0014 airfoil oscillating in pitch around an axis located at 23.7% of the its chord (Lancelot et al., 2017). The gust vanes are supported by an aluminum frame and are placed in front of the outlet of the wind tunnel. The gusts produced by the gust generator have a maximum frequency of 10 Hz and maximum amplitude of 10 degrees. The gust vanes are controlled through the interface implemented in the National Instruments LABVIEW environment.The characteristics and the capabilities of the gust generator are described in more detail in Lancelot et al. (2017).

The measurement systems used in the wind tunnel are the balance, scanning vibrometer and fiber optic sensing. All the measurement systems are synchronized with the gust generator using a trigger signal that is sent from the gust generator controller.

To measure the dynamic response, the dynamic loads are measured at the root of the wing with a six-component balance. The reference point of the balance is 168.5 mm below the mounting plate which needs to be accounted for while processing the wing root moments. Figure 4.10 shows the axis system and the dimension of the balance. The wing is mounted on the balance through the wing mount and the balance is attached to the turn table. The turn table is a device which is used to change the angle of attack that the wing experiences by rotating the balance and wing setup. A splitter table is used to make sure there is clean airflow flowing over the wing.

The Polytec PSV-500 scanning vibrometer is used to measure the static and dynamic displacements of the composite wing. The polytec system is a single point non contact scanning vibration measurement system. With the vibrometer, ten points: five points each along the leading and the trailing edge of the wing, are monitored. Figure 4.9 shows the location of the point on the wing.

The LUNA ODiSI-B, which is a fully distributed strain measurement system with up to 1.28 mm spatial resolution, is used as fiber optic sensing system. The ODiSI system uses a Optical Frequency Domain Reflectometer (OFDR), which is used to analyze the local backscatter light intensity. The optical fiber from the wing is connected to the LUNA ODiSI-B through the OFDR. With this system, the spatial resolution for data acquisition depends on the acquisition frequency: the higher the acquisition frequency the lower the spatial resolution. For the current experiments, the strain data is acquired every 5 mm with an acquisition rate of 100 Hz.

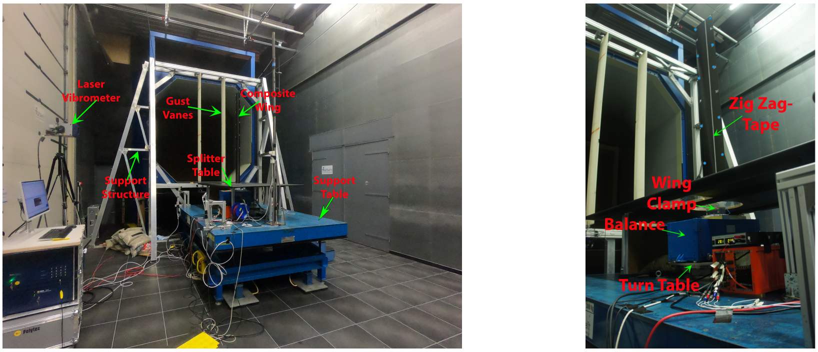

Figure 4.9: Wind tunnel setup (blue dots represent the points monitored by the vibrometer).

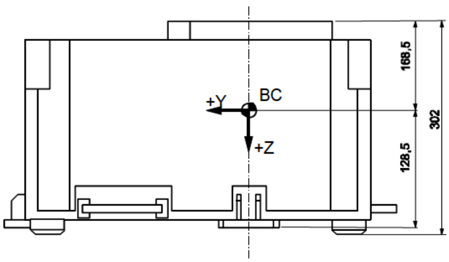

Figure 4.10: Balance axis system and dimension (all the dimensions are in mm).

4.4.2 Fatigue Test

To perform a realistic fatigue test of the composite wing, a distributed load equivalent to the aerodynamic load wing encounters during flight needs to be applied. For this purpose, a whiffle tree is designed and manufactured to distribute the single actuator load from the fatigue machine into several discrete loads on the wing, thus approximating the distributed load on the wing. The discrete loads are applied through a cradle which is a wooden pad with a rubber lining.

The whiffle tree is designed and optimized to match the spanwise distribution of shear force, bending moment and torque obtained from PROTEUS for the first load case described in Table 4.5. This is also the cruise load case. The distributed loads are assumed to scale linearly with the load-factor. Thus all load shapes can be extrapolated from the 1G cruise shape. The design variables for the whiffle tree are as follows

- The number of cradles.
- The fraction of the total load taken by each cradle.
- The spanwise location of each cradle.
- The chordwise location at which the load was introduced in all cradles.

It follows that, for a whiffle tree with N cradles, $2N+1$ optimization variables will be present. The cradles are modelled as point loads and a gradient based optimizer is used to find an optimal design. Since it is possible to generate a different optimal design for each unique number of cradles, several optimal designs are analyzed. Using less than four cradles results in too large of an error between the target distributions obtained by PROTEUS and the load distributions achieved by the whiffle tree. Using more than six cradles only gave very marginal improvements. Figure 4.11 shows the percentage error for the first 1.2 meters of the wing between the bending moment distribution achieved with different number of cradles in the whiffle tree and the target distribution obtained by PROTEUS. Thus, the design with six cradles is selected for manufacturing the whiffle tree.

Table 4.7 shows the details of the whiffle tree design and Figure 4.12 shows the sketch of the assembled whiffle tree. Figure 4.13 compares the spanwise distributions of the shear force, torsion and bending moment induced by the whiffle tree compared to the target distribution obtained by PROTEUS. As can be seen, there is a good match with shear force with maximum error less than 10% and an excellent match with the bending moment where the maximum error is less than 2%. The error with torsional moment is on the higher side with maximum error around 20%. The main reason for a higher error is the design choice that the load distribution between front and rear spar is the same for all the cradles. This design choice is made for the ease of manufacturing. If the load distribution

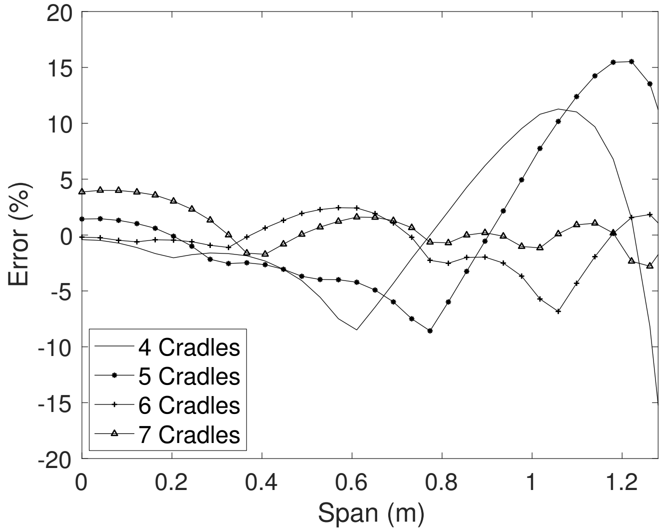

Figure 4.11: Percentage error between the bending moment distribution achieved with different number of cradles in the whiffle tree and the target distribution obtained by PROTEUS.

is tailored for each separate cradle, then the match with the torsion could be improved. As the torsional loads applied by the whiffle tree are lower than the target loads and the angle of rotation of the wing is negligible, the error of 20% is deemed to be acceptable.

Table 4.7: Summary of the final whiffle tree.

Cradle Number	Spanwise location (%)	Fraction of total load (%)	Fraction assigned to front spar (%)
1	13.71	20.65	96.31
2	26.86	21.8	96.31
3	48	17.96	96.31
4	61.71	14.27	96.31
5	78.29	19.2	96.31
6	94.73	6.12	96.31

The whiffle tree is assembled using the spreader bars which are fashioned out of slotted aluminum beams, with a 40 mm by 40 mm cross section. The links between bars are created using carabiner hooks connected to a pair of $M8$ lifting eye bolts (one on each beam). The lifting eye bolts are in turn connected to the beams by means of a T-slot nut that fits in a grove running along the beam's length. The bottom bars are linked to the cradles by means of a carabiner, which is in turn attached to a D-shackle running through the cradle's thickness. The master beam is connected to the actuator of the fatigue machine by means of a

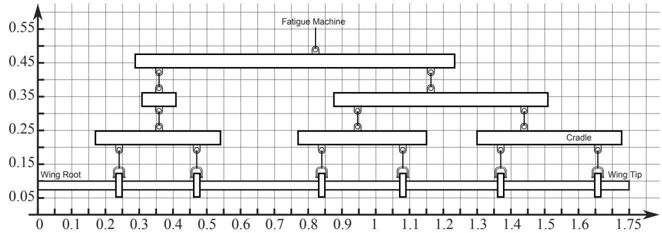

Figure 4.12: Sketch of the whiffle tree setup (dimensions of the axes are in m).

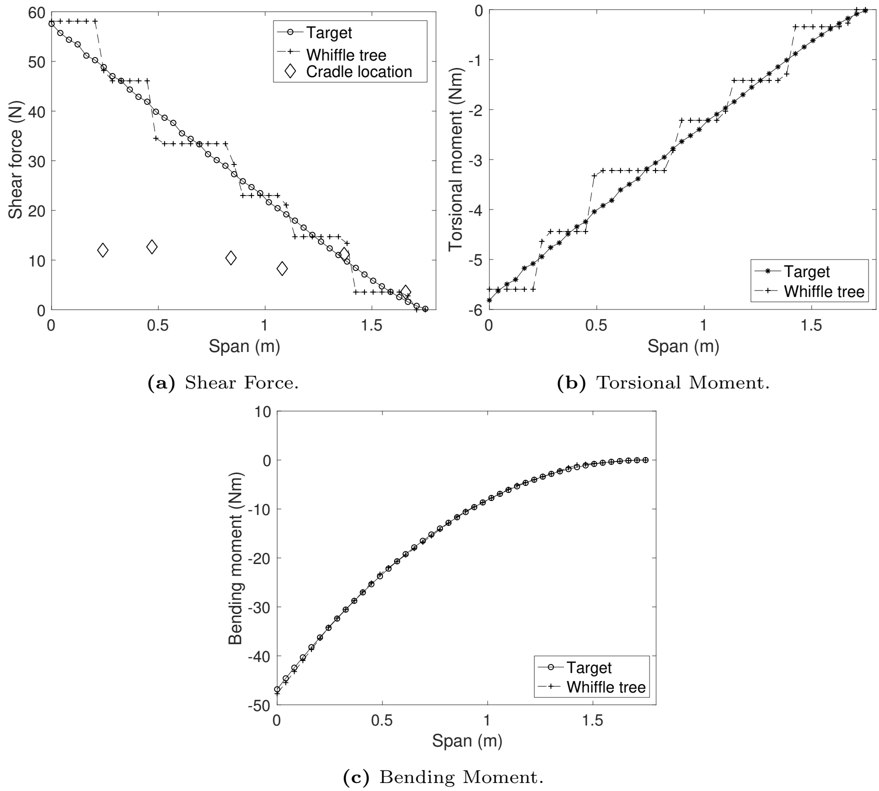

Figure 4.13: Spanwise distributions of the shear force, torsion and bending moment induced by the whiffle tree compared to the target.

lifting eye bolt and a pin. Cradles are fashioned out of 18 mm thick plywood. The majority of these components can be seen in Figure 4.14. Table 4.8 gives information on the materials of the components used to manufacture whiffle tree.

For each whiffle tree component, it was ensured that fatigue failure would never occur during the entire span of testing. If fatigue data for the particular com-

Table 4.8: Details of the components used to build the whiffle tree.

Component	Manufacturer	Material
Slotted aluminum beams	Item24	Aluminum 6060 alloy
Lifting eye bolts	Fabory	Stainless Steel
Nuts and Bolts	Fabory	Stainless Steel
Carabiners	Seilflechter	Stainless Steel
D-shackles	Toolstation	Galvanized Steel
Cradles	Gamma	Plywood

ponent or material was available, it was ensured that the most critical load case would be below the said endurance limit. If no fatigue data was available, it was ensured that the most critical load case would always be at least 10 times smaller than the static failure load

4

The machine used for the fatigue testing of the composite wing is the MTS 100 kN fatigue machine. The machine has a maximum speed of 141 mm/s and a maximum displacement of 200 mm. Figure 4.14 depicts the composite wing mounted in the fatigue setup. The wing is clamped onto the blue steel frame which supports the wing and connects it to the fatigue machine. An external load cell was connected between the machine and the wing through the whiffle tree. To measure the displacement of the wing, a Micro Epsilon laser sensor with a maximum range of 100 mm is mounted on the fatigue machine located at a distance of 650 mm along the span from the wing root.

Figure 4.14: Fatigue test setup.

4.4.3 GROUND VIBRATION TEST

To identify the natural frequencies of the composite wing, a GVT is performed on the wing in the clamped condition when it is attached to the blue steel frame for the fatigue testing. Figure 4.15 displays the setup of the wing during the GVT.

A rowing hammer method is used to perform the GVT. Eighteen excitation points are chosen with 10 points on the wing itself and the remaining eight points on the supporting structure. The response is measured at two locations along the wing: at 75% wing span and at the tip of the wing. At each of these locations, there are two accelerometers; one measuring the in-plane response and another measuring the out-of-plane response. The responses are recorded through a National Instruments data card in the LABVIEW (Elliott et al., 2007) environment. Simcenter Testlab is then used to analyze the response and calculate the modal frequencies of the structure.

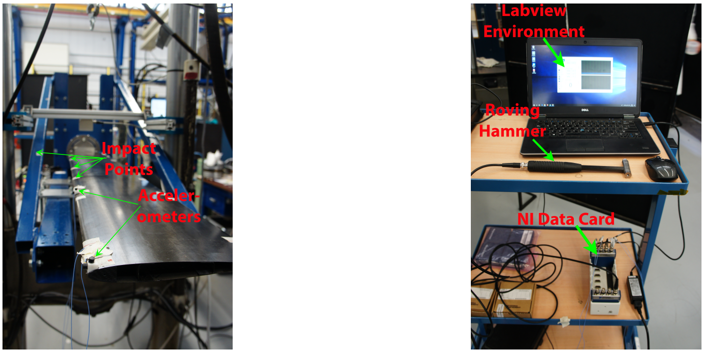

Figure 4.15: GVT setup.

4.5 Results

As mentioned before, the experimental campaign consisted of two wind tunnel tests and one fatigue test. The first wind tunnel test aims at validating the static and dynamic aeroelastic model from PROTEUS and benchmarking the performance of the pristine wing. With the fatigue test, the objective is to validate the fatigue life prediction of the developed analytical fatigue model in PROTEUS. Finally, the aim of the second wind tunnel test is to understand the effect of fatigue on the aeroelastic response of the wing. Before presenting the discussion on the wind tunnel tests, the results from the GVT on the structural dynamic characterization of the composite wing is presented below.

4.5.1 Ground Vibration Test Results

Table 4.9 depicts the measured experimental natural frequency and the calculated natural frequency of the PROTEUS model. As can be seen, except the second and third bending mode, all the other modes differ by more than 10 %. The predictions for the second and third bending are relatively better with an error

Table 4.9: Comparing natural frequency of the wing obtained experimentally with original PROTEUS model.

Mode no.	Mode Description	Experiments (Hz)	PROTEUS (Hz)	Difference (%)
1	First Bending	5.40	6	11.1
2	Second Bending	25.99	26.39	1.9
3	First Inplane Bending	43.21	50.91	17.8
4	Third Bending	67.55	68.97	2.1
5	First Torsion	120	131.75	9.7
6	First Bending and Torsion	133.26	144.82	8.7

Table 4.10: Comparing natural frequency of the wing obtained experimentally with modified PROTEUS model.

Mode no.	Mode Description	Experiments (Hz)	Modified PROTEUS (Hz)	Difference (%)
1	First Bending	5.40	5.66	4.8
2	Second Bending	25.99	25.93	-0.2
3	First Inplane Bending	43.21	49.47	14.4
4	Third Bending	67.55	66.24	-1.9
5	First Torsion	120	126.66	5.5
6	First Bending and Torsion	133.26	136.11	2.1

of around 3%. There are three main reasons for the discrepancy in the natural frequencies. First is the distribution of the masses. In the numerical model of PROTEUS, the LE strip is not modeled. Also, the added weight of the bond line and the four accelerometers are not modeled. This would lead to a different mass configuration, which could impact the natural frequencies. Second is the presence of the bond line and spar flanges, which affects the stiffness of the structure resulting in an effect on the natural frequencies. Both bond line and spar flanges are not modeled in PROTEUS. Finally, in the numerical model, a perfectly clamped boundary condition is used to evaluate the natural frequency, whereas, during the experiments, it is theoretically impossible to obtain a perfectly clamped wing. The clamping mechanism was made out of Aluminum which, because of lower stiffness compared to a material like steel, would induce some flexibility, affecting the natural frequencies.

The PROTEUS model is modified by modeling the LE strip and taking into account the weights of the accelerometers. Table 4.10 shows the comparison of the experimental results and the modified PROTEUS model. As can be seen, except for the first in-plane bending mode, all the other modes have an error of less than 5.5%. The frequency of the first in-plane bending mode is approximately 9 times the frequency of the first bending mode and hence it will not have much influence over the aeroelastic response of the wing. Thus the current modified PROTEUS model is deemed to be sufficient for the objectives of the current experimental tests and hence, no further stiffness update is carried out on the

Table 4.11: Test matrix for the wind tunnel tests.

	Static tests	**Dynamic tests**
Wind Velocity (m/s)	14,26	14,26
Static Angle of Attack (degrees)	-1,2,4,6,8,10	4
Gust frequency (Hz)	(-)	2,4,8
Gust amplitude (degrees)	(-)	5,10

PROTEUS model.

4.5.2 First Wind Tunnel Test

In the wind tunnel test, both static and dynamic tests have been performed on the pristine wing. The test matrix for these tests is shown in Table 4.11. The aim of the first wind tunnel test is to compare the experimental results from static polar and gust envelope with the numerical results obtained from PROTEUS in order to validate the tool. Also, the results are used to benchmark the performance of the pristine wing.

As can be seen in Figure 4.9, the wing is equipped with zig-zag tapes on pressure and suction side of the wing in order to force boundary layer transition from laminar to turbulent and, in this way suppress any potential laminar separation bubble. A tape of 0.2 mm is applied on the suction side at 5% of the chord and a tape of 0.5 mm is applied on the pressure side at 65% of the chord. These values are selected according to the method presented by Braslow and Knox (1958) and using airfoil pressure distributions predicted by XFoil (Drela, 1989).

Static experiments

Figure 4.16 depicts the lift coefficient of the wing for various angles of attack at a velocity of 26 m/s. With a mean error of around 8%, there is a reasonable agreement between PROTEUS and the experimental results with PROTEUS slightly over predicting the lift curve slope. One possible reason for the over prediction of the lift coefficient is the application of the zig-zag tape. The zig-zag tape causes the forced transition of the flow from laminar to turbulent and this effect is not captured by PROTEUS as the aerodynamic solver is based on the inviscid Vortex Lattice Method (VLM). To understand the effect of zig-zag tape on the lift coefficient, a viscous and an inviscid analysis of the NACA 0010 airfoil is carried out using XFoil (Drela, 1989). For the viscous analysis, forced transition at 5% and 65% of the chord on the top and bottom skin of the airfoil is applied, respectively. Figure 4.17 compares the lift coefficient obtained with viscous and inviscid analysis. As can be seen, there is a mean error of around 10% between the two analyses for a 2D airfoil. This contributes to the overprediction of the lift coefficient by PROTEUS compared to the experimental results. Figure 4.18 depicts

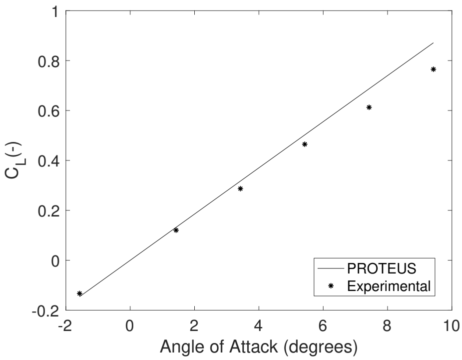

Figure 4.16: Comparison of the lift coefficient of the wing measured experimentally with calculated numerically.

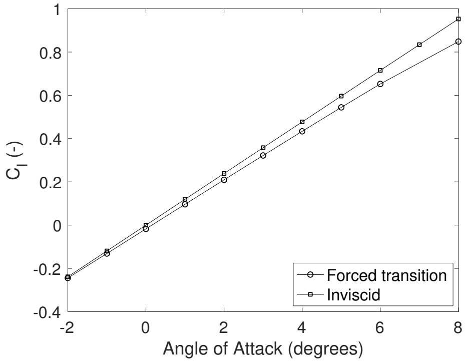

Figure 4.17: Comparison of the 2D lift coefficient between viscous and inviscid solver.

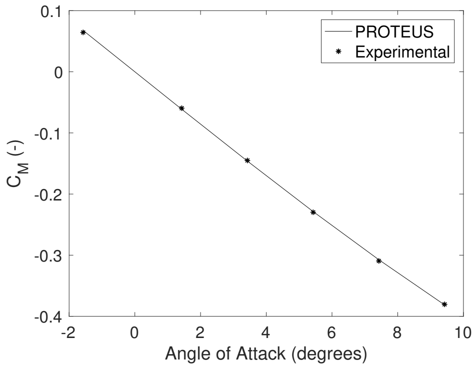

Figure 4.18: Comparison of the root bending moment coefficient of the wing measured experimentally and numerically.

the root bending moment coefficient of the wing for various angles of attack at a velocity of 26 m/s. There is an excellent agreement between PROTEUS and experimental results with an average error of less than 1%.

Figure 4.19 compares the maximum longitudinal normal strain on the bottom skin measured using the optical fiber to the predictions from the PROTEUS. As can be seen, there is a good agreement with an error of less than 3%. The maximum strain occurs at 0.58 m from the root where the first laminate transitions into the second laminate with a ply drop of 4 plies. Figure 4.20 plots the longitudinal normal strain distribution along the span of the bottom skin. There is a good match for the strains predicted from the PROTEUS and the experimental results at a lower angle of attack as the error at the peak strain is less than 0.5%. As the angle of attack increases, the error between the peak numerical and the experimental strain increases to 5.5%. This is due to the fact that as the angle

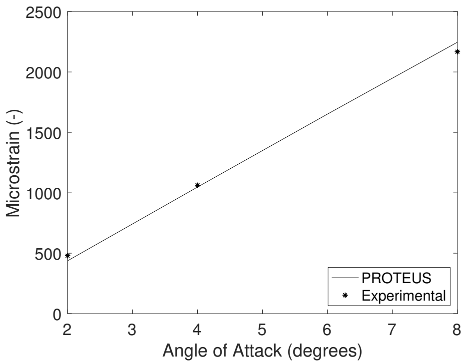

Figure 4.19: Comparison of the maximum longitudinal strain measured numerically and experimentally.

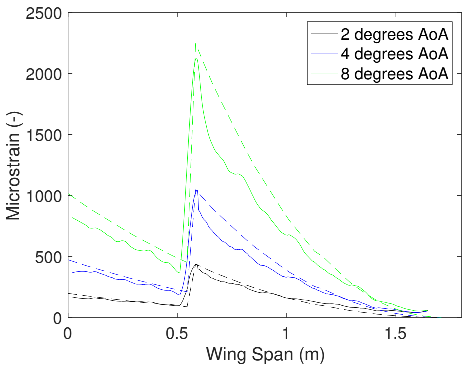

Figure 4.20: Comparison of the longitudinal strain along the span measured numerically and experimentally ((−−) PROTEUS and (-) Experimental).

of attack increases, the difference between the lift predicted by PROTEUS and experiments increases, which leads to a difference in the deformation of the wing leading to a higher difference in the strain experienced by the wing.

Dynamic experiments

For the dynamic measurements, the support table that can be seen in the wind tunnel setup depicted in Figure 4.9 has the first eigenmode at around 5 Hz. Since the first bending mode of the wing is also at 5.4 Hz, the gust response of the wing is influenced by the dynamics of the support table. In an effort to clearly separate the eigenfrequency of the support table and the wing, the wing is fitted with a tip mass of 400 g, which reduces the first bending frequency of the wing from 5.4 Hz to 3.3 Hz.

From here on, all the dynamic results presented will be of the wing fitted with the tip mass. Moreover, only the incremental results due to the gust are considered in the current comparison.

Figure 4.21 and 4.22 depict the maximum lift and root bending moment coefficients measured experimentally and calculated numerically at different gust frequencies and gust amplitudes for a velocity of 26 m/s. For the numerical prediction, a gust speed correction factor of 0.48 is applied to account for a decrease in the gust amplitude experienced by the wing (Lancelot et al., 2017). As can be seen, there is a reasonable match between experimental and numerical predictions with a maximum error of around 10%. The error in the prediction can be attributed to the effect of zig-zag tape and the uncertainty in the gust speed correction factor. In general, the gust speed correction factor depends on the distance of the wing from the gust generator, the speed of the wind tunnel and the frequency of

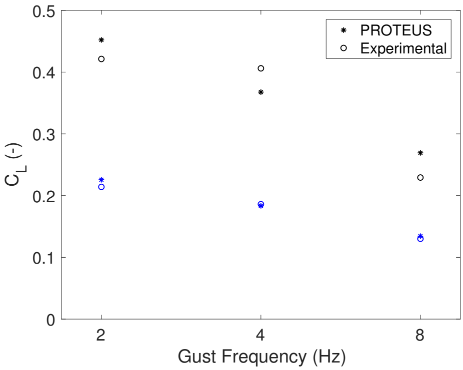

Figure 4.21: Maximum dynamic lift coefficient measured at different gust frequency and amplitude (Blue: 5 degrees gust amplitude, Black: 10 degrees gust amplitude).

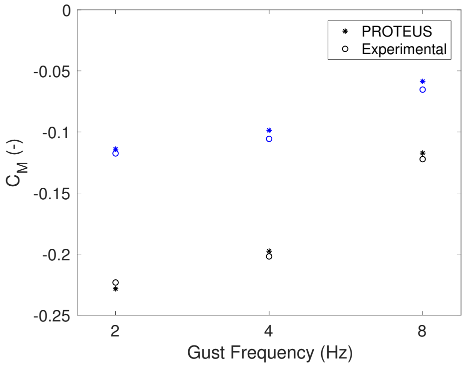

Figure 4.22: Maximum dynamic root bending moment coefficient measured at different gust frequency and amplitude (Blue: 5 degrees gust amplitude, Black: 10 degrees gust amplitude).

4

the gust. A small change in either of these factors could lead to a different correction factor. Based on the data available in Lancelot et al. (2017), a constant correction factor of 0.48 can be reliably estimated. Encouragingly, the trends predicted by PROTEUS for the maximum lift and root bending moment coefficient follow the experimental evidence with the critical gust having a frequency of 2 Hz.

Figure 4.23 compares the maximum tip deflection obtained numerically and experimentally at different gust frequencies and amplitudes and velocities. There is a good match for the tip displacements between the PROTEUS and experimental results with a maximum error of less than 10% except for the two measurement points, which have a frequency of 2 Hz and 4 Hz, gust amplitude of 10 degrees and velocity of 26 m/s. For these two measurement points, the error was due to the scanning vibrometer acquisition system not being able to capture the large tip displacement at those points. Figures 4.24 and 4.25 compare the time history of the tip displacement for a gust frequency of 4 Hz and 8 Hz having a velocity of 26 m/s and gust amplitude of 10 degrees. As can be seen, with a gust frequency of 8 Hz, the numerical tip displacement follows the experimental result quite well. However, for the 4 Hz gust, even though the frequency of the numerical response is in sync with the experimental response, the peak displacement is 30% higher than the experimental result. To measure the tip displacement, the laser from the scanning vibrometer is placed very close to the tip. At high out of plane displacement, the wingtip is out of the field of view of the laser and as a result, there is a loss of information which results in a flat line, as can be seen in Figure 4.24. Nevertheless, if one follows the curvature of the response, the experimental tip displacement would be close to the numerical tip displacement.

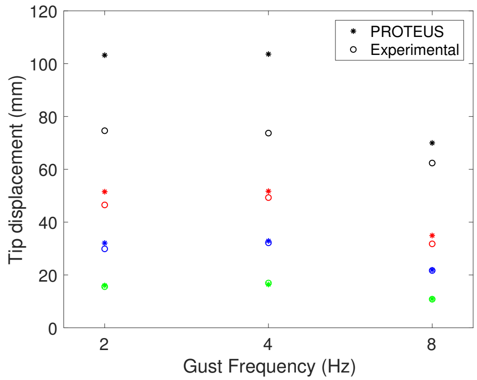

Figure 4.23: Maximum tip displacement measured at different gust frequency, amplitude and velocity (Black: 10 degrees gust amplitude and 26 m/s velocity,Blue: 10 degrees gust amplitude and 14 m/s velocity,Red: 5 degrees gust amplitude and 26 m/s velocity,Green: 5 degrees gust amplitude and 14 m/s velocity).

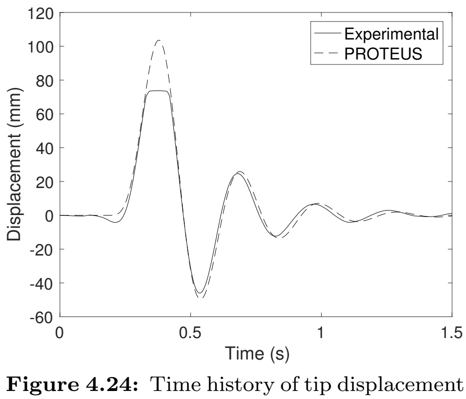

Figure 4.24: Time history of tip displacement for a gust having a frequency of 4 Hz, amplitude of 10 degrees and velocity of 26 m/s.

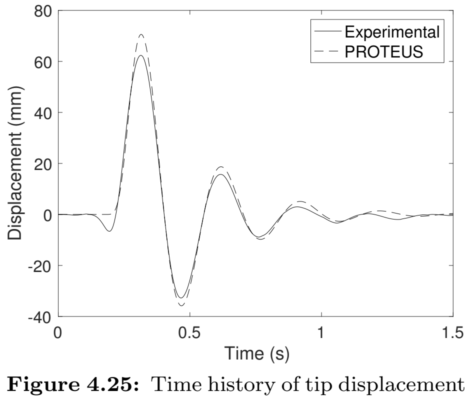

Figure 4.25: Time history of tip displacement for a gust having a frequency of 4 Hz, amplitude of 10 degrees and velocity of 26 m/s.

Looking at the results from the first wind tunnel test, it can be concluded that PROTEUS predicts the static and gust responses of a composite wing with reasonable accuracy. This gives confidence in the tool to be used as a preliminary aeroelastic design tool for composite wing studies. Additionally, with these results, the static and dynamic performance of the pristine wing has been benchmarked and will be used later to compare the effect of fatigue on the aeroelastic response of the wing.

4.5.3 FATIGUE RESULTS

After the first wind tunnel campaign, the wing is installed in the fatigue test machine, as shown in Figure 4.14. The wing is subjected to a load controlled fatigue spectrum. The machine is set up in such a way that the spectrum is applied at a constant load rate rather than constant frequency. Constant load rate is preferred option due to ease in stability and controllability of the specimen. The rate of load applied is set at 60 N/s. With this applied load, a minimum frequency of 0.17 Hz and a maximum frequency of 0.65 Hz is achieved throughout the spectrum. It takes roughly one day to apply one block of $10,000$ cycles. As a result, roughly ten days are required to apply the design life of $100,000$ cycles. As mentioned before, the applied load and the displacement at 0.65 m from the root are continuously recorded. Additionally, at certain time intervals, the fatigue process is paused and a static load of 118 N is applied. The load of 118 N is twice the cruise load. At this load, the strains from the optical fiber and the tip displacement are recorded. The displacement at the point, which is 0.65 m from the root, will be referred to from here on as the mid-span displacement for the sake of brevity.

Figure 4.26 depicts the displacement of the tip measured at the specific interval during the fatigue life. As can be seen, there is approximately 9% increase in the tip deflection at an applied static load of 118 N over the 100,000 cycles. Figure 4.27 depicts the mid-span displacement over the design life. The mid-span displacement is also increased by approximately 10% . As the mid-span displacement is recorded continuously at different load levels along the spectrum, in the current figure, the mid-span displacement of every 100 cycles is interpolated to find the mid-span displacement at 118 N. This assumes that the change in deflection over 100 cycles is negligible compared to the gradual change occurring over the 100,000 cycle duration. This leads to 1000 data points compared to 22 data points for the tip displacement. The gap in Figure 4.27 relates to the error in the data recorded by the fatigue test machine for the respective cycles.

The reason for the increase in deflection can be attributed to a combination of reasons: relaxation of the test fixture, settling of the specimen and adhesive bondlines, and stiffness degradation due to multi-scale damage creation and evolution. For a composite material, a stiffness degradation over a fatigue life consists of

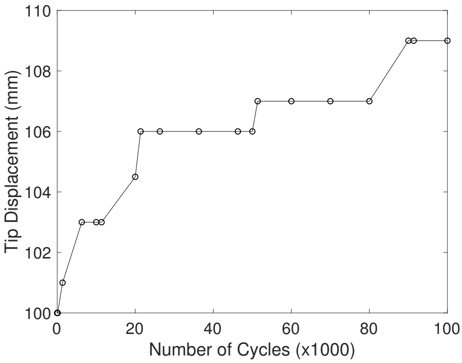

Figure 4.26: Maximum tip displacement with respect to number of cycles.

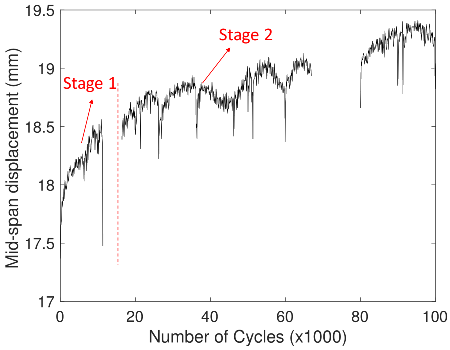

Figure 4.27: Mid-span displacement with respect to number of cycles.

three stages (Talreja, 1987). In stage 1, there is a steep drop in stiffness due to initial defect in the structure and material relaxation, in stage 2, there is gradual degradation in stiffness due to the development of delamination and matrix cracking and finally in stage 3, there is sudden degradation in stiffness because of the fatigue induced fiber breakage leading to final failure. A similar kind of behavior is seen in Figure 4.27, where there is an initial increase in the deflection until 20,000 cycles, after which the increase in the displacement becomes more gradual until 100,000 cycles. The tip deflection curve looks discontinuous with a prolonged period of constant stiffness and a short period of stiffness drops. This is due to the fact that tip displacement is measured manually with an accuracy of 1 mm and at specific intervals. A behavior similar to mid-span displacement would be observed with a continuous recording of the tip displacement over the fatigue life.

Figure 4.28 displays the change in the maximum normal and shear strain experienced by the bottom skin with respect to the number of cycles. The maximum strains occur at the ply drop, as was the case in the wind tunnel test. The points in the figure display the experimental values captured by the optical fiber. Since the data is noisy due to the sensitivity of the optical fiber, a trend line calculated using least squares method, indicated by a solid line helps to understand the pattern of the strain with respect to the number of cycles. There is an increase of 20 microstrains (10%) in shear, whereas the transverse normal strain increases by 30 microstrains (8%) over 100,000 cycles. The maximum increase is observed in the axial strain, which increases by approximately 230 microstrains (10%). This change is partly due to the degradation in axial stiffness of the laminate. This degradation leads to higher deflection as can be seen in Figures 4.26 and 4.27.

Figure 4.29 displays the axial strain along the wingspan at different cycles. As is mentioned before, the maximum strain occurs at ply drop and the maximum strain increases as the number of cycles increases. An interesting observation that can be made is that, as the number of cycles increases, the axial strain increases across the entire wingspan except at the outer part of the wing. This is due to the load redistribution because of the stiffness degradation. As the wing fatigues, the load experienced by the outer part is reduced, resulting in lower strains.

Traditionally, a composite wing, designed with a fatigue knockdown factor of 0.32 on the maximum stress allowables, will not experience strains high enough to cause stiffness degradation of the magnitude measured here. Since the current wings are designed using the analytical fatigue model instead of the knockdown factor, higher strains are experienced by the wing, which leads to an increased degradation in stiffness. The analytical model (Rajpal, Kassapoglou and De Breuker, 2019) is based on the residual strength and does not model the degradation in stiffness. Thus, numerically, the wing is optimized in such a way that the wing will have sufficient residual strength until 100,000 cycles to carry the critical loads. With the experiments, after 100,000 cycles, the fatigued wing is tested again in the wind tunnel as explained in the following section. The wing is able to withstand critical static and gust loads. This proves that even though there was a drop in stiffness, there was no damage at a long enough scale to compromise strength leading to the wing having enough residual strength to carry the applied load. This validates the analytical fatigue model.

With the current methodology, the wing is designed for precisely 100,000 cycles. This means at the $100,001^{st}$ cycle, the wing will theoretically fail. Looking at Figure 4.27, the wing is in the second stage of the fatigue degradation curve and since third phase is about 20% of fatigue life, this specific wing with the specific material batch used and fabrication method accuracy achieved is still a bit far from a failure after the design life of $100,000$ cycles is completed. This points to the fact that the numerical model is conservative in nature and the wing is overdesigned. This conservativeness can be attributed to three phenomena. First is the fact that the fatigue model is implemented within the lamination parameter domain, which is inherently conservative due to the use of the modified Tsai Wu Failure criterion. The second reason is the use of the first ply failure criterion as the fatigue failure criterion of the wing. With this criterion, as soon as a single ply locally fails, the wing is deemed to be failed in fatigue. Whereas in reality, even if there is some kind of damage in the ply, the wing as a whole has sufficient strength to carry the loads. Thirdly, the scatter is quite high in the fatigue of composite materials (Tomblin and Seneviratne, 2011). There is a possibility that this experiment is on the right side of the scatter, which would lead to a conservative result.

To understand how conservative the numerical model is, ideally, the wing would be fatigued until failure. Since in the current experimental campaign focus is also on the effect of the fatigue on the aeroelastic response of the wing, the wing is not fatigued further.

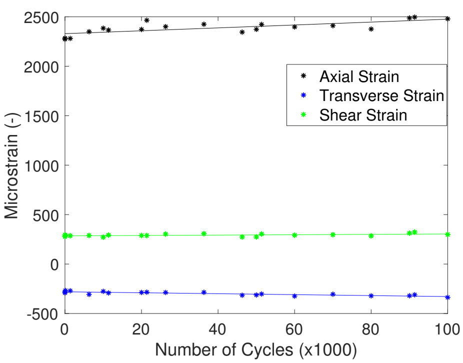

Figure 4.28: Strain history with respect to number of cycles.

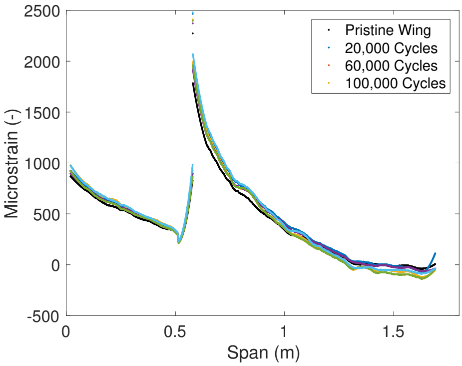

Figure 4.29: Longitudinal normal strain along the span at different cycles.

4.5.4 SECOND WIND TUNNEL TEST

The fatigued wing is tested again in the wind tunnel with a setup similar to the one shown in Figure 4.9. Both static and dynamic measurements are performed with the aim to compare the response of the pristine wing with respect to the fatigued wing.

Figure 4.30 shows the lift coefficient of the pristine and the fatigued wings for different angles of attack at a velocity of 26 m/s. The solid and the dashed line represent the linear fit of the experimental data for the pristine and the fatigued wing, respectively. As can be seen, the lift curve slope of the fatigued wing is 11% lower than that of the pristine wing. This reduction in the lift curve slope can be attributed to the degradation of the stiffness or to the experimental scatter that is caused due to variability in testing conditions. However, looking at Figures 4.26 and 4.27, around 9% increase in the deflection of the wing, indicating degradation in stiffness, does point to the fact that reduction in the lift curve slope could be mainly due to degradation in the stiffness. Due to the degradation in the stiffness, the fatigued wing will go to a higher deflection resulting in a more nose-down twist of the outboard part of the wing leading to reduced forces generated on the wing. This contributes to the lower lift curve slope.

Figure 4.31 shows the force normalized axial strain along the wingspan for the velocity of 26 m/s at 4 degrees angle of attack. Force normalized axial strain is the axial strain normalized by applied force. Force normalized axial strain can be considered as an equivalent to static stiffness where, the higher the value of the force normalized strain, the lower is the stiffness. An approximate increase of 10% in the force normalized strain value agrees well with the increase of about 9% of the tip deflection seen during the fatigue tests.

Figure 4.32 shows the maximum lift coefficient for a different combination of

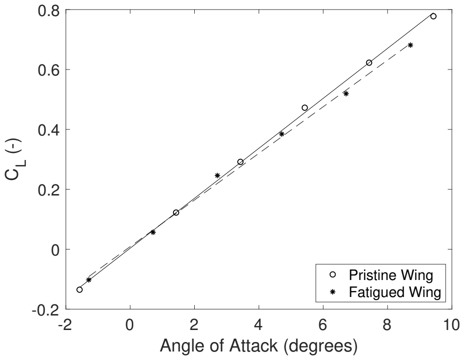

Figure 4.30: Comparison of the lift coefficient of the pristine and the fatigued wing.

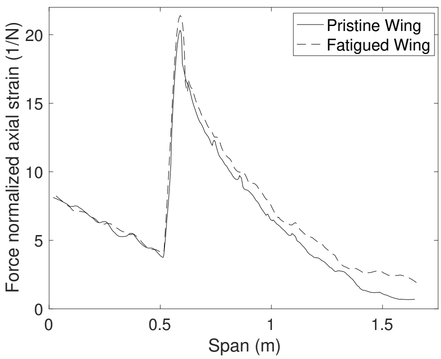

Figure 4.31: Comparison of the force normalized normal strain along the wing span of the pristine and the fatigued wing.

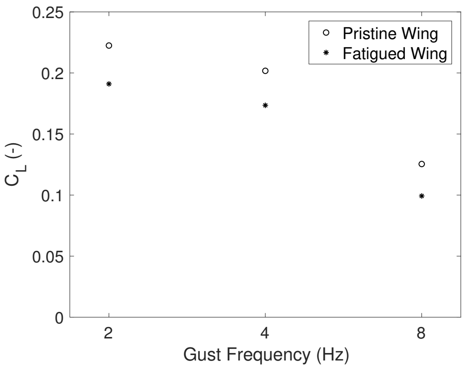

Figure 4.32: Comparison of the maximum lift coefficient of the pristine and the fatigued wing for the gust amplitude of 5 degrees.

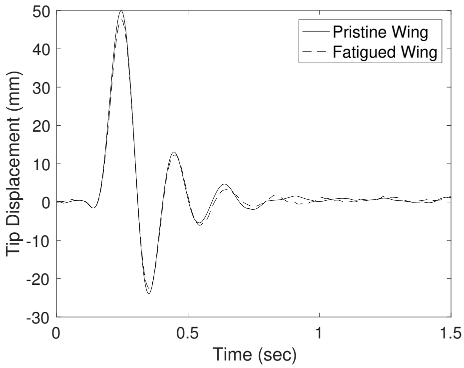

Figure 4.33: Comparison of the tip displacement of the pristine and the fatigued wing for the gust amplitude of 5 degrees.

velocity, gust frequency and gust amplitude. A similar behavior to the static condition is observed where the maximum lift coefficient for the fatigued wing is lower than the pristine wing by approximately 15%. The tip displacement of the pristine and the fatigued wing for a velocity of 26 m/s, frequency of 4 Hz and gust angle of 5 degrees is shown in Figure 4.33. As explained earlier, a combination of lower stiffness and higher nose down twist lead to lower lift which, in turn, results in a lower tip displacement.

Based on the results from the static and dynamic measurements, two main conclusions can be drawn. The first is that even after undergoing fatigue for 100,000 cycles, the wing is strong enough to withstand both static as well as gust loads. This again validates the numerical design methodology of accounting for fatigue through the analytical model instead of the knockdown factor. This, as demonstrated in Rajpal, Kassapoglou and De Breuker (2019) leads to lower weight designs. The second conclusion is that the aeroelastic response of the fatigued wing results in a lower lift coefficient for the same angle of attack compared to the pristine wing. The primary reason for the lower lift coefficient is the degradation in the stiffness caused by the fatigue process. This means that in order to attain a similar cruise lift coefficient, the trim angle of attack for the fatigued wing will be higher than the pristine wing. This would result in an increase in drag coefficient and hence, reduction in the lift to drag ratio leading to degradation in the performance due to an increase in fuel consumption.

In the traditional design of the composite wings, where the fatigue is accounted for by knocking down the stress allowables, the stresses are so low that there would not be any degradation in the stiffness properties of the wing leading to a negligible change in the aeroelastic response of the wing over the design life. This leads to wings being optimized for a single cruise point. With the design methodology proposed in the current research using the analytical model, the stresses in the wing would be higher during the fatigue process, which would lead to stiffness reduction over the life cycle of the aircraft. Even with the degraded stiffness, the wing will still have enough residual strength to carry the applied loads. However, the cruise condition of the wing will change over the design life and to obtain optimum performance over the entire design life, different cruise points need to be taken into account during the optimization of the wings.

4.6 Synopsis

In this chapter, the numerical design methodology for aeroelastic optimization of composite wings designed for gust and fatigue loads was validated. Additionally, since the design methodology did not take into account stiffness degradation during fatigue, the goal was also to understand the effect of fatigue on the stiffness of the wing and, thus, on the aeroelastic response of the wing. For this purpose, a flexible composite wing with a span of 1.75 m and chord of 0.25 m was designed to be critical in strength, buckling and fatigue. For fatigue, a test spectrum load of 100,000 cycles was used as a design life. The optimized wing was manufactured using Hexply 1M7/8552 UD prepreg.

An experimental campaign consisting of two wind tunnel tests and a fatigue test was conducted to meet the goals of this chapter. In the first wind tunnel test, static and dynamic aeroelastic experiments were conducted by mounting the wing in the OJF. The results validated the aeroelastic part of the numerical design methodology as the experimental static and gust response of a composite wing matched the numerical predictions with reasonable accuracy with a maximum error of less than 8%. These results were also used to benchmark the static and gust performance of the pristine wing.

The wind tunnel test was then followed by a fatigue test, in which a whiffle tree was used to replicate a more realistic load distribution on the wing. The wing was fatigued for 100,000 cycles using a spectrum based on the Mini-TWIST. The fatigue process resulted in the degradation of the stiffness, which led to an increase in tip deflection by 9% and in normal axial strain by around 10%. After 100,000 cycles, the wing did not experience any failure and had sufficient strength to withstand the critical load. This validated the analytical fatigue model, however, as the wing was not close to the failure, the analytical model could still be conservative in the fatigue prediction.

Finally, to check the effect of fatigue on the aeroelastic response of the wing, the fatigued wing was again mounted in the OJF and the static and dynamic experiments were once again performed. Comparing the performance of the fatigued wing with the pristine wing, the degradation in the lift curve slope was observed. As the stiffness degrades, the deflection of the wing increases for a given force leading to a more washout, which results in a lower lift. As a result, for a given angle of attack, the pristine wing will generate a higher lift force compared to the fatigued wing. This would lead to a higher cruise angle of attack for a fatigued wing leading to a higher drag coefficient and lower the lift to drag ratio and thus higher fuel consumption.

A wing designed traditionally by considering a knockdown factor for fatigue will result in a heavier wing, but with lower or no degradation in stiffness over its design life. A wing designed with the current methodology of taking into account fatigue through analytical model will result in the lighter wing but with degradation in stiffness over the design life. This degradation results in a change in the cruise angle of attack, which then also needs to be taken into account during the optimization process to avoid degradation in performance because of fatigue over the design life.

5 CONCLUSIONS AND RECOMMENDATIONS

With an aim to improve the wing design by increasing the analysis knowledge in the current preliminary aeroelastic design process of the composite wings, the main research question of this thesis was

> *Can critical gust and fatigue loads be integrated into a preliminary aeroelastic design process of a composite wing and what are there effects on the final design?*

Answers to the following sub-questions were required to answer the global research question mentioned above

- How can critical gust loads be identified and included in every iteration in the aeroelastic optimization process of composite wings? What are the effects of including critical gust loads on the optimized design?

- How can the effect of fatigue be included in the aeroelastic tailoring process of the composite wings? How does the optimized design change due to inclusion of fatigue loads?

- To what extent does the formulated preliminary aeroelastic framework approximate the response of the wing when subjected to critical gust and fatigue loads? What is the effect of the fatigue on aeroelastic performance of the wing?

Before delving into how this thesis tried to answer each of the sub questions, key conclusions from this thesis is summarized below

1. A ROAM, which was based on PROTEUS, was formulated by reducing aerodynamic model using the BPOD method and coupling it to the structural solver. A dynamic aeroelastic optimization study showed that, in the case of a clamped composite wing, static as well as gust loads are critical. Furthermore, the critical loads that sized the wing changed during the optimization process and hence it is important to update the critical loads during the dynamic aeroelastic optimization process.
2. An analytical fatigue model was formulated which was based on the residual strength degradation method developed by Kassapoglou and integrated in PROTEUS. A dynamic aeroelastic optimization study including fatigue requirements was carried out. Results showed that fatigue can be accounted for in the aeroelastic tailoring process using the analytical fatigue model and by doing so a lighter wing with the same level of reliability compared to the traditional method can be achieved.
3. To validate the formulated preliminary aeroelastic optimization framework including gust and fatigue loading requirement, an experimental campaign consisting of two wind tunnel tests and a fatigue test on a flexible composite wing with a span of 1.75 m and chord of 0.25 m designed to be critical in strength, buckling and fatigue was conducted. The test results validated both the dynamic aeroelastic and fatigue part of the preliminary aeroelastic optimization framework. Additionally the fatigue process also resulted in the degradation of the stiffness, which then also need to be taken into account during the optimization process to avoid degradation in performance because of fatigue over the design life.

In the following sections, the conclusions of the chapters discussed in this dissertation are summarized in more detail and the answers to the above-mentioned questions are reflected upon. Subsequently, recommendations for future research are provided.

5.1 DETAILED CONCLUSIONS

The first sub-question to be answered was

How can critical gust loads be identified and included in every iteration

> *in the aeroelastic optimization process of composite wings? What are the effects of including critical gust loads on the optimized design?*

The second chapter of this thesis focused on answering the above-mentioned sub-question. To identify critical gust loads and account for them in the aeroelastic optimization process, MOR strategies were applied to reduce the computational cost of the dynamic aeroelastic analysis. A ROAM, which was based on PROTEUS, was formulated by reducing the order of the unsteady vortex lattice model using the BPOD method and coupling it to the structural solver.

The challenge with the formulated ROAM was the ability to cover the complete flight envelope in an efficient manner. For this purpose, the state-space system was derived such that the influence of the equivalent airspeed was isolated from the state-space matrices. Additionally, the effect of Mach number, implemented using Prandtl-Glauert correction, is negligible on the reduced basis. As a result, a single ROM could therefore be used to analyze the aeroelastic loads throughout the flight envelope, reducing the computational cost significantly. The accuracy of the ROAM was validated by comparing the loads acting on a backward and forward swept version of the NASA CRM obtained with the ROAM and FOM. A considerable saving in the computational cost of about 89% for the analysis of 2,448 flight points, was achieved using this method. Thus, the critical gust loads can be included in the aeroelastic optimization process using the MOR strategies.

Using the developed ROAM, a dynamic aeroelastic optimization of the CRM wing clamped at the root was carried out. The results showed that, in the case of a clamped composite wing, static as well as gust loads are critical. Furthermore, the critical loads that sized the wing changed during the optimization process as the aeroelastic wing properties and hence static and gust response were changing due to the change in the design variables. This showed the importance of updating the critical loads during the dynamic aeroelastic optimization process.

The second sub-question to be answered was

> *How can the effect of fatigue be included in the aeroelastic tailoring process of the composite wings? How does the optimized design change due to inclusion of fatigue loads?*

The third chapter of this thesis was focused on answering this sub-question. To account for fatigue, an analytical fatigue model was formulated which was based on the residual strength degradation method developed by Kassapoglou. There were four key steps involved in formulating the analytical fatigue model. The first one was combining Kassapoglou's method with a Tsai Wu failure theory to determine the failure of the ply. The second one was modifying the degradation equations to account for the fact that the initial strength distribution would follow a Weibull distribution. The third one was extending the fatigue model to account for spectrum loading. And finally, the fourth step was to adapt the analytical model to also work with laminates described by lamination parameters instead of ply angles and stacking sequences. The prediction of the analytical model was compared to the experimental results and reasonable agreements were found with the analytical model being conservative.

The developed analytical fatigue model was then integrated into the dynamic aeroelastic framework formulated in chapter 2. A fatigue life of 40,000 flights/580,000 load cycles could be analyzed for the entire wing within two minutes making the analytical fatigue model computationally efficient. This efficiency sets stage for future optimization studies accounting for fatigue analysis of even longer life or complex models.

To understand the advantage of the analytical fatigue model over traditional knockdown factors, two optimization studies of the CRM wing were carried out, one with fatigue as a constraint using the analytical fatigue model and another was the traditional one using knockdown factors on material allowables to account for fatigue. Results showed that a composite wing is not only critical in strength and buckling but also in fatigue when accounted for explicitly. As the wing was critical in fatigue with the inclusion of the analytical model, the optimum stiffness and thickness distribution lead to a higher washout and therefore reduced load. The inclusion of the analytical model also led to a different critical gust and static loads for the optimum configurations compared to a design with knockdown factors. The middle part along the length of the wing optimized with fatigue constraint was critical with respect to static loads, whereas the middle part optimized with conservative knockdown factor was critical with respect to gust loads. Furthermore, by including a mathematical fatigue model instead of a conservative knockdown factor, the weight of the wing was reduced by 22%.

Thus fatigue can be accounted for in the aeroelastic tailoring process using the analytical fatigue model based on phenomenological methods and by doing so a lighter wing with the same level of reliability compared to the traditional method can be achieved.

The third sub-question to be answered was

> *To what extent does the formulated preliminary aeroelastic framework approximate the response of the wing when subjected to critical gust and fatigue loads? What is the effect of the fatigue on aeroelastic performance of the wing?*

The fourth chapter of this thesis was focused on the answering the above-mentioned sub-question by conducting an experimental campaign consisting of two wind tunnel tests and a fatigue test on a flexible composite wing with a span of 1.75 m and chord of 0.25 m designed to be critical in strength, buckling and fatigue. The test results were used to validate the preliminary aeroelastic optimization framework for composite wings designed for gust and fatigue loads. Additionally, since the design methodology did not take into account stiffness degradation during fatigue, the test results were also used to understand the effect of fatigue on the stiffness of the wing and on the aeroelastic response of the wing.

The first wind tunnel test validated the aeroelastic part of the design framework as the experimental static and gust response of a composite wing matched the numerical predictions with reasonable accuracy with a maximum error of less than 8%. To validate the analytical fatigue model, the wing was fatigued for 100,000 cycles. Even though the fatigue process resulted in the degradation of the stiffness, which led to an increase in tip deflection of 9%, the wing did not experience any failure. It was still strong enough to withstand the critical loads after 100,000 cycles. This validated the fatigue part of the design framework; however, as the wing was not close to the failure, the analytical model was conservative in the fatigue prediction. The degradation in stiffness due to fatigue resulted in the degradation of the lift curve slope of the fatigued wing when compared to the pristine wing. This degradation would result in a change in the cruise angle of attack, which then also need to be taken into account during the optimization process to avoid degradation in performance because of fatigue over the design life.

In conclusion, with the use of MOR techniques and phenomenological methods, gust and fatigue loads can be accounted for in the preliminary design process respectively in an accurate and computationally inexpensive manner. By accounting for gust and fatigue loads, a lighter design with improved aeroelastic efficiency can be created at the preliminary stage of the design process, having the same reliability as the traditional methods.

5.2 Recommendations for future work

The preliminary aeroelastic design framework presented in this thesis improves the state of the art of the aeroelastic design methodology by incorporating critical gust and fatigue loads in the tailoring of the composite wings. To take the presented framework a step further, several recommendations are presented in this section.

In the current framework, wings clamped at root are analyzed and optimized. As a next step, flight dynamics should be incorporated within the aeroelastic framework to analyze and optimize wings with rigid body motion. Also, instead of modeling just the wing, a complete aircraft, including fuselage and empenage should be analyzed. With these modifications, a more accurate estimation of critical loads can be obtained, which would lead to more realistic wing design.

The accuracy of the critical loads can also be improved further by replacing a linear dynamic analysis with a fully non-linear dynamic analysis. Cook et al. (2019) have shown that linear dynamic analysis around non-linear static equilibrium solution works well for predicting vertical shear and bending moments. However, the linear analysis does not perform well while predicting the in-plane, axial and torque loads compared to fully non-linear dynamic solution

In the current framework, only vertical gusts are accounted for to identify critical gust loads acting on the wing. To further improve the framework, lateral and Round the Clock (RTC) gust should also be accounted for to identify the critical gust loads. Cook et al. (2019) have shown that RTC gust can be critical for high aspect ratio wings, especially in torque.

In the analytical fatigue model, the initial static strength is assumed to have a Weibull distribution. In reality, the statistical distribution of the initial static strength could take any form and the residual strength degradation model needs to be adapted to account for a different kind of statistical distribution.

To identify failure during fatigue, a Tsai Wu failure criterion modified for lamination parameters is used. As Tsai Wu has its limitations, especially in the case of biaxial compression, a more detailed failure criterion such as Puck could be used to improve the accuracy of the fatigue model.

For the spectrum loading, stresses and strains in the wing at a given load level are approximated by linearly scaling the mean load. However, to get a more accurate representation of the loads, non-linear static equilibrium analysis should be carried out at each load level and corresponding stresses should be used to calculate the degradation in the residual strength.

Currently, with the fatigue model, there is no information about the degradation in the stiffness and as a result, the effect of fatigue on the aeroelastic properties cannot be approximated. As seen in the experimental campaign, the stiffness degradation due to fatigue leads to a change in the lift curve slope¿ This change affects the aerodynamic and the aeroelastic performance of the wing. Thus the stiffness degradation of the ply should also be modeled in the analytical fatigue model and the effect of the stiffness degradation should be taken into account while performing the aeroelastic tailoring of the wing.

With respect to modeling, finally, a stacking sequence retrieval step should be added to the preliminary aeroelastic design framework to convert the optimum lamination parameters into a manufacturable design. As seen in the experimental campaign, converting lamination parameters to stacking sequences is not straightforward and could result in loss of performance. Therefore the effect of stacking sequence retrieval should be accounted for within the aeroelastic optimization process to minimize the degradation in the performance of the real wing.

In order to further assess the validity of the preliminary aeroelastic design framework, wind tunnel tests with additional load conditions should be carried out. Tests should be performed at higher Mach numbers to assess the validity of the Prandtl-Glauert correction in the unsteady aerodynamic code.

In the current campaign, the fatigue tests were carried out directly on the entire wing with the aim to see if the wing fatigues or not for the given spectrum. As a next step, to get a more fundamental understanding of the fatigue process in a fully bonded composite structure, a more detailed fatigue campaign should be carried out. Starting from the coupon level, each laminate should be tested individually under fatigue to determine the fatigue properties. Then substructures should be tested to understand the behavior under fatigue and finally, the entire structure should be tested under fatigue.

With respect to the instrumentation used during the fatigue tests, a more extensive sensing methods such as acoustic emission and ultrasonic c-scans, should be utilized to understand where the fatigue starts and how does the stiffness degrade along the wing. GVT test should be carried out at regular intervals during the fatigue process to also get a better idea of the degradation in stiffness.

A

APPENDIX A

This appendix consist of additional drawings that gives insight into the inner structure the composite wing that was manufactured for the experiments. Figure A.1 depicts the inner cross section of the outer part of the wing. Figure A.2 depicts the top view of the wing and the isometric views of the aluminum clamp that was fitted inside the wing.

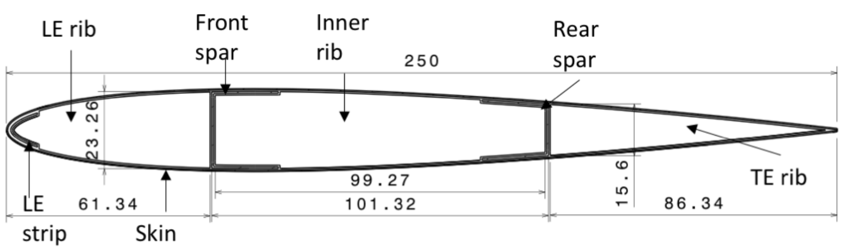

Figure A.1: Scaled drawing of inner cross section of the outer part of the wing (All the dimensions are in mm).

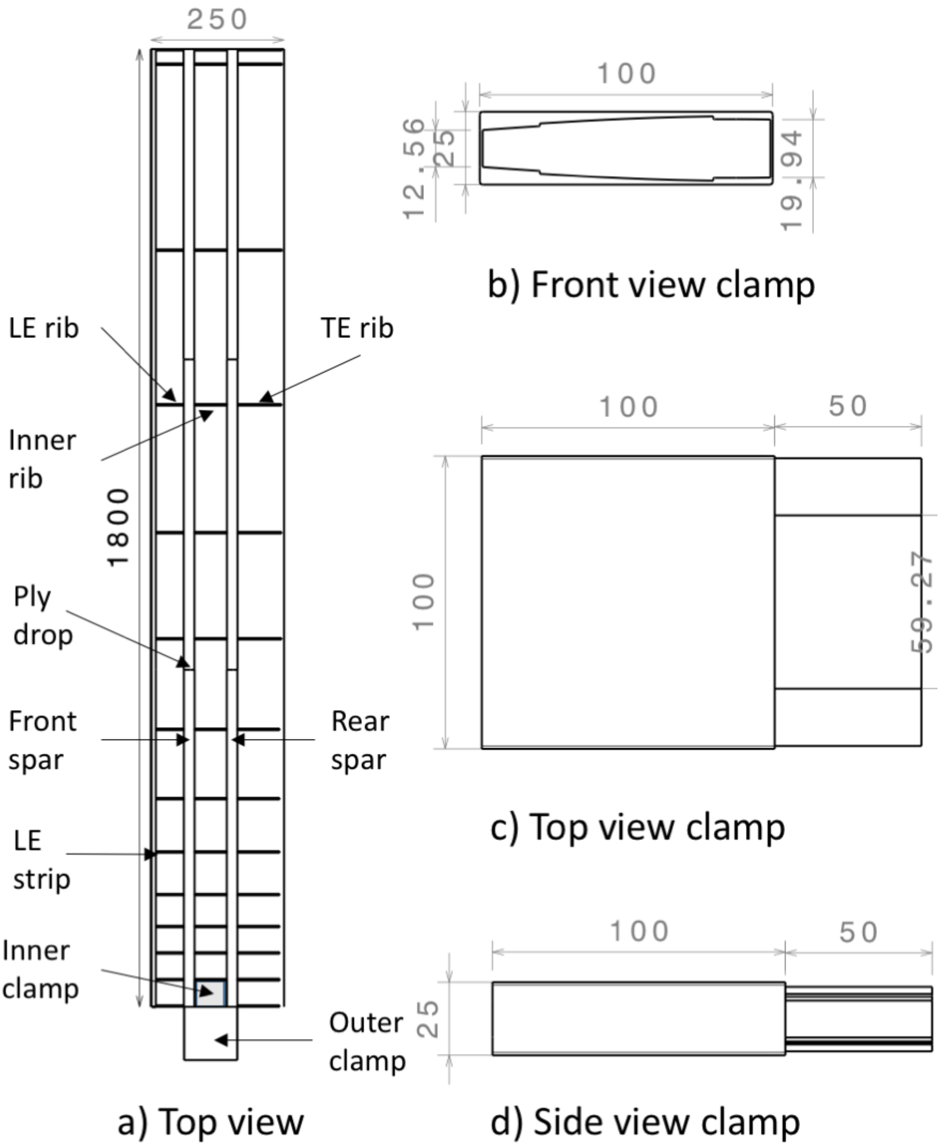

Figure A.2: Scaled drawing of the entire wing and the clamp (All the dimensions are in mm).

Bibliography

Adam, T., Dickson, R., Jones, C., Reiter, H. and Harris, B. (1986), 'A power law fatigue damage model for fibre-reinforced plastic laminates', *Proceedings of the Institution of Mechanical Engineers, Part C: Journal of Mechanical Engineering Science* **200**(3), 155–166.

Airbus (2017), *Global market forecast 2017-2036: Growing horizons*, Airbus. ISBN: 978-2-9554382-2-6.

Amsallem, D. and Farhat, C. (2011), 'An online method for interpolating linear parametric reduced-order models', *SIAM Journal on Scientific Computing* **33**(5), 2169–2198.

Arizono, H. and Isogai, K. (2005), 'Application of genetic algorithm for aeroelastic tailoring of a cranked-arrow wing', *Journal of Aircraft* **42**(2), 493–499.

Benner, P., Gugercin, S. and Willcox, K. (2015), 'A survey of projection-based model reduction methods for parametric dynamical systems', *SIAM Review* **57**(4), 483–531.

Bergmann, H. and Prinz, R. (1989), 'Fatigue life estimation of graphite/epoxy laminates under consideration of delamination growth', *International Journal for Numerical Methods in Engineering* **27**(2), 323–341.

Bergmann, M., Ferrero, A., Iollo, A. and Telib, H. (2016), An approach to predict gust effects by means of hybrid rom/cfd simulations, *in* 'ECCOMAS 2016'.

Boeing (2019), *Commercial Market Outlook 2019 – 2038*, Boeing.

Braslow, A. L. and Knox, E. C. (1958), 'Simplified method for determination of critical height of distributed roughness particles for boundary-layer transition at mach numbers from 0 to 5'.

Brooks, T. R., Martins, J. R. R. A. and Kennedy, G. J. (2019), 'High-fidelity aerostructural optimization of tow-steered composite wings', *Journal of Fluids and Structures* **88**, 122–147.

Broutman, L. J. and Sahu, S. (1972), A new theory to predict cumulative fatigue damage in fiberglass reinforced plastics, *in* 'Composite materials: Testing and design (second conference)', ASTM International.

Brunbauer, J. and Pinter, G. (2015), 'Fatigue life prediction of carbon fibre reinforced laminates by using cycle-dependent classical laminate theory', *Composites Part B: Engineering* **70**, 167 – 174.

Bulder, B., Peeringa, J., Lekou, D., Vionis, P., Mouzakis, F. and Nijssen, R. (2002), 'New wisper creating a new standard load sequence from modern wind turbine data.', http://www.kc-wmc.nl/optimatblades/Publications. [Visited on March 2018].

Bureau, A. T. (2020), 'Effects of novel coronavirus (covid-19) on civil aviation: Economic impact analysis', *International Civil Aviation Organization (ICAO), Montréal, Canada* .

Castellani, M., Lemmens, Y. and Cooper, J. E. (2016), 'Parametric reduced order model approach for rapid dynamic loads prediction', *Aerospace Science and Technology* **52**, 29–40.

Cavagna, L., Ricci, S. and Riccobene, L. (2013), Fast-glp: a fast tool for the prediction of worst case gust loads based on neural networks, *in* '54th AIAA/ASME/ASCE/AHS/ASC Structures, Structural Dynamics, and Materials Conference', p. 1493.

Chen, G.-S. and Dugundji, J. (1987), 'Experimental aeroelastic behavior of forward-swept graphite/epoxy wings with rigid-body freedom', *Journal of Aircraft* **24**(7), 454–462.

Chou, P. C. and Croman, R. (1978), 'Residual strength in fatigue based on the strength-life equal rank assumption', *Journal of Composite Materials* **12**(2), 177–194.

Clarkson, E. (2011), Hexcel 8552 AS4 unidirectional statistical analysis report, Technical report, National Institute for Aviation Research.

Cook, R., Calderon, D., Cooper, J., Lowenberg, M. and Neild, S. (2019), 'Industrially inspired gust loads analysis of various-aspect-ratio wings featuring geometric nonlinearity', *Journal of Aircraft* .

Dahlen, C. and Springer, G. S. (1994), 'Delamination growth in composites under cyclic loads', *Journal of Composite Materials* **28**(8), 732–781.

Degrieck, J. and Van Paepegem, W. (2001), 'Fatigue damage modeling of fibre-reinforced composite materials: Review', *Applied Mechanics Reviews* **54**(4), 279–300.

Dillinger, J. (2015), Static aeroelastic optimization of composite wings with variable stiffness laminates, PhD thesis, Delft University of Technology.

Dillinger, J. K. S., Abdalla, M. M., Meddaikar, Y. M. and Klimmek, T. (2019), 'Static aeroelastic stiffness optimization of a forward swept composite wing with CFD-corrected aero loads', *CEAS Aeronautical Journal* .

Dillinger, J., Klimmek, T., Abdalla, M. M. and Gürdal, Z. (2013), 'Stiffness optimization of composite wings with aeroelastic constraints', *Journal of Aircraft* **50**(4), 1159–1168.

Drela, M. (1989), Xfoil: An analysis and design system for low reynolds number airfoils, *in* 'Low Reynolds number aerodynamics', Springer, pp. 1–12.

Eastep, F. E., Tischler, V. A., Venkayya, V. B. and Khot, N. S. (1999), 'Aeroelastic tailoring of composite structures', *Journal of Aircraft* **36**(6), 1041–1047.

Elliott, C., Vijayakumar, V., Zink, W. and Hansen, R. (2007), 'National Instruments LabVIEW: A programming environment for laboratory automation and measurement', *Journal of the Association for Laboratory Automation* **12**(1), 17–24.

Epaarachchi, J. A. and Clausen, P. D. (2003), 'An empirical model for fatigue behavior prediction of glass fibre-reinforced plastic composites for various stress ratios and test frequencies', *Composites Part A: Applied science and manufacturing* **34**(4), 313–326.

European Aviation Safety Agency (2015), *Certification Specifications and Acceptable Means of Compliance for Large Aeroplanes CS-25.* Amendment 17.

Fidkowski, K. J., Engelsen, F., Willcox, K. E. and Kroo, I. M. (2008), Stochastic gust analysis techniques for aircraft conceptual design, *in* '12th AIAA/ISSMO Multidisciplinary Analysis and Optimization Conference', p. 5848.

Fualdes, C. (2016), Experience and lessons of a full composite passenger aircraft development, *in* 'Congress of the International Council of the Aeronautical Sciences', ICAS.

Gathercole, N., Reiter, H., Adam, T. and Harris, B. (1994), 'Life prediction for fatigue of t800/5245 carbon-fibre composites: I. constant-amplitude loading', *International Journal of Fatigue* **16**(8), 523–532.

Georgiou, G., Manan, A. and Cooper, J. E. (2012), 'Modeling composite wing aeroelastic behavior with uncertain damage severity and material properties', *Mechanical Systems and Signal Processing* **32**, 32–43.

Gillebaart, E. and De Breuker, R. (2015), Reduced-order modeling of continuous-time state-space unsteady aerodynamics, *in* '53rd AIAA Aerospace Sciences Meeting'.

Green, J. A. (1987), 'Aeroelastic tailoring of aft-swept high-aspect-ratio composite wings', **24**(11), 812–819.

Guo, S. (2007), 'Aeroelastic optimization of an aerobatic aircraft wing structure', *Aerospace Science and Technology* **11**(5), 396–404.

Guo, S., Cheng, W. and Cui, D. (2006), 'Aeroelastic tailoring of composite wing structures by laminate layup optimization', *AIAA Journal* **44**(12), 3146–3150.

Guo, S. J., Bannerjee, J. R. and Cheung, C. W. (2003), 'The effect of laminate lay-up on the flutter speed of composite wings', *Proceedings of the Institution of Mechanical Engineers, Part G: Journal of Aerospace Engineering* **217**(3), 115–122.

Guo, S., Li, D. and Liu, Y. (2012), 'Multi-objective optimization of a composite wing subject to strength and aeroelastic constraints', *Proceedings of the Institution of Mechanical Engineers, Part G: Journal of Aerospace Engineering* **226**(9), 1095–1106.

Haddadpour, H. and Zamani, Z. (2012), 'Curvilinear fiber optimization tools for aeroelastic design of composite wings', *Journal of Fluids and Structures* **33**, 180–190.

Hahn, H. and Kim, R. (1975), 'Proof testing of composite materials', *Journal of Composite Materials* **9**(3), 297–311.

Hammer, V. B., Bendsøe, M., Lipton, R. and Pedersen, P. (1997), 'Parametrization in laminate design for optimal compliance', *International Journal of Solids and Structures* **34**(4), 415–434.

Hashin, Z. (1985), 'Cumulative damage theory for composite materials: residual life and residual strength methods', *Composites Science and Technology* **23**(1), 1–19.

Hwang, W. and Han, K. (1987), 'Statistical study of strength and fatigue life of composite materials', *Composites* **18**(1), 47–53.

IATA (2020), *Outlook for Air Transport and the Airline Industry*, IATA.

Isogai, K. (1989), 'Direct search method to aeroelastic tailoring of a composite wing under multiple constraints', *Journal of Aircraft* **26**(12), 1076–1080.

Jovanov, K., De Breuker, R. and Bisagni, C. (2019), High-Fidelity Load and Gradient Corrections for Static Aeroelastic Tailoring of Composite Wings, phdthesis.

Kameyama, M. and Fukunaga, H. (2007), 'Optimum design of composite plate wings for aeroelastic characteristics using lamination parameters', *Computers & Structures* **85**(3), 213–224.

Kassapoglou, C. (2007), 'Fatigue life prediction of composite structures under constant amplitude loading', *Journal of Composite Materials* **41**(22), 2737–2754.

Kassapoglou, C. (2010), 'Fatigue of composite materials under spectrum loading', *Composites Part A: Applied Science and Manufacturing* **41**(5), 663–669.

Kassapoglou, C. (2011), 'Fatigue model for composites based on the cycle-by-cycle probability of failure: implications and applications', *Journal of Composite Materials* **45**(3), 261–277.

Kassapoglou, C. (2013), *Design and analysis of composite structures: with applications to aerospace structures*, John Wiley & Sons.

Kassapoglou, C. (2015), *Modeling the Effect of Damage in Composite Structures: Simplified Approaches*, John Wiley & Sons, chapter 6.

Khani, A., IJsselmuiden, S. T., Abdalla, M. M. and Gürdal, Z. (2011), 'Design of variable stiffness panels for maximum strength using lamination parameters', *Composites Part B: Engineering* **42**(3), 546–552.

Khodaparast, H. H. and Cooper, J. E. (2013), Worst case gust loads prediction using surrogate models and system identification methods, *in* 'Proceedings of 54th AIAA/ASME/ASCE/AHS/ASC Structures, Structural Dynamics and Materials Conference, Boston, MA'.

Khodaparast, H. H., Georgiou, G., Cooper, J. E., Riccobene, L., Ricci, S., Vio, G. and Denner, P. (2012), 'Efficient worst case "1-cosine" gust loads prediction', *Journal of Aeroelasticity and Structural Dynamics* **2**(3).

Kim, T.-U. and Hwang, I. H. (2005), 'Optimal design of composite wing subjected to gust loads', *Computers & Structures* **83**(19), 1546–1554.

Knoblach, A. (2013), 'Robust performance analysis applied to gust loads computation', *Journal of Aeroelasticity and Structural Dynamics* **3**(1).

KPMG (2020), *Aviation 2030 - Disruption beyond Covid-19*, KPMG.

Krein, A. and Williams, G. (2012), 'Flightpath 2050: Europe's vision for aeronautics', *Innovation for Sustainable Aviation in a Global Environment: Proceedings of the Sixth European Aeronautics Days, Madrid, 30 March-1 April, 2011* p. 63.

Lancelot, P. M., Sodja, J., Werter, N. P. and De Breuker, R. (2017), 'Design and testing of a low subsonic wind tunnel gust generator', *Advances in aircraft and spacecraft science* **4**(2), 125.

Landsberger, B. J. and Dugundji, J. (1985), 'Experimental aeroelastic behavior of unswept and forward-swept cantilever graphite/epoxy wings', *Journal of Aircraft* **22**(8), 679–686.

Lieu, T., Farhat, C. and Lesoinne, M. (2006), 'Reduced-order fluid/structure modeling of a complete aircraft configuration', *Computer methods in applied mechanics and engineering* **195**(41), 5730–5742.

Liu, K.-S. and Tsai, S. W. (1998), 'A progressive quadratic failure criterion for a laminate1', *Composites Science and Technology* **58**(7), 1023–1032.

Lowak, H., DeJonge, J., Franz, J. and Schütz, D. (1979), 'Minitwist - a shortened version of twist', *NLR MP 79018 U* .

Lukaszewicz, D. H. J. A., Ward, C. and Potter, K. D. (2012), 'The engineering aspects of automated prepreg layup: History, present and future', *Composites Part B: Engineering* **43**(3), 997–1009.

Macquart, T. (2016), Optibless: An open-source toolbox for the optimisation of blended stacking sequence, *in* 'ECCM17 - 17th European Conference on Composite Materials', European Conference on Composite Materials, ECCM.

Macquart, T., Werter, N. and De Breuker, R. (2017), 'Aeroelastic design of blended composite structures using lamination parameters', *Journal of Aircraft* **54**(2), 561–571.

Manan, A. and Cooper, J. (2009), 'Design of composite wings including uncertainties: A probabilistic approach', *Journal of Aircraft* **46**(2), 601–607.

Mavris, D. N. and DeLaurentis, D. A. (2000), Methodology for examining the simultaneous impact of requirements, vehicle characteristics, and technologies on military aircraft design, *in* '22^{nd} Congress of the International Council of the Aeronautical Sciences', ICAS.

Meddaikar, M. Y., Dillinger, J., Ritter, M. R. and Govers, Y. (2017), Optimization & testing of aeroelastically-tailored forward swept wings, *in* 'IFASD 2017-International Forum on Aeroelasticity and Structural Dynamics', pp. 1–13.

Meddaikar, Y. M., Dillinger, J. K., Sodja, J., Mai, H. and De Breuker, R. (2016), Optimization, manufacturing and testing of a composite wing with maximized tip deflection, *in* '57th AIAA/ASCE/AHS/ASC Structures, Structural Dynamics, and Materials Conference', p. 0489.

Miner, M. et al. (1945), 'Cumulative fatigue damage', *Journal of applied mechanics* **12**(3), A159–A164.

Mitrotta, F. M. A., Rajpal, D., Sodja, J. and De Breuker, R. (2020), Multi-fidelity design of an aeroelastically tailored composite wing for dynamic wind-tunnel testing, *in* 'AIAA Scitech 2020 Forum', p. 1636.

MSCNastran (n.d.), 'MSCNastran', https://www.mscsoftware.com/product/msc-nastran. [Visited on August 2019].

Munk, M. M. (1949), 'Propeller containing diagonally disposed fibrous material', https://patents.google.com/patent/US2484308A/en. [Visited on October 2019].

Murua, J., Palacios, R. and Graham, J. M. R. (2012), 'Applications of the unsteady vortex-lattice method in aircraft aeroelasticity and flight dynamics', *Progress in Aerospace Sciences* **55**, 46–72.

Natella, M. and De Breuker, R. (2019), 'The effects of a full-aircraft aerodynamic model on the design of a tailored composite wing', *CEAS Aeronautical Journal* .

Open Jet Facility (n.d.), 'Open Jet Facility, TU Delft', https://www.tudelft.nl/lr/organisatie/afdelingen/aerodynamics-wind-energy-flight-performance-and-propulsion/facilities/low-speed-wind-tunnels/open-jet-facility. [Visited on October 2019].

OPTIMAT (2002), 'Optimat blades material database', http://www.wmc.eu/optimatblades.php. [Visited on March 2018].

Othman, M. F., Silva, G. H. C., Cabral, P. H., Prado, A. P., Pirrera, A. and Cooper, J. E. (2019), 'A robust and reliability-based aeroelastic tailoring framework for composite aircraft wings', *Composite Structures* **208**, 101–113.

Ouyang, Q., Chen, X. and Cooper, J. E. (2013), 'Robust aeroelastic analysis and optimization of composite wing under μ-analysis framework', *Journal of Aircraft* **50**(4), 1299–1305.

Paepegem, W. V., Degrieck, J. and Baets, P. D. (2001), 'Finite element approach for modelling fatigue damage in fibre-reinforced composite materials', *Composites Part B: Engineering* **32**(7), 575 – 588.

Passipoularidis, V. and Brøndsted, P. (2010), Fatigue evaluation algorithms: review, Technical report, Danmarks Tekniske Universitet, Risø Nationallaboratoriet for Bæredygtig Energi.

Philippidis, T. and Passipoularidis, V. (2007), 'Residual strength after fatigue in composites: Theory vs. experiment', *International Journal of Fatigue* **29**(12), 2104–2116.

Post, N., Case, S. and Lesko, J. (2008), 'Modeling the variable amplitude fatigue of composite materials: A review and evaluation of the state of the art for spectrum loading', *International Journal of Fatigue* **30**(12), 2064–2086.

Pototzky, A. S., Zeiler, T. A. and PERRY III, B. (1991), 'Calculating time-correlated gust loads using matched filter and random process theories', *Journal of Aircraft* **28**(5).

Rajpal, D., Gillebaart, E. and De Breuker, R. (2019), 'Preliminary aeroelastic design of composite wings subjected to critical gust loads', *Aerospace Science and Technology* **85**.

Rajpal, D., Kassapoglou, C. and De Breuker, R. (2019), 'Aeroelastic optimization of composite wings including fatigue loading requirements', *Composite Structures* .

Raju, G., Wu, Z. and Weaver, P. (2014), On further developments of feasible region of lamination parameters for symmetric composite laminates, *in* '55th AIAA/ASMe/ASCE/AHS/SC Structures, Structural Dynamics, and Materials Conference', p. 1374.

Reifsnider, K. L. and Stinchcomb, W. (1986), A critical-element model of the residual strength and life of fatigue-loaded composite coupons, *in* 'Composite Materials: Fatigue and Fracture', ASTM International.

Reyes, M., Climent, H., Karpel, M., Arevalo, F. and Maderuelo, C. (2017), Increased-order aeroservoelastic modeling in practice, *in* 'Proceedings of the International Forum on Aeroelasticity and Structural Dynamics'.

Ritter, M., Dillinger, J. and Meddaikar, Y. M. (2017), Static and dynamic aeroelastic validation of a flexible forward swept composite wing, *in* '58th AIAA/ASCE/AHS/ASC Structures, Structural Dynamics, and Materials Conference', p. 0637.

Scarth, C., Cooper, J. E., Weaver, P. M. and Silva, G. H. C. (2014), 'Uncertainty quantification of aeroelastic stability of composite plate wings using lamination parameters', *Composite Structures* **116**, 84–93.

Schaff, J. R. and Davidson, B. D. (1997*a*), 'Life prediction methodology for composite structures. part ii—spectrum fatigue', *Journal of composite materials* **31**(2), 158–181.

Schaff, J. R. and Davidson, B. D. (1997*b*), 'Life prediction methodology for composite structures. part i—constant amplitude and two-stress level fatigue', *Journal of composite materials* **31**(2), 128–157.

Schmit, R. and Glauser, M. (2003), Improvements in low dimensional tools for flow-structure interaction problems: using global pod, *in* 'APS Division of Fluid Dynamics Meeting Abstracts', Vol. 1.

Sherrer, V., Hertz, T. and Shirk, M. (1981), 'Wind tunnel demonstration of aeroelastic tailoring applied to forward swept wings', *Journal of Aircraft* **18**(11), 976–983.

SHIRK, M. H., HERTZ, T. J. and WEISSHAAR, T. A. (1986), 'Aeroelastic tailoring - theory, practice, and promise', *Journal of Aircraft* **23**(1), 6–18.

Silva, G. H. C., do Prado, A. P., Cabral, P. H., De Breuker, R. and Dillinger, J. K. S. (2019), 'Tailoring of a composite regional jet wing using the slice and swap method', *Journal of Aircraft* **56**(3), 990–1004.

Simcenter Testlab (n.d.), 'Simcenter Testlab', https://www.plm.automation.siemens.com/global/en/products/simcenter/testlab.html. [Visited on August 2019].

Stanford, B. K. and Jutte, C. V. (2017), 'Comparison of curvilinear stiffeners and tow steered composites for aeroelastic tailoring of aircraft wings', *Computers & Structures* **183**, 48–60.

Stanford, B. K., Jutte, C. V. and Chauncey Wu, K. (2014), 'Aeroelastic benefits of tow steering for composite plates', *Composite Structures* **118**, 416–422.

Stanford, B. K., Jutte, C. V. and Wieseman, C. D. (2016), 'Trim and structural optimization of subsonic transport wings using nonconventional aeroelastic tailoring', *AIAA Journal* **54**(1), 293–309.

Starnes Jr, J. H. and Haftka, R. T. (1979), 'Preliminary design of composite wings for buckling, strength, and displacement constraints', *Journal of Aircraft* **16**(8), 564–570.

Stodieck, O., Cooper, J. E., Weaver, P. M. and Kealy, P. (2013), 'Improved aeroelastic tailoring using tow-steered composites', *Composite Structures* **106**, 703–715.

Stodieck, O., Cooper, J. E., Weaver, P. M. and Kealy, P. (2015), 'Optimization of tow-steered composite wing laminates for aeroelastic tailoring', *AIAA Journal* **53**(8), 2203–2215.

Stodieck, O., Cooper, J. E., Weaver, P. M. and Kealy, P. (2017), 'Aeroelastic tailoring of a representative wing box using tow-steered composites', *AIAA Journal* **55**(4), 1425–1439.

Svanberg, K. (2002), 'A class of globally convergent optimization methods based on conservative convex separable approximations', *SIAM journal on optimization* **12**(2), 555–573.

Talreja, R. (1987), *Fatigue of composite materials*.

Tenhave, A. (1992), 'Wisper and wisperx: Final definition of two standardised fatigue loading sequences for wind turbine blades', *NASA STI/Recon Technical Report N* **94**.

Thormann, R., Bekemeyer, P. and Timme, S. (2016), Reduced order modelling of gust analysis using computational fluid dynamics, *in* 'ECCOMAS 2016'.

Timme, S., Badcock, K. and Da Ronch, A. (2017), 'Gust analysis using computational fluid dynamics derived reduced order models', *Journal of Fluids and Structures* **71**, 116–125.

Tomblin, J. and Seneviratne, W. (2011), 'Determining the fatigue life of composite aircraft structures using life and load-enhancement factors', *Final report, Air Traffic Organization, Washington DC, USA* .

Vassberg, J. C., DeHaan, M. A., Rivers, S. M. and Wahls, R. A. (2008), Development of a common research model for applied cfd validation studies, *in* '26th AIAA Applied Aerodynamics Conference, Honolulu, Hawaii'.

Wales, C., Gaitonde, A. and Jones, D. (2016), 'Reduced-order modeling of gust responses', *Journal of Aircraft* **54**(4), 1350–1363.

Weisshaar, T. A. (1981), 'Aeroelastic tailoring of forward swept composite wings', *Journal of Aircraft* **18**(8), 669–676.

Werter, N. P. M. (2017), Aeroelastic Modelling and Design of Aeroelastically Tailored and Morphing Wings, PhD thesis, Delft University of Technology.

Werter, N. P. M. and De Breuker, R. (2016), 'A novel dynamic aeroelastic framework for aeroelastic tailoring and structural optimisation', *Composite Structures* **158**, 369–386.

Werter, N. P. M., De Breuker, R. and Abdalla, M. M. (2017), 'Continuous-time state-space unsteady aerodynamic modeling for efficient loads analysis', *AIAA Journal* pp. 1–12.

Werter, N. P., Sodja, J. and De Breuker, R. (2016), 'Design and testing of aeroelastically tailored wings under maneuver loading', *AIAA Journal* **55**(3), 1012–1025.

Whitehead, R., Kan, H., Cordero, R. and Saether, E. (1986), 'Certification testing methodology for composite structures', *Volumes I and II, Report No. NADC-87042-60 (DOT/FAA/CT-86-39)* .

Whitworth, H. (1997), 'A stiffness degradation model for composite laminates under fatigue loading', *Composite structures* **40**(2), 95–101.

Williams, S. P., Jones, D., Gaitonde, A., Wales, C. and Huntley, S. J. (2017), Reduced order modelling of aircraft gust response for use in early design stages, *in* '35th AIAA Applied Aerodynamics Conference', p. 3906.

Wilson, T., Azabal, A., Castrichini, A., Cooper, J., Ajaj, R. and Herring, M. (2017), Aeroelastic behaviour of hinged wing tips, *in* 'Proceedings of the International Forum on Aeroelasticity and Structural Dynamics'.

Wu, Z., Raju, G. and Weaver, P. M. (2015), 'Framework for the buckling optimization of variable-angle tow composite plates', *AIAA Journal* **53**(12), 3788–3804.

Yang, J. and Du, S. (1983), 'An exploratory study into the fatigue of composites under spectrum loading', *Journal of Composite Materials* **17**(6), 511–526.

Yang, J. N. (1978*a*), 'Fatigue and residual strength degradation for graphite/epoxy composites under tension-compression cyclic loadings', *Journal of Composite Materials* **12**(1), 19–39.

Yang, J. N. (1978*b*), 'Fatigue and residual strength degradation for graphite/epoxy composites under tension-compression cyclic loadings', *Journal of Composite Materials* **12**(1), 19–39.

Yang, J. N. and Jones, D. L. (1978), 'Statistical fatigue of graphite/epoxy angle-ply laminates in shear1', *Journal of Composite Materials* **12**(4), 371–389.

Yang, J. and Sun, C. (1980), 'Proof test and fatigue of unnotched composite laminates', *Journal of Composite Materials* **14**(2), 168–176.

Yao, W. and Himmel, N. (1999), 'Statistical analysis of data from truncated fatigue life and corresponding residual strength experiments for polymer matrix composites', *International journal of fatigue* **21**(6), 581–585.

List of publications

Journal publications

1. D. Rajpal, F. Mitrotta, C. Socci, J.Sodja, C. Kassapoglou and R. De Breuker (2021), "Design and testing of a aeroelastically tailored composite wing under fatigue and gust loading including the effect of fatigue on the aeroelastic performance of the wing", *Composite Structures*, under review.

2. D. Rajpal, C. Kassapoglou and R. De Breuker (2019), "Aeroelastic optimization of composite wings including fatigue loading requirements", *Composite Structures.*

3. D. Rajpal, E. Gillebaart and R. De Breuker (2019), "Preliminary aeroelastic design framework for composite wings subjected to gust loads", *Aerospace Science and Technology.*

Chapter

1. J. Vos, D. Charbonnier, T. Ludwig, S. Merazzi, H. Timmermans, D. Rajpal, A. Gehri (2019), "Aeroelastic Simulations Using the NSMB CFD Solver Including results for a Strut Braced Wing Aircraft", *Flexible Engineering Toward Green Aircraft.*

Conference publications

1. F. Mitrotta, D. Rajpal, J.Sodja and R. De Breuker (2020), "Multi-Fidelity Design of an Aeroelastically Tailored Composite Wing for Dynamic Wind-Tunnel Testing", In *AIAA Scitech 2020*, Florida, USA.

2. P. D. Ciampa, P. S. Prakasha, ...D. Rajpal, ... and M. Voskuijl (2019), "Streamlining Cross-Organizational Aircraft Development: Results from the AGILE Project", In *AIAA Aviation 2019 Forum*, Texas, USA.

3. D. Rajpal and R. De Breuker (2019), ”Dynamic Aeroelastic Tailoring of a Strut Braced Wing Including Fatigue Loads” In *Proceedings of the 18th International Forum on Aeroelasticity and Structural Dynamics*, Georgia, USA.

4. D. Rajpal, et al. (2018), ”Including Aeroelastic Tailoring in the Conceptual Design Process of a Composite Strut-Braced Wing” In *ICAS 2018*, Belo Horizonte, Brazil

5. F. Torrigiani, JP. Bussemaker, ...D. Rajpal, ... ans D. Charbonnier, (2018), ”Design of the Strut Braced Wing aircraft in the AGILE Collaborative MDO Framework”, In *ICAS 2018*, Belo Horizonte, Brazil

6. D. Rajpal, C. Kassapoglou and R. De Breuker (2018), ”Aeroelastic Optimization of Composite Wings Subjected to Fatigue Loads”, In *AIAA Scitech 2018*, Florida, USA.

7. D. Rajpal and R. De Breuker (2017), ”Preliminary aeroelastic design framework for composite wings subjected to gust loads” In *Proceedings of the 17th International Forum on Aeroelasticity and Structural Dynamics*, Como, Italy.

ACKNOWLEDGMENTS

A wise woman once said ”It is good to have an end to journey towards, but it is the journey that matters in the end.” This thesis was the end objective of the journey that was started 6 years ago but indeed it was the journey that mattered the most and this journey would not have been possible without the help and support of my family, friends and colleagues

To start with first I would like to thank Dr. Roeland De Breuker for believing in me and offering me a chance to work on this interesting topic. Over the years he has donned many hats - promoter/supervisor/friend/mentor and many more. There have been times when I have doubted myself and my abilities but you have always had confidence in me and motivated me when the chips were down. You have an innate ability to connect with each of your PhD student on deeper level which definitely makes the journey definitely more enjoyable. I have always enjoyed your company and am definitely gonna miss among other things our weekly Friends trivia session.

I am also grateful to my promoter Prof. dr. Christos Kassapoglou for his help, support and supervision during this journey. Your academic experience combined with industrial exposure has given different perspective to my thesis. I am always amazed by your enthusiasm towards academia and research. Your simplicity and practical outlook is rare to find in academia and this thesis would not have been what it is today without your support and guidance.

I would like to thank my promoter Prof. dr. Chiara Bisagni for providing the necessary critical note which helped me improve the quality of my research. I would also like to thank the committee members, Prof. Cooper, Prof. Van Paepegem, Prof. Dransfled, Prof. Benedictus and Dr. Martinez for taking the time to read my thesis, provide feedback, and take part in the doctoral ceremony. Special thanks go to Dr. Martinez who was also instrumental in offering me a chance to work on this topic as well.

This journey would not have been the same without my fellow colleagues. The old guard: Noud, Erik, Paul, Jurij and Kristofer made me feel right at home and helped me tackle the beautiful world of aeroelasticity. Thank you for your collaboration and feedback over the years. Along with them I will like to thank my fellow PhDs and post-doc colleagues Andres, Daniël, Edgars, Innes, Javier, Mario, Marta, Mayank, Natalia, Tito, Tigran, Tutu and Yasir. I have so many fond memories with all of you of the nice lunches, Friday drinks, counter strike nights and conference trips. I would also like to thank my master students Carlo and Francesco for their important contributions to this thesis. A especial thanks goes to Laura without whom this department will not be as enjoyable. Thank you for your support in tackling the more bureaucratic part of the PhD.

Living more than 7000km from your home is difficult and to survive one needs a family and I found that family in Varun, Ram, Bhattu, Aritra, Nakul, Chirag, Karwal, Sujaya, Mayuri, Laxmi, Nanda, Silky and two newest members Vihaan and Inaya. Without you guys I would not have been able to enjoy my time in Delft. Special thanks goes to Varun. We started our journey in aerospace 14 years ago in PEC and have been tackling the world of academia together since. He was the one who inspired me to do my masters and thats how I ended up at Delft.

Finally but most importantly I would like to thank my family. My parents who have always supported me and shown faith in my decisions. Without them I would not have been the where I am today. My brother Aakash who always encourages me take a chill pill and follow my own decisions. His zeal to travel and his efforts to bring the whole family together is something that inspires me. I am also very grateful to my extended family consisting of my in laws, cousins, chachas, chachis, mama and mamis and ofcourse my nani for your love and support.

This PhD journey became all more memorable as I was able to find my life partner in Bhawna during this time. Marrying her was the best decision of my life. Of course doing a PhD comes close second. She has been standing like a rock supporting me for the past two years and without her constant support I would not have been able to finish my thesis in time. Thank you for your never-ending love and support.

Biographical note

Darwin was born on March 26, 1990, in Mumbai, India. Darwin completed his higher secondary education in Mumbai itself. After high school, he decided to move to Chandigarh which is 2500 km north of Mumbai to pursue a bachelor in aerospace engineering from PEC University of Technology. During the next four years, he undertook numerous internship in India as well as around the globe to complement academic learning with practical exposure. He did a two-month internship during the winter of 2009 in Zambia, Africa and another two-month internship in summer of 2010 in China. He presented a paper at the AIAA Scitech conference in Florida, USA in the final year of his studies. In 2011 he graduated from his university with a Bachelor degree in aerospace engineering.

After his Bachelor, his interest in aerospace and his love for football led him to a beautiful country of Europe called The Netherlands. He started his Master degree in 2011 in Flight Performance and Propulsion at Delft University of Technology. Along with the studies, he was also involved with SSVOBB, a non-profit foundation of students, to design S-Vision, a 2-seater very light aircraft.

After finishing his courses in the first year, he went to DLR in Hamburg, Germany for a year-long graduation project on multi-disciplinary design optimization of novel concepts. He was involved in the development of a distributed multi-disciplinary design optimization (MDO) framework capable of analyzing non-planar wing concepts such as C-wing and Box-wing. The goal of this thesis was to find an optimum novel wing configuration for an A320 like aircraft having minimum fuel consumption and thus maximum efficiency.

Darwin graduated with a Master degree in aerospace in 2013 from Delft University of Technology. After his studies, he wanted to take a break and travel for a while before deciding his next step. In 2014, there was an exciting position on loads and aeroelasticity at the chair of Aerospace Structures and Computational Mechanics offered by Dr. Roeland De Breuker that piqued his interest. He successfully applied for this position and started his PhD in 2015 in Delft, The Netherlands. This dissertation on dynamic aeroelastic optimization of composite wings, including fatigue considerations, is the result of his PhD project.